UNIVERSIDADE FEDERAL DE PERNAMBUCO
CENTRO DE TECNOLOGIA E GEOCIÊNCIAS
DEPARTAMENTO DE ELETRÔNICA E SISTEMAS
PROGRAMA DE PÓS-GRADUAÇÃO EM ENGENHARIA ELÉTRICA

HAFIZ ZEESHAN MAHMOOD

A STUDY OF METALLIC AND POLYMERIC NANOSTRUCTURE-SOLUTION BASED PLATFORMS FOR OPTICAL AND CHEMICAL ARBOVIRUS BIOSENSING

Recife
2019

HAFIZ ZEESHAN MAHMOOD

A STUDY OF METALLIC AND POLYMERIC NANOSTRUCTURE-SOLUTION BASED PLATFORMS FOR OPTICAL AND CHEMICAL ARBOVIRUS BIOSENSING

Thesis submitted to the post graduate program in Eletrical Engineering of the Universidade Federal de Pernambuco to obtain the Ph.D. degree in Eletrical Engineering.

Área of concentration: Photonics.

Supervisor: Prof. Dr. Emery Cleiton Cabral Correia Lins.

Recife

2019

Catalogação na fonte
Bibliotecária Margareth Malta, CRB-4 / 1198

M215s Mahmood, Hafiz Zeeshan.
A study of metallic and polymeric nanostructure-solution based platforms for optical and chemical arbovirus biosensing / Hafiz Zeeshan Mahmood. – 2019.
97 folhas, il., gráfs., tabs.

Orientador: Prof. Dr. Emery Cleiton Cabral Correia Lins.

Tese (Doutorado) – Universidade Federal de Pernambuco. CTG. Programa de Pós-Graduação em Engenharia Elétrica, 2019.
Inclui Referências e Apêndice.

1. Engenharia Elétrica. 2. Sensoriamento. 3. Ressonância plasmônica de superfície. 4. Nanopartículas. 5. Nanomateriais. 6. Biossensores poliméricos. I. Lins, Emery Cleiton Cabral Correia. (Orientador). II. Título.

UFPE

621.3 CDD (22. ed.) BCTG/2019-429

HAFIZ ZEESHAN MAHMOOD

A STUDY OF METALLIC AND POLYMERIC NANOSTRUCTURE-SOLUTION BASED PLATFORMS FOR OPTICAL AND CHEMICAL ARBOVIRUS BIOSENSING

Thesis submitted to the post graduate program in Eletrical Engineering of the Universidade Federal de Pernambuco to obtain the Ph.D. degree in Eletrical Engineering.

Aprovada em: 25/09/2019.

BANCA EXAMINADORA

_____
Prof. Dr. Emery Cleiton Cabral Correia Lins (Orientador)
Universidade Federal de Pernambuco

_____
Profa. Dra. Rosa Amália Fireman Dutra (Examinadora Externa)
Universidade Federal de Pernambuco

_____
Prof. Dr. Renato Evangelista de Araújo (Examinador Interno)
Universidade Federal de Pernambuco

_____
Profa. Dra. Erika Ketlem Gomes Trindade (Examinadora Externa)
Universidade Federal de Pernambuco

_____
Prof. Dr. Diego José Rátiva Millán (Examinador Externo)
Universidade de Pernambuco

I would like to dedicate this dissertation to my beloved parents who have been a source of inspiration, encouragement, and perseverance to face the eventualities of life with patience and enthusiasm!

Along With all hard working and respected **TEACHERS!**

ACKNOWLEDGEMENTS

I have had the pleasure of getting to know many inspiring and intelligent people during my stay as a Post-graduate student. I would like to sincerely thank them for sharing their experience and knowledge for making all the work worthwhile. I wish to express my sincere gratitude to my supervisor Prof. Dr. Emery Cleiton Cabral Correia Lins and my co-supervisor Profa. Dra. Rosa Amalia Fireman Dutra. They have provided me direction and technical support. Due to their persistence, understanding and kindness I am able to conclude this gigantic task in a smooth fashion. Your enthusiasm, fundamental view on research and mission for providing high-quality work has made a deep impression on me. I don't know how to fully express my appreciation, but I owe you my sincere gratitude.

This research work would have never been completed without the assistance of my colleagues at LAPED. Thanks to all other senior researchers especially Dra. Erika Ketlem Gomes Trindade for her guidance and constructive discussions. I really appreciate your advice, encouragement and support throughout my research work. I can't thank to my beloved parents enough for giving me the highest gifts of unconditional love and continuous support throughout my life. It is impossible to describe in words how much you have done for me. Without their enormous sacrifices and encouragement, I could never have reached current level of success.

My sincere regards to my ever-supporting brothers, sister and nieces Arfan Mahmood (Late), Farhan Mahmood, Rameen, Areeba and Eman Sohail. You are always there for me and I feel blessed for having such a wonderful family.

Last but not least, words cannot describe my sentiments and esteem affection that I constantly have for my beloved spouse for her encouragement and understanding to accomplish my goals and aspirations. Her unconditional affection and trust have always increased my strength without which I would not have been able to complete this task. Thank you for everything you have done and standing beside me through thick and thin. My sincere love goes to my son Muhammad Abu Bakar. His smiles always brighten my world.

ABSTRACT

The metallic nanoparticles support localized surface plasmon resonance (LSPR) by interacting with time varying electromagnetic field. LSPR of noble metal nanoparticles are reliant on multiple factors such as size, shape and material composition. It is found that metallic nanoparticles (NPs) scatter or absorb light with remarkable efficiency at the plasmon resonance frequency. Therefore, metal nanostructures are increasingly receiving attention as important starter for the development of molecular biosensors for medical diagnosis. In this study, several parameters that govern on LSPR sensor performance such as refractive index sensitivity, figure of merit and molecular sensing, were evaluated. Finite Element Method and experimental results were used to explore the optical characteristics of plasmonic structures to employ their uses for LSPR sensors. Firstly, we had investigated theoretically the sensing performance of the dielectric-metal core-shell that support plasmon resonances as a function of refractive index of the surroundings in connection with varying core radius and shell thickness. Furthermore, our results possess high figure of merit for Ag nano shell (3.0), higher than Au nano shell (2.50) having same silica shell thickness 5 nm but different metallic core radius (46 nm & 34 nm) for Au/Ag nano shells, respectively. Then we had explored the optical behaviour in dimmer of gold nanorod (AuNR) bridge by thin silica cylinder to sub-nanometer regime, where light−matter interactions have been anticipated in which quantum nature of free electrons in metals might be strongly affected. Our results reveal that an increase in aspect ratio causes a red shift in dimer connected mode, leading to significantly higher sensitivity 717 nm/RIU and figure of merit 16.9 compared to a single dimer having 300 nm/RIU sensitivity with similar dimensions. Due to high surface to volume ratio, Au nanorods prove good candidate for LSPR-based optical sensors as compared to Au/Ag nanoshells. Moreover, in this work, the application of polymeric nanoparticles for the detection of chikungunya virus will be elucidated. A Sandwich like structure was designed for the detection of chikungunya RNA and it was observed that our proposed structure was suitable and stable for chemical sensor under probe.

Keywords: LSPR sensor. Finite element method. Nanoparticles. Chikungunya. Polymeric Biosensors.

RESUMO

As nanopartículas metálicas suportam a ressonância plasmônica de superfície localizada (LSPR) interagindo com campos eletromagnéticos variáveis no tempo. O LSPR de nanopartículas de metal nobre depende de múltiplos fatores, como tamanho, forma e composição do material. A mudança na função dielétrica devido à mudança no meio circundante sobre ou ao redor da superfície da nanopartícula é bastante impressionante e sensível para calcular a sensível sensibilidade granular e o sensor molecular. O LSPR é atribuído a uma oscilação coletiva dos elétrons livres nas nanoestruturas metálicas de dimensões abaixo do comprimento de onda ressonante. Verifica-se que as nanopartículas metálicas (NPs) dispersam ou absorvem a luz com notável eficiência na frequência de ressonância plasmônica. Portanto, as nanoestruturas metálicas estão recebendo cada vez mais atenção como importante iniciador para o desenvolvimento de biossensores moleculares para o diagnóstico médico. Neste estudo, vários parâmetros que governam o desempenho do sensor LSPR, como a sensibilidade do índice de refração, a figura do mérito e a detecção molecular, foram avaliados. Método dos Elementos Finitos e resultados experimentais foram usados para explorar as características ópticas das estruturas plasmônicas para empregar seus usos para os sensores LSPR. Em primeiro lugar, investigamos teoricamente a performance sensora do núcleo dielétrico-metálico que suporta ressonâncias de plasmon como uma função do índice de refração do ambiente em conexão com raio de núcleo variável e espessura de casca. Além disso, nossos resultados possuem alto valor de mérito para nanocascas de núcleo de Ag (3.0), em comparação à nanocascas de núcleo de Au (2.50) com cobertas com uma camada de sílica com espessura de 5 nm, mas diferentes raios de núcleo metálico (46 nm e 34 nm) para Au / Ag nanocascas, respectivamente. Em seguida, exploramos o comportamento óptico na ligação do dímero de nanobastões de ouro (AuNR) por um regime de sílica cilíndrica a um subnanômetro, onde as interações luz-matéria foram antecipadas, nas quais a natureza quântica de elétrons livres em metais pode ser fortemente afetada. Nossos resultados revelam que um aumento na razão de aspecto causa um desvio para o vermelho no modo conectado ao dímero, levando a uma sensibilidade significativamente maior 717 nm / RIU e figura de mérito 16.9 comparado a um único dímero com sensibilidade 300 nm/ RIU com dimensões similares. Existe a necessidade de projetar sensores plasmônicos altamente sensíveis que conferem uma boa biocompatibilidade e estabilidade óptica para detectar baixos níveis de analitos em meio

biológico. Devido à alta relação entre superfície e volume, os nanobastões de ouro são bons candidatos a sensores óticos baseados em LSPR, em comparação com as nanoesferas de ouro. Além disso, o valor mais elevado do índice de refracção, isto é, 353 nm / RIU de ouro @ sílica nanorod, seria muito atractivo para a investigação de analitos em fluidos biológicos. Neste trabalho, será elucidada a aplicação de nanopartículas poliméricas para a detecção do vírus chikungunya. Uma estrutura tipo sanduíche foi aplicada para a detecção de chikungunya e foi observado que nossa estrutura proposta era adequada e estável para o sensor químico sob sonda.

Palavras-chave: Sensoriamento. Ressonância plasmônica de superfície. Nanopartículas. Nanomateriais. Biossensores poliméricos.

LIST OF FIGURES

Figure 1- Geographic distribution of Chikungunya…… 17

Figure 2- Schematic diagram showing components of a sensor……. 19

Figure 3- Schematic view of Propagation of the SPR wave…… 24

Figure 4- Graphical representation of the dispersion relation of SPR wave…… 25

Figure 5- Schametic representation of the interacion of EM radiation and matellic nanostructure…… 26

Figure 6- The Lycurgus cup illustrates King Lycurgus is being dragged by Greek nymph Ambrosia……. 27

Figure 7- TEM images and related LSPR spectrum for single Au nanoparticles…… 30

Figure 8- Absorption response of single and silica linked Au dimer……... 31

Figure 9- LSPR peak position as a function of change in refractive index of Au rods... 32

Figure 10- Refractive index sensitivity plots for Ag dispersed in water and immobilized on glass substrate…… 34

Figure 11- Bulk and Molecular sensing……. 37

Figure 12- Schematic diagram of a biosensing system……. 40

Figure 13- Schematic Structure of an antibody……. 43

Figure 14- Schematic depiction of random immobilization of antigen on the sensing surface……. 46

Figure 15- Components of UV-Vis spectrophotometer……. 51

Figure 16- Schematic model of the metallic core with dielectric (SiO_2) coated nanoshell……... 55

Figure 17- 3D simulations model region composed of model nanostructure in embedding medium and PML layers…… 57

Figure 18- Schematic representation of an electrochemical cell……... 60

Figure 19- Graphical representation of the CV technique……. 61

Figure 20- Geometrical representation of a FTIR spectrometer in the generation of a spectrum……... 64
Figure 21- The LSPR extinction for gold and silver nanoshells…… 67
Figure 22- LSPR peak shift of gold and silver nanoshells on changing the refractive index of the surrounding……. 68
Figure 23- The sensitivity of gold and silver nanoshells as a function of their respective silica shell thickness……. 69
Figure 24- The bulk sensitivity of gold versus silver nanoshells as a function of core radius and their respective figure of merit……... 70
Figure 25- The product of RIS×FoM (unit: nm/RIU^2) for Au/Ag nanoshell with SiO_2 shell (5nm) and Au/Ag core (10-50nm) ……... 71
Figure 26- Plasmonic spectral shift as a function of the adsorbent layer thickness…… 72
Figure 27- LSPR peak shift of single AuNR and AuNR dimer connected with silica cylinder……. 74
Figure 28- Bulk sensitivity and FoM of AuNR dimer with various aspect ratios……. 75
Figure 29- Bulk sensitivity and FoM as a function of silica nano-cylinder with different lengths…….. 76
Figure 30- Effect of different concentrations of EDA on PEDOT: PSS……... 77
Figure 31- Schematic representation of nanostructured platform development and Cyclic voltammograms of the electrode modified……... 78
Figure 32- CVs obtained from the PEDOT-EDA/GCE and Plot of anodic and cathodic peak current……. 79
Figure 33- Immunosensor response for Anti-IgG 5 µg/mL and Anti-IgG 10 µg/mL……. 81
Figure 34- Effect of Different Concentrations of IgG and Different Concentrations of NPs……... 82
Figure 35- Matrix effect and selectivity studied on successive incubations in positive and negative serum……... 83

LIST OF TABLES

Table 1-	Effect of Material on LSPR of Nanoscopic Particles of Same Shapes……	33
Table 2-	Different Nanostructures and respective Figure of merit (FoM), Bulk Sensitivity (η_b)…….	36
Table 3-	Comparison of biological molecules with detection limit using various structures of Au or Ag…….	39
Table 4-	Comparison of electrochemical sensors based on polymers…….	49
Table 5-	Brief survey of Bulk sensitivity and Figure of Merit of plasmonic nanostructures……	75

LIST OF ABBREVIATIONS

AFM	Atomic Force Microscopy
Ag	Silver
Au	Gold
CV	Cyclic Voltammetry
EM	External Electromagnetic Field
ECP	Electronically conducting polymer
EDA	Ethylenediamine
EDC	N-Ethyl-N'-3-Dimethylaminopropyl Carbodiimide
E_{pa}	Anodic peak potential
E_{pc}	Cathodic peak potential
CHIK	Chikungunya
DEN	Dengue
WHO	World Health Organization
YF	Yellow Fever
ZIK	Zika
eV	Electron Volt
FEM	Finite Element Method
FoM	Figure of Merit
FWHM	Full width at Half Maximum
FT-IR	Fourier Transform Infrared Spectroscopy
GCE	Glassy carbon electrode
I_{pa}	Anodic peak current

I_{pc}	Cathodic peak current
LSPR	Localized Surface Plasmon Resonance
NHS	N-Hydroxy Succinimide
PEDOT: PSS	Poly(3,4-ethylenedioxythiophene): poly (styrene sulfonate)
PCP	Proton conducting polymer
PML	Perfectly Matched Layer
SEM	Scanning electron microscopy
SWV	Square Wave Voltammeter
nm	Nanometer
RIU	Refractive Index Unit
η_b	Bulk sensitivity

TABLE OF CONTENTS

1 INTRODUCTION 16

1.1 Objectives 21

2 REVIEW OF LITERATURE 22

2.1 Plasmonics 22

2.1.1 Phenomena of SPR 24

2.1.2 Features of Localized Surface Plasmon Resonance 26

2.2 Factors Governing LSPR 29

2.2.1 Impact of shape and size 29

2.2.2 Impact of Material and Medium 31

2.3 Parameters Analytically Measure Plasmonic Sensors Efficiency 33

2.3.1 Bulk Sensitivity 33

2.3.2 Figure of Merit 35

2.3.3 Affect of Analyte Attachment 37

2.5 Biosensor 40

2.5.1 Immunosensor 43

2.5.2 Antibody immobilization 45

2.5.3 Sensors based on conductive polymers 48

3 MATERIALS AND METHODS 51

3.1 UV-Vis Spectroscopy 51

3.2 Computational Simulations 52

3.3 Modelling and Calculations 54

3.3 Materials and Electrochemical Techniques 57

3.3.1 Characterization of electrode surface 58

3.3.2 Immobilization of Chikungunya on the glassy carbon electrodes: 59

3.3.3 Electrochemical Cell 59

3.3.4 Cyclic Voltammetry (CV) 61

3.3.5 Square Wave Voltammetry (SWV) 62

3.4 Structural and topographic characterization 63

3.4.1 Fourier Transform Infrared Spectroscopy (FT-IR) 63
3.4.2 Atomic Force Microscopy (AFM)..... 65
3.4.3 Scanning Electron Microscopy (SEM)..... 66
4 RESULTS AND DISCUSSION..... 67
4.1 Plasmonic Properties of Silica Coated Au/Ag nanoshells..... 67
4.2 Gold nanorods dimer structure for sensing platform..... 73
4.3 Construction of PEDOT-EDA film on the GCE for the detection of chikungunya. 77
5 CONCLUSION..... 84
REFERENCES..... 85
APÊNDIX A - Articles and Conference Contributions……97

1 INTRODUCTION

The alphaviruses (Barmah Forest, Mayaro, o'nyong-nyong and Ross River viruses) are enveloped particles and their genome consists of a single strand of positive sense RNA molecule .[1] There are five structural proteins (capsid, E3, E2, 6K, and E1), Among these E2 and E1, the envelope proteins, play an important role in binding of the virus to the host cell membrane and get translated during the virus replication.[2]

Chikungunya virus (CHIKV), Dengue virus (DENV), Yellow Fever virus (YFV) and Zika virus (ZIKV) are arboviruses associated to worldwide outbreaks. CHIKV was first reported (1952) in southern Tanzania during an outbreak [3] and Geographic distribution of Chikungunya is depicted in Figure 1. It is an enveloped positive-sense single-stranded RNA virus, member of the *Togaviridae* family, genus Alphavirus, with a genome just under 12Kb nucleotides coding nonstructural proteins and structural proteins (capsid, envelope and two polipeptides).[4] Transmission between species and individuals mainly caused due to infected female mosquitoes bites Aedes agypti and Aedes albopictis[4] and predominantly transmitted to humans in a sylvatic cycle.

It is a significant public health concern and has been identified in more than sixty (60) countries around the globe.[5] According to World Health Organization (WHO) statistics, out of 6,93,489 suspected 37,480 were confirmed cases of CHIK as reported by Pan American Health Organization. By September 2014, first indigenous CHIKV sufferers in Brazil were identified in the cities of Oiapoque (North Brazil) and Feira de Santana (Northeast Brazil).[6] This arboviral disease shares some clinical manifestations similar to dengue virus and zika virus which makes the diagnosis of CHIKV difficult, especially in endemic areas with DENV and ZIKV co-circulation [2,7], severe joints pain alongside by edema differentiates it from the for mentioned diseases.[7] Despite from chronic arthralgia, an infected individual may suffer, headache, myalgia, nausea, fatigue, hair loss, rash and depression are some of the long-term complications.[8] Rheumatic manifestations (endocrine disorder) are common in all the stages of CHIK infection. However, many chikungunya-infected individuals have reported prolonged arthralgia which can last for months to years.[2]

Figure 1 - Geographic distribution of Chikungunya

Countries and territories where chikungunya cases have been reported*
(as of May 29, 2018)

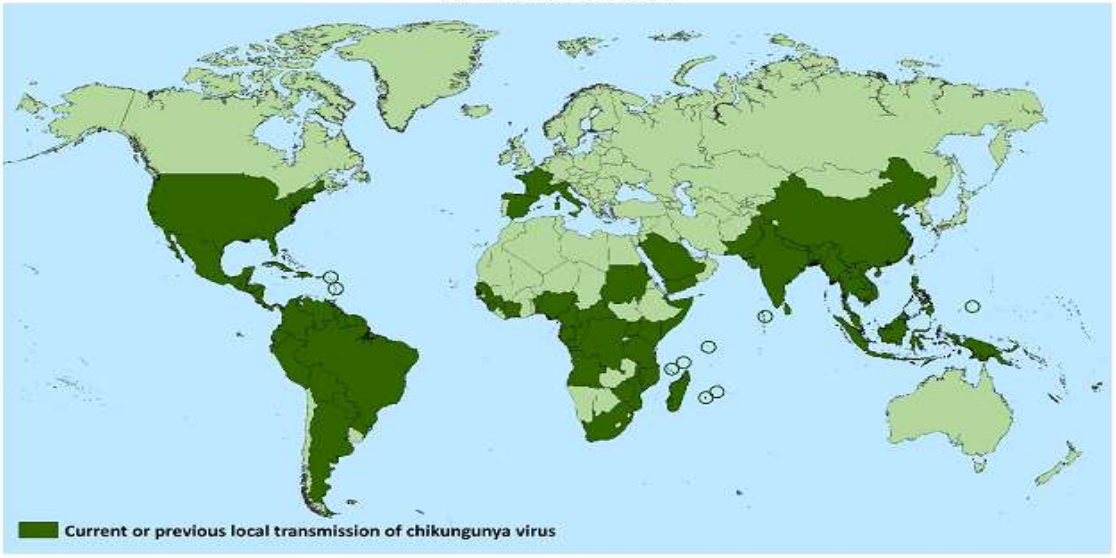

*Does not include countries or territories where only imported cases have been documented.

Data table: Countries and territories where chikungunya cases have been reported

AFRICA	ASIA	AMERICAS	
Angola	Bangladesh	Anguilla	Panama
Benin	Bhutan	Antigua and Barbuda	Paraguay
Burundi	Cambodia	Argentina	Peru
Cameroon	China	Aruba	Puerto Rico
Central African Republic	India	Bahamas	Saint Barthelemy
Comoros	Indonesia	Barbados	Saint Kitts and Nevis
Cote d'Ivoire	Laos	Belize	Saint Lucia
Dem. Republic of the Congo	Malaysia	Bolivia	Saint Martin
Djibouti	Maldives	Brazil	Saint Vincent & the Grenadines
Equatorial Guinea	Myanmar (Burma)	British Virgin Islands	Sint Maarten
Gabon	Nepal	Cayman Islands	Suriname
Guinea	Pakistan	Colombia	Trinidad and Tobago
Kenya	Philippines	Costa Rica	Turks and Caicos Islands
Madagascar	Saudi Arabia	Cuba	United States
Malawi	Singapore	Curacao	US Virgin Islands
Mauritius	Sri Lanka	Dominica	Venezuela
Mayotte	Thailand	Dominican Republic	
Mozambique	Timor-Leste	Ecuador	
Nigeria	Vietnam	El Salvador	**OCEANIA/PACIFIC ISLANDS**
Republic of the Congo	Yemen	French Guiana	American Samoa
Reunion		Grenada	Cook Islands
Senegal		Guadeloupe	Federal States of Micronesia
Seychelles	**EUROPE**	Guatemala	Fiji
Sierra Leone	France	Guyana	French Polynesia
Somalia	Italy	Haiti	Kiribati
South Africa	Spain	Honduras	Marshall Islands
Sudan		Jamaica	New Caledonia
Tanzania		Martinique	Papua New Guinea
Uganda		Mexico	Samoa
Zimbabwe		Montserrat	Tokelau
		Nicaragua	Tonga

Source: Adapted from (61).

Mosquitoes that spread chikungunya bite aggressively during the day. Avoid infection by preventing mosquito bites by wearing long-sleeved shirts and long pants or permethrin (Odorless insect repellents) treated clothing. Treatment is directed primarily at relieving the symptoms, including the joint pain using antipyretics (medication used to lower body temperature due to fever), optimal analgesics/ painkiller and fluids. There is no specific commercial antiviral drug/vaccine available to treat chikungunya infection.

It can be potentially treated with immunosuppressive therapies. Conventional assays are based on genetic and immune techniques, however due limitation in real-time polymerase chain reaction (RT-PCR) for non-acute disease phase and MAC-ELISA sensibility reduced due cross-reaction caused by arbovirus similarity are associated with false negative results.[9] Conventional diagnostic assays that are exploited for CHIKV detection are RT-PCR[10], a real-time accelerated reverse-transcription-loop-mediated isothermal amplification RT-LAMP[9], indirect immunofluorescent test and the Chikungunya IgM antibody capture enzyme-linked immunosorbent assay (MAC-ELISA[11], using serum, plasma, urine, placental tissue, brain tissue and amniotic fluid.[10] However, the said methods are cumbersome, required skilled individuals to operate and as well as sensitivity of MAC-ELISA was below 50%[11], in view of the above limitations these assays are hard to carry out.

Novel diagnostic methods such as biosensors can be a distinguished choice, owing to their excellent sensitivity, selectivity, portability, low cost and a nominal input signal required for their operation.[12] These systems are high in demand because they can provide in situ, robust and rapid automation analyses[13] as well as previous studies suggested electrochemical immunosensors as diagnostic methods for arboviruses. [9]

Among the electrochemical antibody-based biosensors known as immunosensors, have revolutionized the diagnostics and recent advancement in electrochemical biosensor-based technology has been accomplished through the development of novel immunosensors, as they exploit the high specificity provided by the molecular recognition of an antigen- antibody interaction. On contrary, the known drawbacks of electrochemical immunosensors, they required frequent washes and several transducer modifications steps that shrinkage its efficacy. A

transducer or biological sensing element converts the biochemical signal into an electronic signal[14] as depicted in Figure 2 different components of biosensing setup.

Figure 2 - Schematic diagram showing components of a sensor.

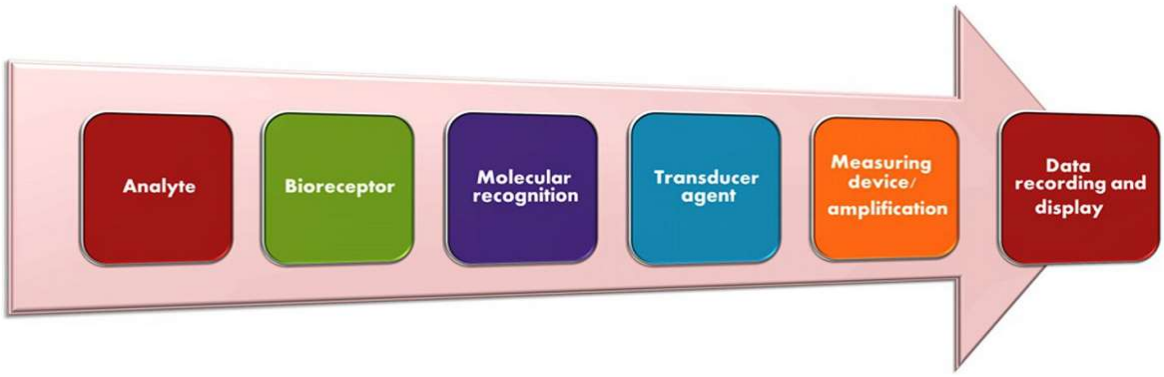

Source: Adapted from (62).

In biosensing systems, different transduction can be employed in the conversion of the electric-biochemical response, highlighting the optical, piezoelectric and electrochemical transducers. In general, the monitoring of antigen-antibody interaction in electrochemical transducers uses electroactive species as indirect markers of analyte detection. The successful biomolecule immobilization on the transducer surface is considered a crucial step in the development of stable and reproducible biosensors. The biomolecule must be effectively immobilized, without losing its activity, deterioration over time and it should not undergo leaching processes. One way to overcome this challenge is to use coating of functionalized polymeric film. In clinical diagnostics, electronically conducting polymers (ECP) have gained much intention as suitable matrices of biological component that can be used to exploit stability, speed, and sensitivity of the biosensor.[15][16] Polymers have advantages over metal or inorganic materials, for instance easy to synthesize and processing, structural and chemical diversity, light weight[17] as well as better electrical and optical properties.[18] The efficiency of electrochemical transducer depends on the electroactive properties and material's conductivity utilized for the immobilization matrix .[19]

Polymeric films that are excellent materials for the immobilization of biomolecules have been used in electrochemical biosensors include polypyrrole[20], polyaniline[21] and polythiophene derivatives[22] among others. For instance, in this study an ECP i.e., poly(3,4-ethylenedioxythiophene): poly (styrene sulfonate) PEDOT: PSS has been utilized as sensing plate form and their nanoparticle as labelling agent to identify the target analyte.

As compared to other conducting polymers, PEDOT has an advantage due to the presence of a dioxyalkylene bridging group across the 3-positions and 4-positions of its heterocyclic ring which results in its lowers band gap and thus provides superior electrical conductivity apart from better chemical, thermal and environmental stability.[23] Particularly PEDOT:PSS has received considerable attention in recent years due to their well-defined redox properties, high electrical conductivity, large volumetric capacitance and stability in water when mixed with PSS as a dopant, this state of the art conducting polymer has become a de facto standard material for bioelectronics.[24] Since polymeric films can be chemically functionalized[25] hence yielding desirable functional groups on the transducer surface.

The optimization of the antigen-antibody interaction at the sensor interface is one of the critical steps for obtaining more sensitive, stable and reproducible electrochemical immune sensors. Signal enhancement is mainly achieved by coupling different kinds of labels with a secondary bioreceptor in sandwich-type electrochemical immunosensors.[26] In order to enhance signal, sandwich-type immunosensor is best option.[27] To optimize sensitive detection, the sandwich architecture utilizes the substrate material along with nanomaterial conjugated to secondary antibodies (Ab2). Although a major breakthrough for electrochemical immunoassays with prospects to obtain mono-use immune assays at the large scale, cost of bioreactor biomolecules for the best specificity and use of monoclonal antibodies is still desirable. In order to overcome these limitations, biomimetic systems based on glassy carbon electrode (GCE) was analyzed. These have many important advantages which include chemically inert, high thermal shock resistance, Wide Electrochemical potential limits(stability window).[28]

1.1 Objectives

In view of the foregoing, in this thesis we will investigate plasmonic sensors to explore the optical characteristics of noble metal nanostructures with different geometry to engineer new platforms for optical biosensing. Basic concepts regarding localized surface plasmon resonance (LSPR) response and how to scrutinize it for bio-applications will be analyzed. Mathematical simulations in frequency domain will be carried out to evaluate the light-matter interactions by the use of finite element method (FEM) with COMSOL Multiphysics. This computational approach focused on the assessment of the LSPR spectral peak position and spatial distribution of electromagnetic field enhancement near the surface of the metallic structure under probe, in order to understand the behavior of crucial parameters such as figure of merit and bulk sensitivity which predicts the LSPR sensor performance.

Furthermore, an immune sensor based on recombinant protein monoclonal antibodies utilizing glassy carbon electrodes (GCE) modified with PEDOT: PSS previously dispersed in ethylenediamine (EDA) for electrochemical detection of arbovirus (Chikungunya and Dengue) Virus will also be studied. A sandwich-type electrochemical immunosensor based on a new signal amplification strategy will be prepared for the detection of CHIK. Among the electrochemistry techniques, square-wave voltammetry and cyclic voltammetry will applied to investigate the stability and reliability of the proposed electrochemical sensor.

Upcoming chapters will review the physical basis for plasmonic sensor and electrochemical sensor as well as the relevant parameters and techniques used to evaluate, assemble, and characterize the LSPR and electrochemical sensors.

2 REVIEW OF LITERATURE

This chapter deals with a brief introduction of plasmonic, Surface Plasmon Resonance (SPR) Phenomena, Localized surface plasmon resonance (LSPR), metallic nanostructures and their applications in optical sensing. Important parameters on which LSPR performance is reliant on, such as shape, size, surrounding dielectric medium and material compositions, as well as, the Campbell's model to predict the LSPR peak shift due to adsorbate molecules layer was analyzed. Furthermore, the Electrochemical immuno sensor based on conducting polymers and techniques related to analyze efficacy of this type of sensor were also discussed briefly in the second part of this chapter.

2.1 Plasmonics

Plasmons are made up of electrons rather than an electron but a gang or collection of electrons that get together prompted by long-range Coulomb force. In order to describe their behavior, they may be considered as a single entity, like an orchestra or a choir following the same conductor.[29] The basic model for the electronic properties of a metal is the Drude model, based on the classical description which makes the approximation of a free electron gas/plasma that moves within a crystalline lattice of fixed positive nuclei of a metal. The dielectric function for a free electron is:

$$\varepsilon = 1 - \frac{\omega_p^2}{\omega^2 + i\gamma\omega} \tag{2.1}$$

With real and imaginary parts:

$$\varepsilon_{real} = 1 - \frac{\omega_p^2}{\omega^2 + \gamma^2} \tag{2.2}$$

$$\varepsilon_{img} = 1 - \frac{\omega_p^2 \gamma}{\omega(\omega^2 + \gamma^2)} \tag{2.3}$$

This is Drude model for the optical properties of free electrons in metals.[29] According to this model, when the metal is exposed to an external electromagnetic field, the non-uniform charge distribution will set up an electric field that produce oscillations which results in applied force on the electron plasma and displaces it from its initial uniform equilibrium position. The electric field set up due to the displacement of electron plasma can be expressed by means of Gauss's Law in eq. (2.4):

$$E = \frac{-\rho x e}{\varepsilon_0} \tag{2.4}$$

Where 'ρ' is the free electron density, 'x' is the displacement from mean/equilibrium position, 'e' charge on an electron and 'ε_0' is the permittivity of free space. As aforementioned, the 'E' exerts a force on free electron gas/plasma yields E.e. By comparing this relation 'E.e' with Newton's 2nd law can be written as:

$$E.e = m_e \cdot \frac{\partial^2 x}{\partial t^2} \tag{2.5}$$

Here m_e is the effective mass of an electron. By putting the eq. (2.4) in eq. (2.5) implies that:

$$\frac{-\rho x e^2}{\varepsilon_0} = m_e \cdot \frac{\partial^2 x}{\partial t^2} \tag{2.6}$$

$$\frac{\partial^2 x}{\partial t^2} + \frac{\rho x e^2}{\varepsilon_0 m_e} = 0 \tag{2.7}$$

$$\frac{\partial^2 x}{\partial t^2} + \omega^2 x = 0 \tag{2.8}$$

After substitution Eq. (2.8) takes the form of simple harmonic oscillator. It is clear from the comparison of eq. (2.7) and eq. (2.8), the natural frequency at which the free electrons in a metal will naturally oscillate, called the plasma frequency 'ω_p', can be determined as particularly expressed in eq. (2.9):

$$\omega_p = \sqrt{\frac{\rho e^2}{\varepsilon_0 m_e}} \tag{2.9}$$

When light is incident upon the metal, long-range correlation of the electron plasma collectively tends to oscillate caused by Coulomb forces. This collective oscillation is called a plasma oscillation.[29] This frequency holds only for plasmons existing in the bulk material and for

metals it falls in visible and ultraviolet regions of electromagnetic spectrum and ranges from about 3 eV to 20 eV. [29]

2.1.1 Phenomena of SPR

Surface Plasmon waves are excited along the interface between the metal and the dielectric layer with negative and positive permittivity i.e. real part corresponding to dielectric constant of the metal and the dielectric are of opposite sign and decay exponentially with distance normal to the interface, Conceptual view of the SPR wave propagation is depicted in Figure 3.

Figure 3 - Schematic view of Propagation of the SPR wave

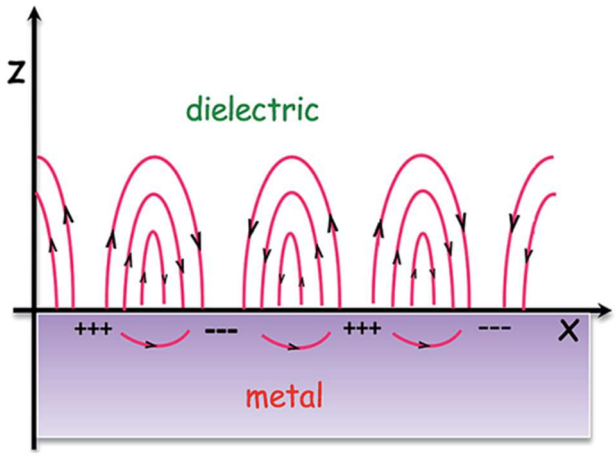

Source: Adapted from (30).

By solving Maxwell's equation within proper boundary conditions, it will lead to understand the SPR phenomenon, its main characteristics as well as the dispersion relations (A relationship between the wave vector 'K' and angular frequency 'ω'). The dispersion relations also correlate the wave vector 'K' with metal 'ε_m' and dielectric 'ε_d' permitvities respectively.

$$K_x = \frac{2\pi}{\lambda}\sqrt{\frac{\varepsilon_m \varepsilon_d}{\varepsilon_m + \varepsilon_d}} \qquad (2.10)$$

It is worthwhile to keep in mind in order to propagate a SPR wave along the metal-dielectric interface, the phase matching condition should be satisfied i.e. the energy and momentum of the incident TM polarized light must match the energy and momentum of a propagating SPR wave

($k_x = \omega_{sp}$) as illustrated in Figure 4.

Figure 4 - Graphical representation of the dispersion relation of SPR wave

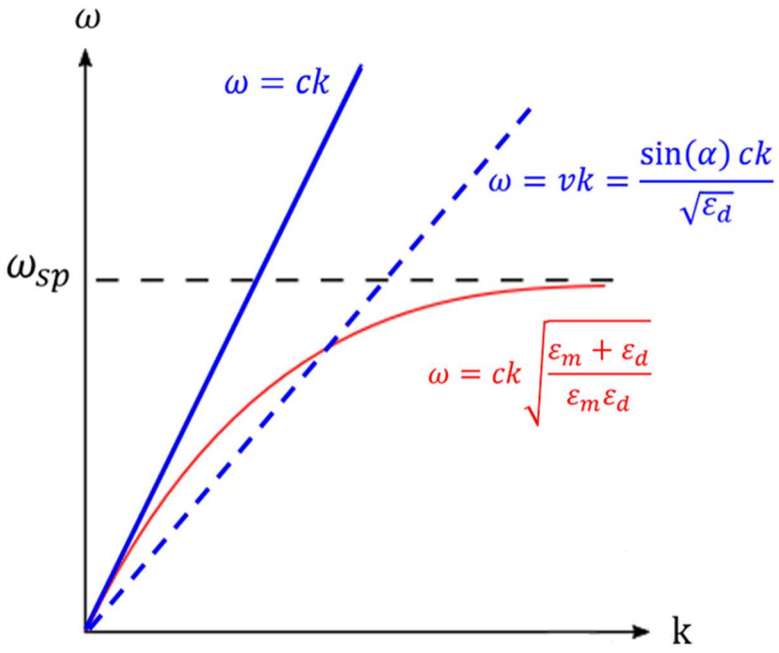

Source: Adapted from (31).

Here solid blue line represents the dispersion relation for a vacuum photon, red line for SPR and the dotted blue line is regarded as a photon traveling through a coupling medium as in the Kretschmann and Otto configuration. This coupling medium e.g. Prism, in case of both Kretschmann and Otto coupling techniques which are classified under prism coupling, alters the dispersion relation and thus allows for phase matching of the momenta and energies of the incident TM polarized light and the SPR waves. The intersection of dotted blue line with the SPR line satisfies the conditions at which an SPR wave can be excited. Hence to summarize that, the conditions in order to excite the SPR waves are: [32]

- Incident light is Transverse Magnetic (TM) polarized.
- The real part related to dielectric constant of the metal and the dielectric bears opposite sign.
- The energy and momentum of the incident TM polarized light and the propagating SPR wave must fulfill the phase matching condition ($k_x = \omega_{sp}$).

2.1.2 Features of Localized Surface Plasmon Resonance

Localized surface plasmon resonance (LSPR) is a novel phenomenon that occurs in metallic nanostructures that possess dimensions 3-100 nm which are much smaller than the incident wavelength.[33] The free electrons in a metal can be excited by the presence of an external electromagnetic (EM) field as depicted in Figure 5. LSPR are non-propagating excitations, so they don't have any momentum, instead requires only the additional energy for their propagation. In case of metallic nanoparticles, oscillation of the surface plasmons is confined to the material due to their small size.[34] On the other hand, When resonance arise from the conductive nanoaggregate due to scattering in the transverse electromagnetic field and in turn the electrons oscillate as a result of surface polarization that provides a restoring force with respect to the positive ionic cores, [35] leading to an intense surface plasmon absorption band both inside and outside of the particle as well as in the near-field zone.[36] This phenomenon is termed as Localized surface plasmon resonance.

Figure 5 - Schametic representation of the interacion of EM radiation and matellic nanostructure.

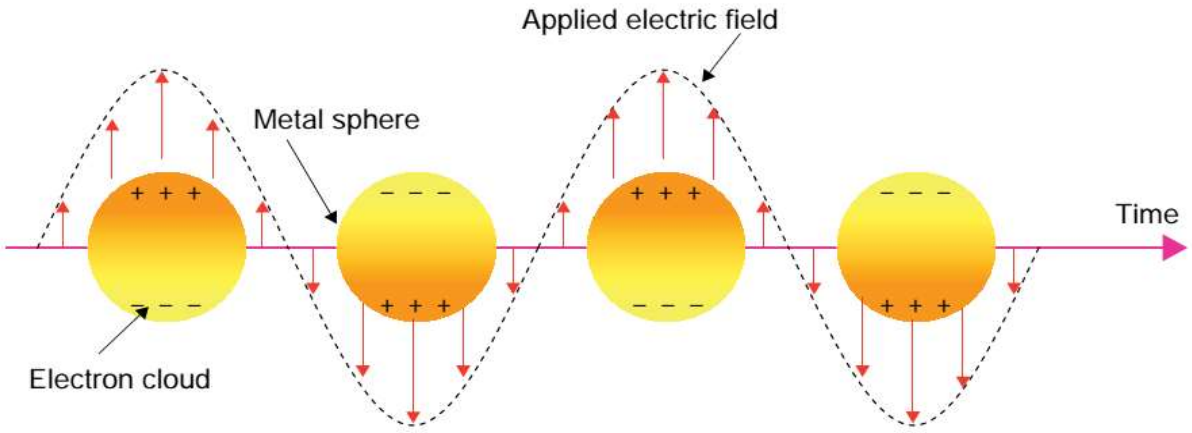

Source: Adapted from (32).

For most bulk metals the LSPR is in the ultraviolet range; however, when this electron oscillation is confined within a nanoparticle metal atoms, the resonances for Au/Ag can instead fall in the visible region i.e. 400-700 nm. [36]

This strong interaction between plasmonic nanoparticles and visible light, what causes nanoparticle ensembles to exhibit their distinctive and vibrant colors that can be exploited for plasmon coupling. As shown in Figure 6, The Lycurgus cup exhibit different colors, when light is

reflected (green) and illuminated from inside or Transmitted light (ruby red) due to plasmonic nanoparticles response embedded within the cup. The plasmonic metallic nanostructures have been extensively investigated substantial subject which stimulated the interest of the researchers due to their fascinating optical characteristics, conspicuous features linked with geometric tunability.[37] The specific wavelength at which this resonance occurs is a property which depends on a number of factors: the bulk LSPR of the metal, the dielectric medium in which the structure is immersed, the particle's size and shape, and any local EM fields.[38] Control over these factors, and the strong coupling between plasmons and light, along with advancements in particle synthesis makes plasmonic nanoparticles a very flexible platform for a number of different applications; ranging from the controlled drug delivery, imaging, nonlinear optics all the way to bio and chemical sensing modalities. [39]

Figure 6 - The Lycurgus cup illustrates King Lycurgus is being dragged by Greek nymph Ambrosia.

Source: Adapted from (40).

Due to their unique optical properties and multifaceted approach, a plethora of studies based on plasmonic nanostructures showed that LSPR of the subwavelength nanoparticles is directly attributed to the shape, size and metal composition which make them pragmatic for the optical phenomenon (absorption, scattering, extinction) of light and bio sensing.[34][41-44] To foster the sensitivity, phenomenon of sensing utilizes the capability of metallic nanostructures to concentrate the external radiation in the vicinity of their small local entity. The basis of plasmonic sensors is the resonant coupling between the oscillations of free electrons, called plasmons, and incident visible light waves. By confining these oscillations within a nanostructure, the coupling efficiency is enhanced by the creation of localized surface plasmon resonant (LSPR) states. For single particle LSPR sensor, the fundamental principle utilizes the fact that LSPR spectrum position varies as a function of dielectric host medium.[29] Jensen et al[45] pointed out that LSPR wavelength of metallic nanoparticles shift with respect to variation in the RI of the proximity of surrounding media. To investigate which metal nanostructures is a good candidate for bio or chemical sensing applications as well as their efficiency can be characterized by measuring their RI based sensitivity. Bulk sensitivity (η_b), A sensing parameter which qualitatively analyse the sensing efficiency and correlates the change in LSPR wavelength as function of varying refractive index of the surrounding medium has been evaluated i.e: $\eta_b = \Delta\lambda LSPR / \Delta n$.Figure of Merit (FoM) is second analytical parameter which elucidate well sensor reliability by, FoM = η_b/FWHM, where (FWHM) is full width at half maximum or line width of the LSPR peak.[46] Therefore, a plasmonic sensor simultaneously requires both prerequisites: high bulk sensitivity and a fine LSPR spectrum.

In 1905, Gustav Mie was the first who solved the Maxwell equations to calculate the optical properties for spherical metallic nanoparticles and derived the extinction cross section σ_{ext} :[29]

$$\sigma_{ext} = 9\frac{\omega}{c}\,\varepsilon_m^{\frac{3}{2}}\,V\frac{\varepsilon_i}{(\varepsilon_r+\varepsilon_m)^2+(\varepsilon_i)^2} \qquad (2.11)$$

Here '$\varepsilon = \varepsilon_r + i\varepsilon_i$' is the dielectric function of nanoparticle, 'ε_m' surrounding medium dielectric function, 'V', 'ω' and 'c' are volume of sphere, angular frequency and speed of light in vacuum respectively. LSPR spectroscopy of metal nanostructures is considered a powerful tool in biological and chemical sensing.[47] When the surface of the metallic particle under probe is

modified it will change the dielectric constant as well, thereby changing the optical response of that metal. A common technique applies to detect changes as a result of binding or analytic adsorption on the metallic surface. This is the basis for surface plasmon resonance related sensing. Due to excellent plasmonic response of noble metals (Au or Ag) in nano-regime (because of high surface to volume ratio) make it possible to utilize these nanostructures in wide variety of applications. The interaction of NPs with proteins or bio-molecules has provided the base for a number of applications including label free detection, cell imaging, imaging enhancers, kinetic and binding sensing as well as molecular biosensors.[48-52] Based on this study, the key relationship between LSPR spectral shift and sensitivity to the surrounding media including shape, size and particularly molecular sensing had been widely investigated [53-56] and will be discussed briefly in the upcoming section.

2.2 Factors Governing LSPR

LSPR is widely utilized to improve and investigate the different characteristics of noble metal NPs. For example, LSPR based Electric field enhancement leads to surface enhanced Raman scattering (SERS) and other kind of surface enhancement related process. [57] However, there are several factors that can manipulate the nature of the LSPR based sensors.

2.2.1 Impact of shape and size

According to the Mie–Gans theory, shape and size of the NPs strongly influenced the plasmon resonance.[58] LSPR spectra related to different geometrical shapes have specific peak values such as for triangles (506 nm), trapezoids (537 nm), irregular circular cylinder (548 nm), hexagonal (603 nm) and parallelograms have (629 nm).[59]

Figure 7 - TEM images and related LSPR spectrum for single Au nanoparticles.

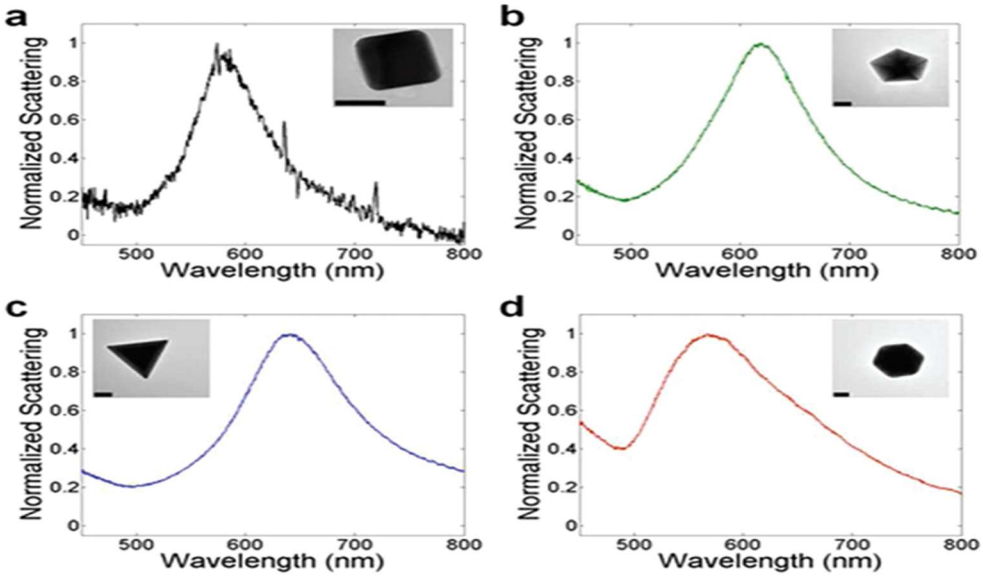

Source: Adapted from (60).

Note: (a) Au cube, (b) Au decahedron, (c) Au icosahedrons and (d) Au triangle.

Figure 7 shows the different images of transmission electron microscopy (TEM) and corresponding LSPR peak positions for the various shapes of single Au nanostructures. This varied response to shape and size allows for a continuous range of plasmon peaks and one can analyze from the results depicted in Figure 7, that LSPR frequency falls in the visible range (400 nm -700 nm) in case of noble metals (Au and Ag) nanostructures. On the other hand, NPs with Sharpe edges are expected to exhibit LSPR at longer wavelength as compared to spheroids. For instance, the plasmonic spectra of individual Ag triangular nanoplate demonstrated red shift in contrast to the spherical NP.[63] Due to high symmetry of nanosphere, they have a single resonant mode but increasing the aspect ratio and more complex geometries of NPs can split the resonant frequencies into transverse and longitudinal as well as multiple different modes. [31]

Figure 8 - Absorption response of single and silica linked Au dimer

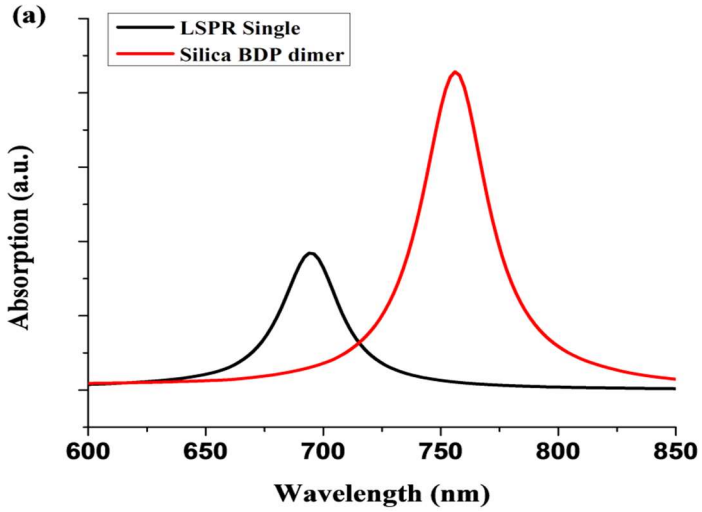

Source: The Author, 2019.

It has been found that while going towards the isotropicity of the particle size, a blue shift occurs. However, the edges effect in the Au dimer (single and silica junction) can cause red shift in the plasmonic spectra as illustrated in Figure 8. This plays an important role in the refractive index-based sensing technique. On contrary, Ringe et al investigated that the influence of size on the dipolar plasmon frequency and line width or Full width at half maximum (FWHM) of NPs with different shapes but proportional to Plasmon length (the length between two poles created in the particle due to the incident electromagnetic field) have similar plasmonic spectra.[60] This finding suggests that describing the size-dependent (50 nm - 350 nm particularly edge effects) plasmonic properties of NPs, Plasmon length should be focused rather than their intrinsic shape.

2.2.2 Impact of Material and Medium

In LSPR based sensing, noble metals Au and Ag are widely used metals with negative real part and small positive imaginary part of dielectric function. Other than noble metals, like aluminum (Al), Copper (Cu), Sodium (Na), Lithium (Li) and Gallium (Ga) are plasmon metals that exhibit

the LSPR resonance in Ultraviolet-Visible region[64-67] where several organic molecules absorb light.[68] However, these metals are easily oxidized and highly reactive to the surrounding medium which makes them difficult to utilize like Au or Ag.[69]

Figure 9 - LSPR peak position as a function of change in refractive index of Au rods.

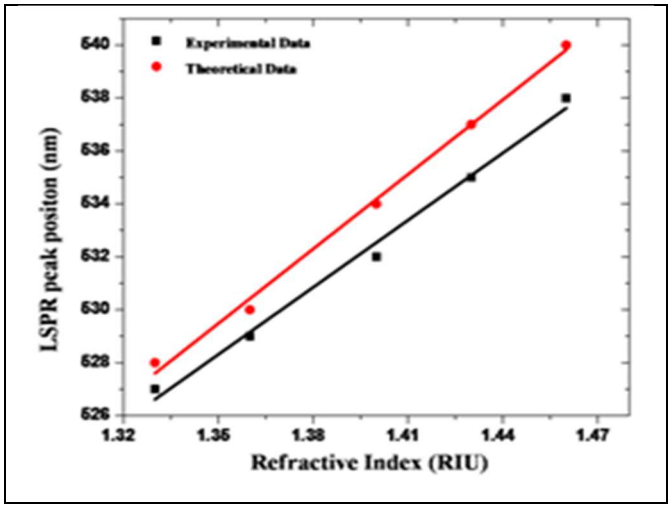

Source: The Author, 2019.

The surface of plasmon NPs is very sensitive to the change in local medium and LSPR sensing is based on the shift of plasmonic peak as a function of change in local dielectric medium due to analytic adsorption e.g. in molecular sensing. Figure 9 demonstrates the theoretical and experimental analyses of the LSPR spectral peak position of Au nanorods in diverse surrounding medium, as water (n = 1.33), ethanol (n = 1.36), tetrahydrofuran (n = 1.40), dimethylformamide (n = 1.43) and polyethylene glycol (n = 1.46). As depicted LSPR peak position is linearly dependent on the refractive index of the local medium and a clear red shift of LSPR peak wavelength (λ_{LSPR}) can be observed. The oscillating electric field around the NP generates the polarization in the local environment and the polarized medium has the influence on the restoring force in presence of the external electromagnetic field. The relationship between LSPR and refractive index of the medium is according to:

$$\lambda_{max} = \lambda_{LSPR}\sqrt{1 + 2n_m^2} \tag{2.12}$$

Where 'λ_{LSPR}' is the LSPR wavelength in bulk material and 'n_m' is the refractive index of the medium. This relationship shows the linear dependence of the λ_{peak} on the refractive index for a small range of 'n'. A brief description regarding the effect of material on LSPR peak and sensitivity is illustrated in Table 1.

Table 1 - Effect of Material on LSPR of Nanoscopic Particles having Same Shapes

Particle Type	Size (nm)	LSPR Peak (nm)	Sensitivity (nm/RIU)
Gold Nanospheres	50	530	60
Silver Nanospheres	60	435	160
Gold Nanocube	44	538	83
Silver Nanocube	30	510	146

Source: Adapted from (56).

Although, when solvents have different functional groups, the relationship becomes non-linear. This non-linear response can be attributed due to interactions between the particle surface and functional groups. The factor that influence the sensitivity due to change in RI of the surrounding medium can be determined by the properties of dielectric constant of the local materials as well as plasmon peak shift.[70] In fact, the metallic dielectric function can be perturbed by the oxide layers on the surface of metallic NPs.[71]

2.3 Parameters Analytically Measure Plasmonic Sensors Efficiency

This section briefly describes the factors that can quantitatively analyze the efficacy of LSPR based sensor e. g. Bulk Sensitivity η_b , Figure of Merit (FoM) and molecular sensing.

2.3.1 Bulk Sensitivity

When metallic nanoparticle surface interacts with the solvent or substrate as a result of this interaction, the dielectric constant or refractive index change near the particle-solvent or particle-

substrate interface. A parameter that correlates the shift in LSPR peak '$\Delta\lambda_{LSPR}$' and change in refractive index 'Δn_m' of the medium under probe is termed as Bulk sensitivity (η_b), this effect can be expressed as:

$$\eta_b = \frac{\Delta\lambda_{LSPR}}{\Delta n_m} \tag{1.13}$$

With its unit nm/RIU or eV/RIU.[72] The sensitivity η_b (nm/RIU) can also be defined as the slope of a linear fit. [73]

Figure 10 - Refractive index sensitivity plots for Ag nanoparticle dispersed in water and immobilized on glass substrate.

.

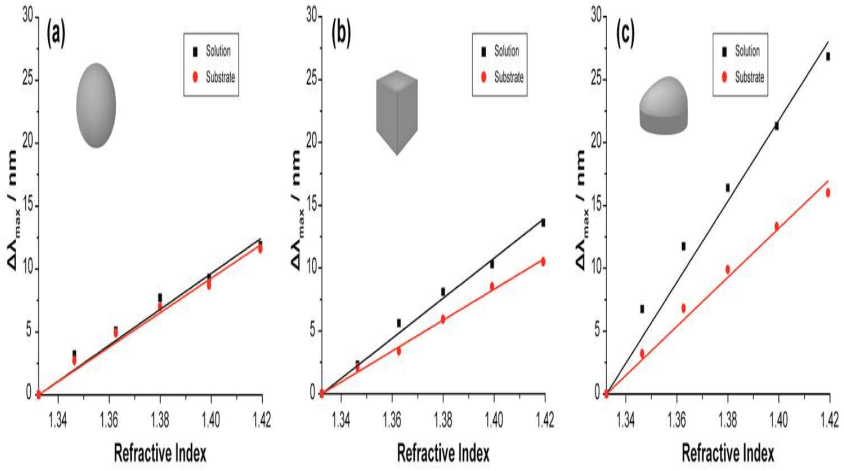

Source: Adapted from (73).

Note: (a) Ag nanosphere (b) Ag nanocube and (c) Ag nanoplate.

Miller et al analytically investigated the sensitivity for various shapes and structures of AuNPs, in frequency range where the plasmonic peak linearly varies to the real part of metallic dielectric constant while change in imaginary part was minor.

According to this study, 'η_b' linearly increases with respect to the real part of dielectric constant of the metallic NPs as a function of 'λ_{LSPR}' regardless of their structure and properties of the NPs.[74] Furthermore, the influence of the substrate, dielectric constant and extent of the radiation

damping also play a critical role in 'η_b'.[75] For instance, Martinsson et al had investigated the sensitivity 'η_b' of Ag NPs of different shapes (nanosphere, nanocube and nanoplate) dispersed in water and immobilized on a solid support theoretically and experimentally. They proposed a strong correlation between NPs surface area in contact with substrate and found that as a result of immobilization of Ag NPs on solid media will decrease the RI based sensitivity. Based on their findings the shape dependent sensitivity η_b increases as, $\eta_{plate} > \eta_{cube} > \eta_{sphere}$.[73]

2.3.2 Figure of Merit

LSPR sensing depends on plasmonic peak shift and the precision in sensing can be obtained by the variations of RI of the surrounding medium that affect the sensitivity and Full width at half maximum (FWHM) of the peak as depicted in Table 2.[56] Larger NPs show tendency to have larger sensitivity but their peaks are broad due to radiative damping and multipolar excitations.[76] Hence, we define a dimensionless parameter termed as Figure of merit (FoM), to directly compare the overall performance of single nanoparticles as chemical sensors that can be described as the ratio of sensitivity η_b and FWHM of LSPR peaks as overall refractive index sensitivity also depends on the FWHM.[41]

$$FoM = \frac{\eta_b}{FWHM} \tag{2.14}$$

Moreover, it has been reported that FWHM consistently increase with the increase of RI of surrounding medium.[77] Borja et al have studied surface and bulk sensitivities to reveal the fact that FoM are equivalent in wavelength and energy scales for both cases.[78]

Table 2 - Different Nanostructures and respective Figure of merit (FoM), Bulk Sensitivity (η_b)

Particle	Type	λ_{Peak}		Δλ		Shift/RIU		FOM
		nm	eV	nm	eV	nm	eV	
Au Branches	Ensemble	1141	1.09	879	0.983	703	0.415	0.8
Au/Sio$_2$ Shell	Ensemble	770	1.61	350	0.732	314	0.657	0.9
Au/AuS Shell	Ensemble	700	1.77	400	1.01	409	1.04	1.0
Au nanorice	Ensemble	1600	0.775	600	0.291	801	0.388	1.3
Au nanorod	Ensemble	720	1.72	125	0.301	170	0.327	1.3
Au Sphere	Ensemble	530	2.34	60	0.265	090	0.397	1.5
Au/AuS Shell	Single	660	1.88	77	0.220	117	0.333	1.5
Ag Cube	Single	510	2.43	91	0.433	146	0.695	1.6
Ag NSL	Ensemble	564	2.20	104	0.405	191	0.745	1.8
AU Star	Single	675	184	125	0.340	238	0.649	1.9
Au Pyramid	Single	680	1.82	114	0.310	221	0.450	2.2
Au Sphere	Single	520	2.38	73	0.335	160	0.734	2.2
Au Crescent	Ensemble	1795	0.69	209	0.080	596	0.190	2.4
Au Rattle	Single	570	2.18	52	0.198	199	0.568	3.8
Au Triangle	Single	760	1.63	80	0.172	350	0.751	4.4
Au Bipyramid	Ensemble	681	1.82	52	0.140	352	0.620	4.5
Ag Cube-Sub	Single	430	2.88	22	0.146	118	0.792	5.4

Source: Adapted from (56).

2.3.3 Affect of Analyte Attachment

The plasmonic response of metal NPs shifts upon refractive index changes of surrounding medium through the binding/attachment of analytes to the NPs surface. In principle, the main advantage of utilizing nanoscopic particles for sensors as an alternative of metal films is their extremely small size which allows one to measure analytes in volumes down to attoliters.[79] The interaction of nanoparticle with the substrate, plasmon length, volume of analyte and surface roughness play a significant role in order to tune the plasmonic spectra of NPs.[80-82] Furthermore, sensitivity due to molecular binding decreases exponentially as the distance between the biomolecule and the NPs increases.[83] Figure 11 shows comparison of the Bulk refractive index sensing and molecular sensing by LSPR. In case of Figure 11 (a), the change to the particle's dielectric environment is confined to the sensing volume.

Figure 11 - Bulk and Molecular sensing

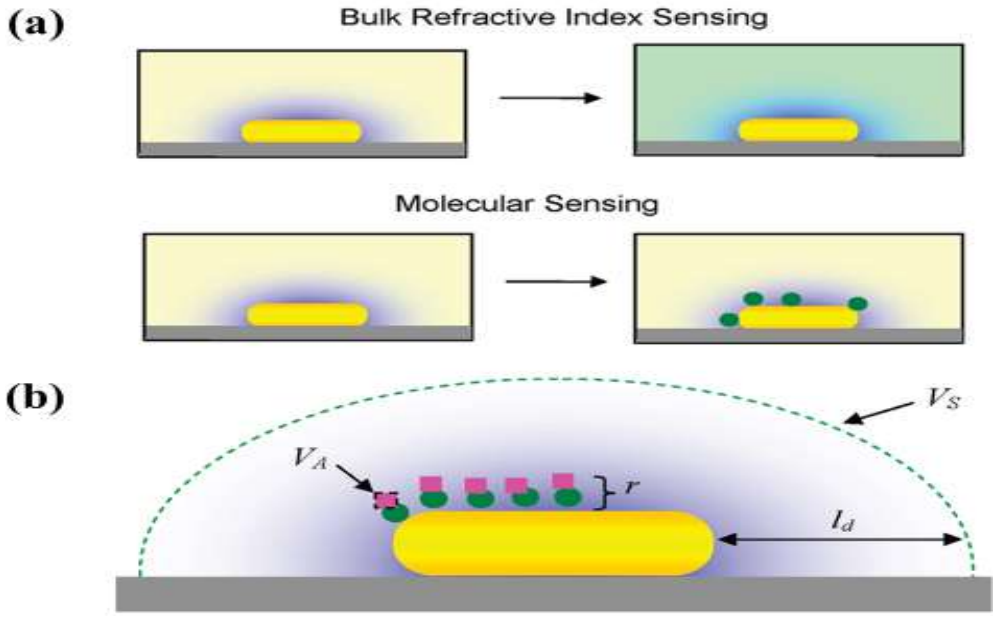

Source: Adapted from (56).

Note - (a) Bulk Refractive index Vs Molecular sensitivity (b) Schematic geometry of Analyte binding with single Au nanorod.

Here in Figure 11 (b) different geometric parameters are given which are very effective for plasmon spectra as a result of biomolecular binding e.g. V_s is total sensing volume, V_A is the volume of the analyte, l_d is the EM field decay length in cubic nm and r is the distance from the particle surface to where the analyte binds. These parameters can describe the maximum shift in the peak position of LSPR spectra for molecular sensing. The plasmonic wavelength shift, either with effective thickness of adsorbed molecular layer (surface sensitivity) or surrounding medium (bulk sensitivity) due to adsorption on a metallic NP surface, can be expressed mathematically by the Campbell's model as.[84]

$$\Delta\lambda = \eta_b(n_{ads} - n_m)(1 - e^{-\frac{2d}{l_d}}) \tag{2.25}$$

Where η_b denotes the bulk sensitivity, n_{ads} is the RI of adsorbate layer, n_m is the RI of surrounding medium and d is the effective thickness of adsorbate layer in nm.[83] Comparison of biological molecules with detection limit using various structures of Au or Ag are presented in Table 3. The shift in LSPR peak decreases exponentially with respect to increase in distance as a result of the decrease of EM field which dependents on size and anisotropy of NPs.[57] It has been reported that LSPR peak response is not too sensitive if the distance of analyte to NP surface is greater than 40 to 50 nm.[85]

Table 3 - Comparison of biological molecules with detection limit using various structures of Au or Ag.

Nanostructures	Biological Molecules	Detection Limit
Au NPs	IgG	0.1 nM
Ag plates	Anti-ADDL	50 nM
Au NPs	Streptavidin	0.05 µM
Au NPs	Streptavidin	16 nM
Ag triangles	Streptavidin	1.0pM
Au nanorod	Streptavidin	19 nM in serum
Au nanorod	IgG	200 nM
Au nanorods	Anti-rabbit IgG	10.0nM
Au NPs	BSA	0.01 µM
Au@SiO_2	Mellitin	10 nM
Single Au NP	Streptavidin	50 µM
Single Au nanorod	Streptavidin	1.0nM

Source: Adapted from (38).

2.4 Biosensor

The development of bioanalytical devices has gained space and collaborated in the elucidation of biochemical and biological phenomena on a particular analyte of clinical, pharmaceutical or environmental importance. The pioneering study of CLARK & LYONS (1962) in the determination of glucose, through a system of sensing, opens the first perspective in the development of biosensors offering a potential alternative to traditional systems.

In recent years, the biosensor industry has been witnessing major advances in incorporation of these devices into clinical and non-clinical applications. According to research, the biosensor market was valued at US 30.82 billion $ in 2018 and is expected to reach US 85.98 billion $ by the end of 2024. The increased demand for these diagnoses' tests, especially in the form of prompt are the main drivers of market growth due to threesome diseases such as diabetes, aging of the population and the need to improvement of the current health infrastructure. Biosensors are analytical devices capable of converting physical-chemical, such as chemical transformations, heat release, electron transfer, biological interactions (enzyme-substrate / antigen-antibody) in an analytical, quantitative or semi-quantitative. Basically, the biosensor consists of three integrated parts: the element, a transducer and signal processing system [86-87] and can be seen in Figure 12.

Figure 12 - Schematic diagram of a biosensing system.

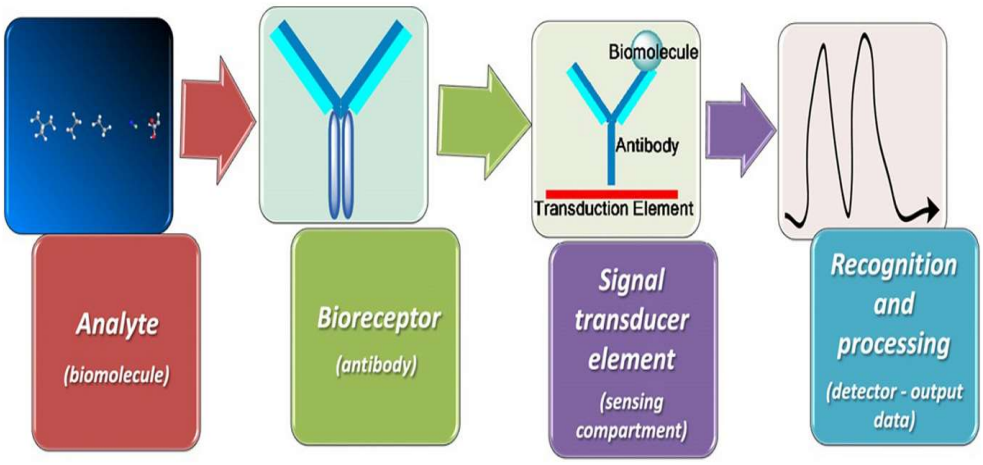

Source: Adapted from (62).

The biological recognition element (bioreactor, a biologically active component,) is linked in a specific way to the analyte on a sensing surface, generating a change in one or more physical-chemical parameters such as, enzyme, antibody, DNA fragment, organelle, cell or even a microorganism.[88] The interaction can produce ions, electrons, light and heat. Thus, the receiver is responsible for the recognition of the analyte and also for the specificity and sensitivity of the biosensor. The transducer is the element that perceives the changes caused by the interaction between the receptor and its analyte and converts them into an analytically measurable signal. This signal is converted and amplified by transducer element in an electrical signal whose magnitude is proportional to the concentration of the analyte of interest. The data is processed by software and converted into a significant parameter.[89] Different transducers can be used in biosensors and their selection depend on the biological component immobilized on the sensing surface and the properties of each sample of interest. According to the energy principle involved, the transducers in biosensors can be classified as acoustic or piezoelectric, optical and electrochemical.[90]

Acoustic transducers detect variations of acoustic wave frequencies generated by piezoelectric crystals in response to the biomolecule-analyte interaction. In this type of transduction, the piezoelectric crystal is subjected to an alternating electric field that modifies the vibrational state of the crystal, generating a measurable acoustic wave, behaving as a microbalance for the detection of the biomolecule-analyte interaction. At variations in the frequency of acoustic waves are then proportional to the amount of material adsorbed in the bi-recognition event.[87,89]

Optical transducers are based on variations in response to light stimuli as a consequence of the interaction of the analyte of interest with the biological element. According to the detection mechanism, the quantification of the analyte in this type of transduction is performed through measurements of the refractive index, amount of light absorbed, fluorescent and phosphorescent properties. A variety of optical systems have been used in these types of transduction, such as different types of spectroscopies (fluorescence, Raman), interferometry and surface plasmon resonance systems (SPR).[91; 92]

Electrochemical transducers have stood out among the most employed in biosensors. The principle of this transduction system is based on the measurement of variations of an electric

property resulting from the analyte-bioreceptor interaction. According to the exploited electrical property, the electrochemical detection can be (1) amperometric, by measuring the electric current produced by movement of species on the sensing surface when the system is subjected to a controlled potential; (ii) potentiometric, by measuring the potential difference due to accumulation or depletion of ion at the sensor interface submitted to a source of constant current or zero current;(iii) conductimetric, measuring changes in the conductance of the resulting electrode surface of catalytic reaction products; or (iv) impedimetric, measuring changes in the impedance due to a sinusoidal current or potential surface sensing.[93] Different biological molecules can be used as bioreactors in biosensors, subdividing these according to the type of biochemical interaction involved in the recognition of the analyte. Catalytic biosensors use electroactive enzymes such as element of recognition, being characterized by measuring products resulting from the enzymatic bioactivity in the presence of its specific substrate. [90] The affinity biosensors are based on the formation of complexes between the substrate and the receptor.

Among the bio affinity systems, antigen-antibody interactions, lectin-carbohydrate and hybridization between single-stranded nucleic acid sequences.[87,94] Electrochemical biosensors measure the electrical changes of the medium according to properties such as current, potential, conductivity, electrical resistance among others. To capture the signal and convert it into an electrical signal, the bioreceptors element is fixed on a conducting surface, called the electrode. Electrodes in general, consist of inert metals for example, gold, carbon, glassy carbon, ITO (indium doped tin oxide), platinum, steel stainless etc. Before immobilization of the analytes, these electrodes can be modified with conductive polymers or in combination with nanomaterials that help to increase conductivity such as carbon nanotubes, graphene and gold nanoparticles. ([95-97])

In case of modification of electrode surfaces, the conjugated polymers (those alternating single-sigma- and double-sigma- and pi- chemical bonds throughout their chain) have attracted interest for use as matrices where the biomolecules will be immobilized; serve as intermediates in receptor-to-analyte binding, in addition to improving response time, sensitivity and limit of detection. Another advantage of these polymers is the possibility of their electrochemical synthesis allowing an immobilization of biomolecules on the modified surface of the electrode.

Relatively, it becomes possible to control of the spatial distribution of the immobilized material, film thickness and biomolecule activity. Thus, the development of any type of technology in this field knowledge is dependent on understanding the interactions at the molecular level between species and the polymer matrix.[98] Among the many characteristics that favor the use of a biosensor are: the most specificity, high sensitivity, responsiveness leading to short-time analysis, integration in integrated systems, ease of automation, work in real time, versatility and low cost.

2.4.1 Immunosensor

Immunoassay-based methods are usually used for the detection of pathogens in food, diseases caused by viruses, bacteria and pollutants in the water intended for consumption. The immunoassay diagnoses the ability of an antibody to bind chemically and specifically to a single molecule or a very limited group of molecules, called antigen. In an immunoassay, the highly specific antigen-antibody binding is sensitive, is used for the detection of proteins, viruses, bacteria among other substances, present in a fluid sample (blood, saliva, aqueous solution, among others). In this sense, the antibody or virus antigen, bacterium etc., is immobilized and the antigen or antibody to be detected is immersed or comes in contact and a non-covalent bond occurs. Using this the presence or absence of the analyte and the amount (mass or concentration) of the analyte may be measured.[99] When the specificity of molecular recognition of the analyte of interest (between antigens and antibodies) is given by the formation of stable immunocomplexes, this kind of biosensor is called an immunosensor. The antibodies belong to a family of glycoproteins, called immunoglobulins (Ig), responsible for triggering the specific immune defense mechanism in response to the presence of a given antigen. There are five distinct classes/groups of glycoproteins (IgA, IgG, IgM, IgD and IgE), with IgG being the most abundant class/group (approximately 70%) and more frequently used in immune analytic techniques. [100]
The basic structure of IgG composed of two identical heavy polypeptide chains (5575 kDa), linked/connected together by disulfide bridges (-S-S-), and two light polypeptide chains (25 kDa), which form a characteristic structure in Y shape/pattern as depicted in Figure 13.[101]

Figure 13 - Schematic Structure of an antibody.

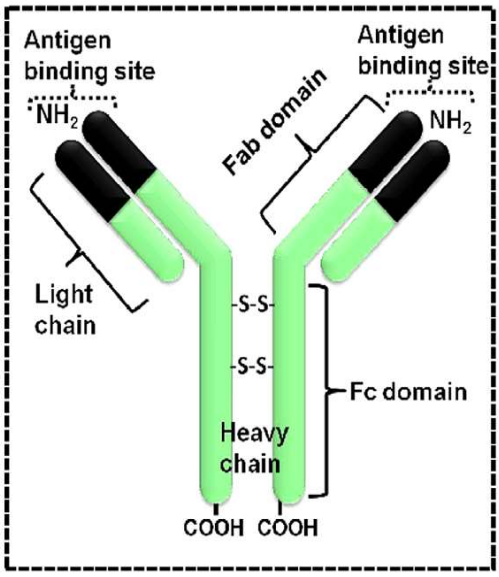

Source: Adapted from. (102).

The amino-terminal portion, located at the top of the Y-frame, is the sites of antigen-binding fragments. This region is called the paratopo and have specific amino acid variable sequences for a particular portion of the antigen, called the epitope, thus determining its specificity. Already in the carboxy-terminal portion is the constant fraction of Ig, responsible for the regulation of the immune response.[103] In general, the antibodies have high molecular weight and mean diameter of 10 to 40 nm.[101] Electrochemical transducers, especially ampere metric, have been development of immuno-sensors for clinical diagnosis, due to its high sensitivity, low cost and compatibility with micro-manufacturing technologies. The principle of signal transduction in ampere metric sensors is based on the measurement of an electric current that is directly proportional to the concentration of the species of interest (analyte).[104] During ampere metric measures, a constant potential is maintained between the working electrode (WE) and the reference electrode (RE). The current generated by processes of oxidation and reduction of species on the surface of the working electrode is measured and generated signal is directly proportional to the concentration of the electroactive species. The antibody-antigen interaction is

monitored by small physical/chemical changes, involving hydrogen bonds, hydrophobic forces, electrostatic forces and van der Waals forces. [105]

Regarding the type of response desired, the immunosensors are classified into marked and unmarked. The labeled immunosensors described in the literature exploit the principle of competitive enzyme and sandwich immunoassays utilize enzymes, fluorophores and nanoparticles as markers. Although selective, this method implies high operational costs, including increased sample processing steps.[106] In label-free assays the immunosensor response is obtained directly after the bio reacquisition event. In this type of assay, the antigen-antibody interaction on the sensing surface can be obtained by monitoring changes in physical properties, such as the refractive index in SPR systems [92], mass changes in piezoelectric transducers using a quartz crystal microbalance [107] and electrical properties in electrochemical transducers. In particular, electrochemical transducers have been development of immune suppressors free of marking, due to their high sensitivity, low cost and compatibility with sensor microfabrication technologies.

2.4.2 Antibody immobilization

It is a critical aspect to choose antibody immobilization method in the development of immunosensors, since maintaining antigen recognition and antibody specificity may directly influence sensitivity of the device. As shown in Figure 14, the layout of the antigenic sites properties on the sensor surface clearly shows how the orientation affects the surface of immobilized antibodies and the bio reactuation interaction. The random immobilization of the antibodies makes it difficult to adequately expose the antigenic sites, antigen-antibody interaction on the sensing surface. [108]

Figure 14 - Schematic depiction of random immobilization of antigen on the sensing surface.

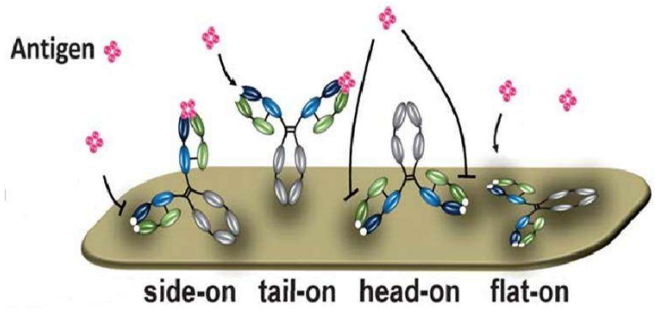

Source: Adapted from (108).

Among the several immobilization protocols, some are described and are used in the construction of immuno-sensors e.g. adsorption, covalent bonding, encapsulation, crosslinking or electrostatic interaction. Adsorption, whether physical or chemical, is a simple method that requires little preparation; through.[109,110] However, in non-covalent immobilization of antibodies by physical adsorption explores mainly weak bonds, such as ionic bonds, electrostatic, hydrophobic and van der Waals interactions. Although quite traditional due to the simplicity, the physical adsorption method allows low control over the conformation of the molecule on the sensing surface. In addition, the interaction forces are susceptible to variation in pH, ions and temperature. [110]

Already encapsulation, the biomolecule to be immobilized is surrounded by a membrane that prevents it from contamination and deterioration as well as can protect against changes in temperature, pH, ionic chemical composition. Another variant of this process may be the encapsulation in an array which may hinder the diffusion of the analyte and cause loss of functionality. This will certainly affect the qualities of the biosensor. Another possibility is the immobilization of biomolecules in nanostructures of conjugated polymers, which, elaborated by several routes chemical and physical properties, may aid in the control of the hybrid-polymer interface / biological element molecular level.

To achieve a better presentation of the recognition element for the analyte, the use of ordered layers on the electrode surface has been introduced. In this case, the most commonly used electrode material is gold (either as a printed/traditional), which allows the formation of self-assembled monolayers (SAMs), through the thiol-gold in a very reproducible and orderly manner. Antibodies immobilized by covalent binding is the stable method of bio functionalization on immunosensor surfaces. According to this method, utilization of mutually reactive chemicals results in a more precise control of antibody on the sensing surface. Most of the study in literature explore the activity of functional groups present on the amino acid chains of the antibody, such as Thiol (-SH), Amino ($-NH_2$), Hydroxylic (-OH) and Carboxylic (-COOH) groups. In Particularly, carboxylic groups present in the Fc (Crystallizable fragment of immunoglobulin) portion of the antibody can be used strategically for specific and targeted covalent site immobilization. The carboxylic groups acids may react with amino functionalized surfaces when previously activated with N-Ethyl-N'-3-Dimethylaminopropyl Carbodiimide (EDC) and N-Hydroxy Succinimide (NHS) due to amide bonds formation.[111] The resulting monolayer is well orientated on the surface of the electrode and a better antibody - antigen binding. [112]

In this reaction, EDC reacts with the carboxyl group to form a reactive ester (Esters are fairly reactive because of electrophilicity of the C=O carbon and due to its capacity to stabilize alpha enolate anions), o -acryl isourene. However, the reaction of this compound with the amino groups (are excellent nucleophiles that may react with esters yielding amides) on the sensing surface is slow and coupling does not occur. Thus, the NHS provides increased reaction yield through the nucleophilic attack forming a highly reactive ester intermediate, and consequent formation of a stable amide bond between the antibody and the sensor surface. The EDC / NHS reaction is pH-dependent to maximize the electrostatic forces between biomolecule and the negative charge of the carboxylic groups. [113,114]

2.4.3 Sensors based on conductive polymers

The word polymer originates from the Greek word poly (many) meros (parts). They are macromolecules which are bounded together by the repetition of a large number of similar chemical units (monomers). For instance, Proteins (natural polymers) have polypeptide molecules linked with various amino acid monomer units and resins, plastics (synthetic organic materials) etc. The polymers molar mass can be of the order of thousands (atomic mass unit) amu. [115] Traditionally, polymers were developed as an insulator and any electrical conduction was normally considered as an undesirable phenomenon caused by loosely bound protons. The most prominent feature of conducting polymers is their inherent electrical conductivity which is closely associate with charge transfer rate and electrochemical redox efficiency. Conductivity is a key parameter for many applications particularly in the field of sensors and electroanalytical chemistry. Conductive polymers show interesting electrical and optical properties. [116] They can be divided into two classes based on their mode of conduction: Electron conducting polymers (ECP) and Proton conducting polymers (PCP). [117]

For the preparation of films many materials e.g., characterized by their structural complexity and functional diversity, can be used to deposited on the surface of the electrodes which serve as basis for the anchoring of biomolecules. Electronically conducting polymers (ECP) are utilized in sensor technologies for electrode modification in order to enhance and impart selectivity, to suppress interference and to support as a matrix for sensor molecules. All electrochemical transducer principles can be realized with ECP modified electrodes. The role of the conducting polymer may be active e.g., as a catalytic layer, redox mediator, switch, or as a chemical modulated resistor or passive e.g., as matrix. [118]

ECP have a conjugated chain structure consists of extended π- bond system which leads to the formation of broad valence and conduction bands. Typical examples are polyacetylene, polypyrrole, polythiophene and polyaniline and they can be synthesis by chemically or electrochemically.[118] In the field of electrochemical sensors, their use seems to be very promising because they allow the enhancement of speed, sensitivity and versatility. For sensor construction, electroactive polymers seem to have the best qualities for sensor construction

among all types of conjugated polymers. [119] Furthermore, due to high conductivity they can act as electron donors or acceptors, exhibiting electrocatalytic effects and the possibility of redox mediation.

This type of polymers are being utilized as fuel cells, electrochemical capacitors, batteries, memory devices, electrochromic devices, electrochemical actuators, field emission devices, superhydrophobic coatings and biosensors.[120,121] PCP shows a cation or proton conductivity along the polymer backbone due to the presence of carboxylated or sulfonated groups with a cationic counter ion, whose mobility can be increased by water swelling. For this feature, they present low electrical resistance due to increasing ion exchange capacity, decreasing membrane thickness and water content, high permed selectivity for anions and nonionized molecules as well as good mechanical and chemical stability over long periods. [117] Their properties depend on many factors such as the chemical nature of the polymer-backbone, molecular weight and its distribution in the polymer, the nature of the solvent used for casting and the possible presence of residual solvent in the polymeric film. [122] These polymers find applications in cell separators, effluent treatment, recycling and energy production in fuel cells.[117][123][124] A brief analytical figure of merit of electrochemical sensors based on nanostructured polymer are given in table 4.

Table 4 - Comparison of electrochemical sensors based on polymers.

Ploymers	Modified Electrode	Analyte	Detection Method	Detection Limit (µM)	Sample
2-amino-1,3,4-thiadiazole	p-ATD/GCE	AA	DPV	2.01	Human urine
		DA		0.33	
		UA		0.19	
		XN		0.59	
PEDOT	Graphene-PEDOT/AO/GCE	AA	Amperometry	2	Commercial juices
PEDOT	PEDOT/AG/GCE	Paracetamol	Amperometry	0.041	Pharmaceutical samples
5-amino-2-mercapto-1,3,4-thiadiazole	GCE/OD/FMWCNTs/p-AMT	Rutin	Amperometry	0.0003	Pharmaceutical samples

Source: Adapted from (125).

Treatment with sulfuric acid vapor reduces the Coulomb interaction between the PEDOT and poly (styrensulfonate) (PSS) chains. This results in giving rise to a structural rearrangement between the PEDOT and the PSS chains, which in turn an increase in the power factor of PEDOT:PSS.[126] Electroactive polymers can be connected with other conductive polymers, for instance poly(3,4-ethylenedioxythiophene) (PEDOT) to enhance electrode performance. In particular, PEDOT shows high conductivity, moderate band gap, low oxidation potential, high chemical stability (in aqueous solutions) and a good biocompatibility with biological media[127][128], which allows its application in the field of supercapacitors and electrochemistry. PEDOT can be used alone [129], in combination with electroactive polymers to obtain composites with improved properties [130][131], or in combination with nanoparticles [132] to improve the efficiency of various types of sensors.

3 MATERIALS AND METHODS

Different techniques to investigate the performance of LSPR and Electrochemical biosensors are briefly described in this chapter.

3.1 UV-Vis Spectroscopy

The UV-Vis spectroscopy was used to analyze the samples in aqueous medium to obtain the LSPR extinction spectrum, from 400–850 nm, using Ocean Optics spectrophotometer (HR +4000) and placing the samples in quartz cuvettes of 1 cm width. Fiber bundles were used to guide light from a Halogen–Deuterium light source to the sample and to send light from sample to the spectrophotometer.

A spectrophotometer is usually considered as an instrument to measure absorbance or transmittance of the sample as a function of wavelength of EM radiation. The key components of the UV-Vis spectroscopy are as light source that produces broad band of EM radiation, dispersion device that is used to select from broad bond of the light source, a simple area and one or more detectors to detect light intensity as shown in Figure 15. The light source that is used here is deuterium lamp. The deuterium light source is considered to yield a good intensity continuum in UV as well as visible region. The light source should be normally switched on twenty minutes to make it stabilized before starting the experiment.

Figure 15 - Components of UV-Vis spectrophotometer.

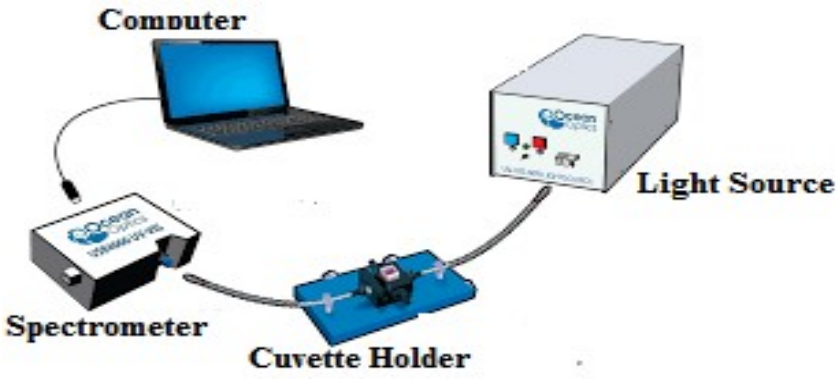

Source: Adapted from (47).

The beam of light is collected from the light source using fiber optics and passes through the sample, for example cuvette, and collected by the second fiber and directed to the spectrometer. The light that enters to the spectrometer after passing the sample and spectrometer analyze the intensity of the transmitted light to the incident intensity. The reference spectra or incident intensity of the light is obtained by taking water in the cuvette and compares this with the transmitted intensity after replacing water with colloidal solutions of Au or Ag. The extinction coefficient of metallic nanostructures is calculated by Beer's Law. If I_0 and I_T are incident and transmitted intensities of the light, then transmittance is given by:

$$T = \frac{I_0}{I_T} = e^{-\varepsilon bc} \tag{3.1}$$

where ε is extinction coefficient or molar absorbance, b is the path length in cm and c is the concentration of the sample. The absorbance (A) is expressed as:

$$A = -\log\frac{I_0}{I_T} = \varepsilon bc \tag{3.2}$$

This is termed as Beer's Law.

3.2 Computational Simulations

Plasmonic nanostructures strongly interact with light resulting in size-dependent scattering, absorption and intensive near field enhancement. These outstanding optical features of nanoscale particles led to remarkable interest along with their potential applications, which make them suitable candidate for their use on a large scale of miniature devices and nanophotonics applications. These optical characteristics are governed by collective coherent oscillations of free electrons that can harness the localized surface plasmon resonance (LSPR) phenomenon due to their ability by confinement of light into nanoscale spatial regions. [(132)] A plethora of studies reveal that plasmonic properties of the metallic nanostructures have been demonstrated successively and efficiently by controlling the geometry (size, shape), composition and the refractive index of their surrounding medium. [(133)(134)] Several studies discuss two significant approaches to employ electrodynamics modeling techniques: the Finite Element Method (FEM)

and the Finite Difference Time Domain(FDTD) but FEM employed as more appropriate approach in describing the plasmon peak position and field amplitude of metallic nanoparticles when area of interest is near- field optics.[135][136][137] Comsol Multiphysics with radio frequency (RF) module is numerical method based on FEM for simulation package that engages accurately and has been used extensively for studying EM field properties in vicinity of irregular nanostructures, therefore, its accuracy correspondent to analytical analysis is more appropriate for designing and characterizing such geometries. [138][139] This study had investigated the behavior of Au/Ag NPs with different geometry in 3-D space using Comsol Multiphysics 5.0. and RF module was applied to calculate Frequency-domain scattering electric field using a background oscillating field of arbitrary amplitude 1 (Vm^{-1}). A perfectly matched layer (PML) was additionally incorporated to avoid any reflection artifact during the simulation and extinction cross sections as well as normal electric field were calculated for 300–1000 nm for different wavelengths at different step size. Data required for Au/Ag for simulation and interpolation had been obtained from Johnson and Cristy.[140]

To foster the sensitivity, phenomenon of sensing utilizes the capability of metallic nanostructures to concentrate the external radiation in the vicinity of their small local entity. It has been studied that Refractive index (RI) based sensitivity and figure of merit, (defined as the ratio of sensitivity to the linewidth), depends on the geometry of the Au nanoparticles. [68][141] For single particle LSPR sensor, the fundamental principle utilizes the fact that LSPR spectrum position varies as a function of dielectric host medium.[142] Jensen and Mock et al [143] pointed out that LSPR wavelength of metallic nanoparticles shift with respect to variation in the RI of the proximity of surrounding media.

El-Sayed and coworkers have theoretically suggested that the different possible positioning between gold nanorods can dominate greatly their plasmonic behavior.[144] Several feasible adaptations in a nanostructure that exist between gold nanorods can affect the plasmon coupling but it is difficult to calibrate as well. The spectrum of LSPR excitations have been the subject of hintensive research efforts and encourage researchers to synthesize the growth of complex shapes nanostructures such as nanoshells, nanorice, nanocages, nanostars, nanorods and nanopyramids[145] which shows plasmon peaks in various spectral regions.

Moreover, gold nanostructures are increasingly receiving attention as an important starting point for label-free sensing. LSPR sensors can be explored as fast, reliable, cheap, and fairly facile tool for medical diagnosis. Pramod et al have proposed to investigate the effects of orientation factor on plasmon response, gold nanorod (AuNR) dimer are ideal candidates.[146] Firstly, Au/Ag nanoshell based on gold/silver core encapsulated by silica shell having nano scale varying thickness likewise their tune ability linked with surface plasmon resonance were theoretically investigated. Secondly, to develop an efficient LSPR sensor, an evaluation of plasmon peak shift as a function of the gold nanorod dimer, connected with silica nano-cylinder, with several aspect ratios and silica junction thickness were investigated.

To investigate which metal nanostructures is a good candidate for bio or chemical sensing applications as well as their efficiency can be characterized by measuring RI based sensitivity. In order to correlate the varying RI of the surrounding medium and peak shift of the LSPR wavelength that governs the sensing performance of LSPR sensor, an important sensing parameter to analyze the sensing efficiency has been evaluated qualitatively i.e Bulk sensitivity: $\eta_b = \Delta\lambda LSPR / \Delta n$, where $\Delta\lambda LSPR$ is change in LSPR wavelength as function of change in refractive index of the surrounding medium (Δn). Second parameter to analytically describe the sensor reliability is the Figure of Merit, FoM = η_b/FWHM, where (FWHM) is full width at half maximum or linewidth of the LSPR peak. Therefore, a LSPR sensor requires to attend simultaneously both prerequisites: a high bulk sensitivity and a fine LSPR spectrum. This condition can be depicted by a relation given as RIS×FoM which will be discussed in next chapter.

3.3 Modelling and Calculations

Firstly, the schematic geometry of Au/Ag silica coated nano shell is illustrates in Figure 16. The inner most region is attributed as core having radius and dielectric function r_1 and ϵ respectively. The second portion represents the shell with radius r_2 and dielectric function ϵ_d, where shell thickness is given by $t = r_2 - r_1$.

Figure 16 - Schematic model of the metallic core with dielectric (SiO_2) coated nanoshell

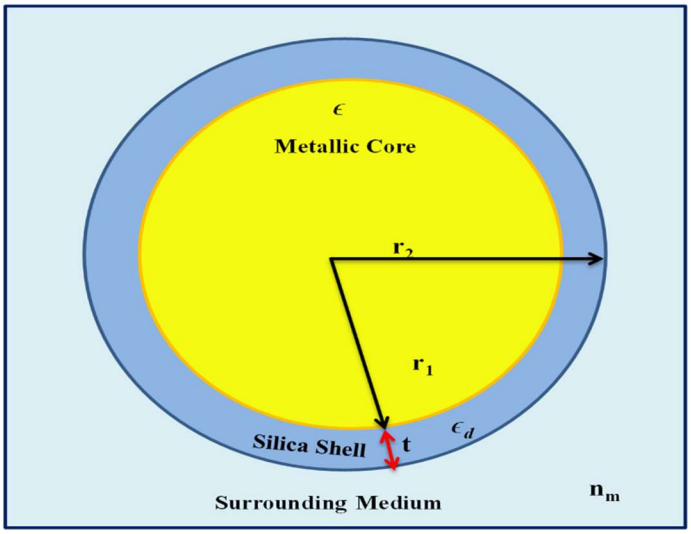

Source: The Author, 2019.

The interaction between core-shell based metallic nanostructures and electromagnetic radiation in this study was ascribed by Mie theory which elucidated well the solution of Maxwell's equation with appropriate boundary conditions. Let N be the number of particles per unit volume were contained in a dilute colloidal solution illuminated by incident light, the measured attenuation in the intensity of light I_o, for a path length I_d in cm is given by.[35]

$$M_a = \log\frac{I_0}{I_d} = NC_{ext}\,\frac{d}{2.303} \tag{3.3}$$

Where C_{ext} is extinction cross section which can be calculated by the following relation given by.[29]

$$C_{ext} = \frac{2\pi}{k^2}\,\Sigma\,(2n+1)R_e(a_n + b_n) \tag{3.4}$$

where R is the radius and k are the wave number in the surrounding medium, a_n and b_n are scattering coefficients as well as the function of radius. To determine the position of LSPR extinction spectra, the extinction cross section (C_{ext}) can be estimated after figuring out the values

of (σ_{abs}) and (σ_{sec}). From Mie theory the values for absorption and scattering can be calculated as[147]:

$$\sigma_{abs} = \frac{2\pi}{\lambda\epsilon_0} \operatorname{lm}(\alpha) \quad \text{and} \quad \sigma_{sca} = \frac{8\pi^3}{3\lambda^4\epsilon_0^2} |\alpha|^2 \tag{3.5}$$

It is obvious from eq. (3.5), both are functions of ϵ_0 and λ, therefore it is quite feasible to plot the σ_{ext} in order to get the position of Plasmon peak. In this study the silica thickness and the diameter of the core both are variable i.e. the dielectric function is size-dependent. When the dielectric function is geometrically tuneable, the effect of electron scattering can be interpreted by practicing the modified bulk collision frequency:

$$\Gamma = \Gamma_{bulk} + \frac{Av_f}{m_f} \tag{3.6}$$

Where Γ_{bulk} , mf and v_f are collision bulk frequency, electron mean free path and Fermi velocity respectively. In case of single refractive scattering and for simple Drude model, A = 1 (Averitt et al.). But customarily its value lies in between 1-5. [147] Whereas, A is a dimensionless geometrical parameter. For nanoshells, the bulk dielectric function can be modified to analyze the free electrons scattering, which is given by:

$$\epsilon\left(m_f, \omega\right) = \left(1 - \frac{\omega_{bp}^2}{\omega^2 + \iota\omega\Gamma}\right) + \epsilon(\omega)_{int} \tag{3.7}$$

Here, the second term represents the interband transitions, ω_{bp} bulk plasama frequency, m_f mean free path of reduced electrons and ϵ (m_f, ω) is metallic dielectric function (size dependent).

In second case, Finite Element Method (FEM) calculations were employed to predict the unprecedented dependence of the plasmonic properties of the gold nanorod (AuNR) dimers which are linked with a thin silica cylinder. In 3D simulations, the AuNR dimer surface was divided into small tetrahedral mesh elements with size ‘extremely fine’. The dimers were modeled as shown in Figure 17.

Figure 17 - 3D simulations model region composed of model nanostructure in embedding medium and PML layers.

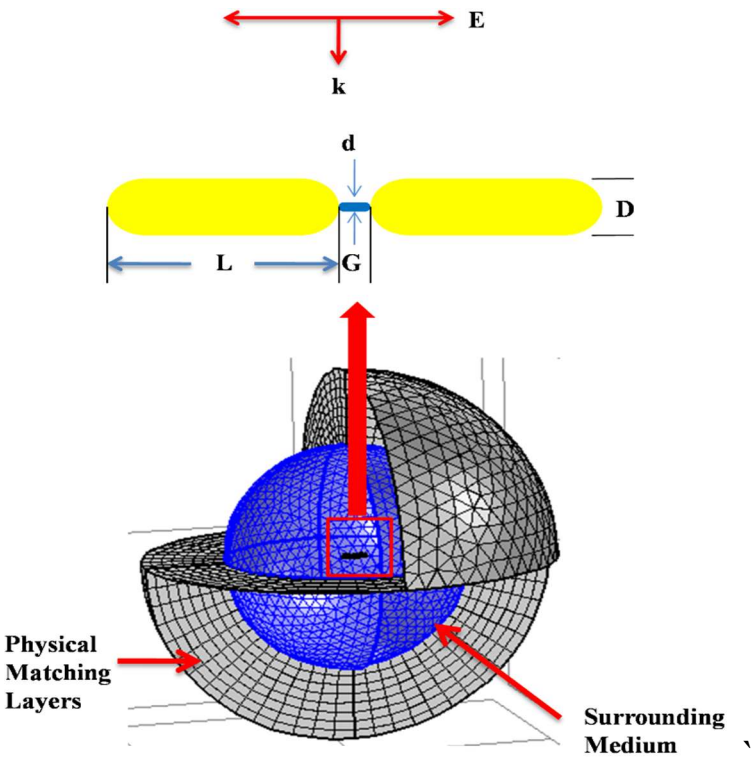

Source: The Author, 2019.

The plasmonic nanostructure consist of two hemispherically-capped cylinders forming the gold nanorod (AuNRs) dimer with length = L, diameter = D and junctioned by a silica cylinder (length = G, diameter = d). Furthermore, perfectly matched layer (PML) around the nanostructure was used to avoid any kind of reflection artifacts on the simulations. The data of the metal dielectric functions (real and imaginary) for Au were obtained from Johnson and Christy.[140]

3.3 Materials and Electrochemical Techniques

The poly (3, 4-ethylenedioxythiophene):Poly(styrene sulfonate) PEDOT:PSS, PEDOT nanoparticles, 1-ethyl-3-(3 dimethylaminopropyl) carbodiimide (EDC), N-hydroxysuccinimide (NHS), potassium ferricyanide (K_3 [Fe $(CN)_6$]), potassium ferrocyanide (K_4 [Fe $(CN)_6$]) and

ethylenediamine (EDA) were obtained from Sigma-Aldrich (USA). The level of all other chemicals used without any purification was of analytical grade and solutions were prepared in Phosphate buffered saline (10 Mm, pH = 6.5). Ultrapure water (18.2 MΩ cm) was obtained from a Milli-Q water purification system (Millipore Inc., United States).

3.3.1 Characterization of electrode surface

Electrochemical measurements were performed in a three-electrode system containing a helical platinum wire as counter electrode, Ag/ AgCl (3 M KCl Sat.) as reference and glassy carbon electrode (GCE), as working electrode. The electrochemical measurements were performed with a potentiostat/galvanostat Ivium Compact Stat (Eindhoven, Netherlands) coupled to a microcomputer and controlled by IviumSoft software. To characterize the surface modifications of the electrodes, electrochemical measurements and analytical responses were recorded by cyclic voltammetry (CV) to analyze the formation of polymers and their characterization while square wave voltammetry (SWV) was used for indirect detection of the oligonucleotides on the electrode surface respectively. CVs measurements were analyzed at 50 mVs^{-1} scan rate in a potential range between -0.1 V to 0.5 V using 5 mM [K_3 $Fe(CN)_6$] and [K_4 $Fe(CN)_6$] prepared in 100 mM KCl. The Square wave voltammetry was carried out at 10 Hz with 10 mV pulse amplitude, 10 mV step potential in a potential window from 1V to 0 V by using 5 mM [K_3 $Fe(CN)_6$] and [K_4 $Fe(CN)_6$] prepared in 100 mM KCl as redox probe. Morphological analyses of modifications on the GCE surface were carried out by means of Atomic Force Microscopy (AFM) in the noncontact mode, using the Nanosurf Flex AFM (Liestal, Switzerland) equipped with a C3000 controller and the TAP190AI-G tip. The images obtained were treated and analyzed by Gwyddion (free version 2.49). Chemical surface characterization of the platform was accomplished by attenuated total reflectance with Fourier transform infrared spectroscopy (ATR-FTIR) using the Bruker IFS 66 model FT-IR spectrometer (Billerica, USA), set up for spectra from 4000 to 500 cm^{-1}.

3.3.2 Immobilization of Chikungunya on the glassy carbon electrodes:

Prior to modifications, the glassy carbon electrode (GCE) was cleaned on a polishing cloth with 0.3, 0.05 μm alumina powder, after sonication and rinsed washed with ultra-pure water. The GCE was drop casted with 4 μL of PEDOT@EDA solution previously dispersed in EDA (0.5%) was pipetted onto the electrode surface and dried at room temperature overnight. Then a mixture of 20 mM EDC and 50 mM NHS solution [1:1] prepared in 0.1M sodium acetate buffer, pH = 5.5), combined together with anti-Chikungunya (5 μgmL^{-1}) in phosphate buffer saline (10 Mm, pH = 6.5) in order to activate the carboxyl groups of anti- CHIK. Subsequently, an aliquot (4 μL) of carboxyl activated anti- CHIK was pipetted onto the GCE surface and incubated for 50 min at 4 °C to obtain the activate anti- CHIK/ PEDOT@EDA /GCE, followed by washing with Phosphate buffer saline/PBS (pH = 6.5) to remove the physically adsorbed proteins. The carboxyl activated anti- CHIK/ PEDOT@EDA /GCE was incubated with 4μL of carboxyl activated CHIK (1μg mL^{-1}) solution for 60 min at 4 °C, followed by washing with PBS (pH = 6.5). Furthermore, activated CHIK/activated anti-CHIK/ PEDOT@EDA /GCE was incubated with 4 μL of PEDOT@EDA -NPs+ activated anti-CHIK (0.5 μgmL^{-1}) solution for 10 min at 24°C, followed by washing with PBS (pH = 6.5) to remove unbound PEDOT@EDA-NPs. The anti-CHIK/PEDOT@EDA-NPs/activatedCHIK/activatedanti-CHIK/PEDOT@EDA/GCE (sandwich-type electrochemical immunosensor) was finally obtained.

3.3.3 Electrochemical Cell

Electrochemistry evaluates an interrelationship between physical and chemical phenomena e. g., the transfer of electrons that can occur homogeneously in a solution or heterogeneously on the surface of the electrode, making it possible to establish direct link between analyte concentration and some electrical properties such as current, electric charge, potential, conductivity and resistance. The evaluation of these parameters is easily accessible via experimentally so the electrochemical techniques are suitable for the quantification of species of interest in different areas of study. [148]

Figure 18 - Schematic representation of an electrochemical cell.

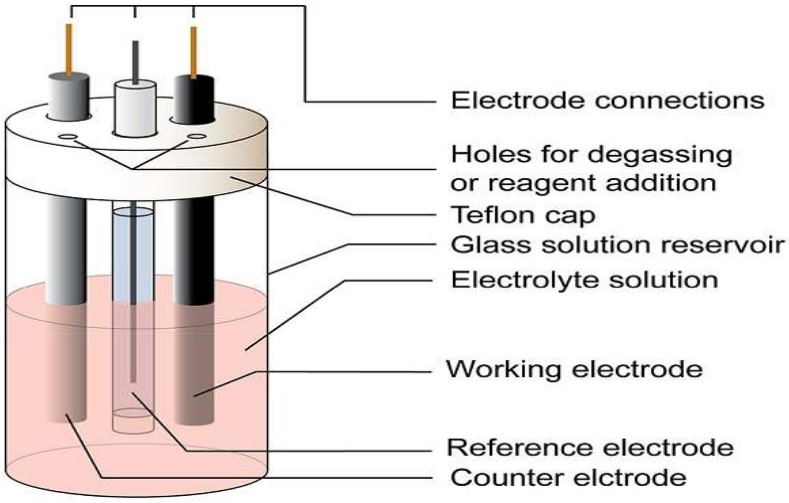

Source: Adapted from (149).

In general, different electrochemical techniques use a system composed of an electrochemical cell consisting of three electrodes for data acquisition: A working electrode, where the electrochemical processes of interest occur, A reference electrode (silver / silver chloride - Ag / AgCl or saturated calomel - Hg_2Cl_2 / Hg) which is a potential alternative to the working electrode and an auxiliary electrode/ Counter electrode (platinum wire) used for the discharge of over potency without working electrode as depicted in Figure 18. These electrodes are connected to a potentiostat and immersed in a cell containing the solution of the electroactive species with an excess of one inert electrolyte/ supportive electrolyte, responsible for ensuring the diffusional control of species. The information on the analyte is obtained by measuring the magnitude of the electrical current between the working electrode and the counter electrode due to applied potential between the working electrode and the reference electrode.[150] Among electrochemical techniques, cyclic voltammetry (CV) and square wave voltammetry (SWV) are the most suitable for characterization of biosensing platforms as they allow to follow different stages of modification on the electrode surface as a function of the various electrical parameters (current density, capacitance, resistance etc).

3.3.4 Cyclic Voltammetry (CV)

Voltammetry comprises a group of electroanalytical techniques in which the analyte information is measured by analyzing current variations in response of oxidation and reduction reactions resulting from applied potential. In this process, a capacitive current is generated, corresponding to the double layer of the electrode after application of the potential, which decays rapidly. In addition, faradic currents can be measured by the transfer of charge during redox reactions on the sensing surface. This process is in accordance with Faraday's law, which determines that the number of reagents formed/consumed on the surface of the electrode is proportional to the current.[151][152] Although CV technique is used in quantitative analysis as well to obtain information about electrochemical processes, such as redox reactions, detection of reaction intermediates, observation and monitoring of reactions involving products formed on the electrodes etc. The current is obtained when the working electrode is subjected to a triangular wave of potential which is linearly varied over time starting from an initial value and end to final values assigned. During the scanning of the potential, the potentiostat registers the current that is generated in response of the applied potential.

Figure 19 - Graphical representation of the CV technique.

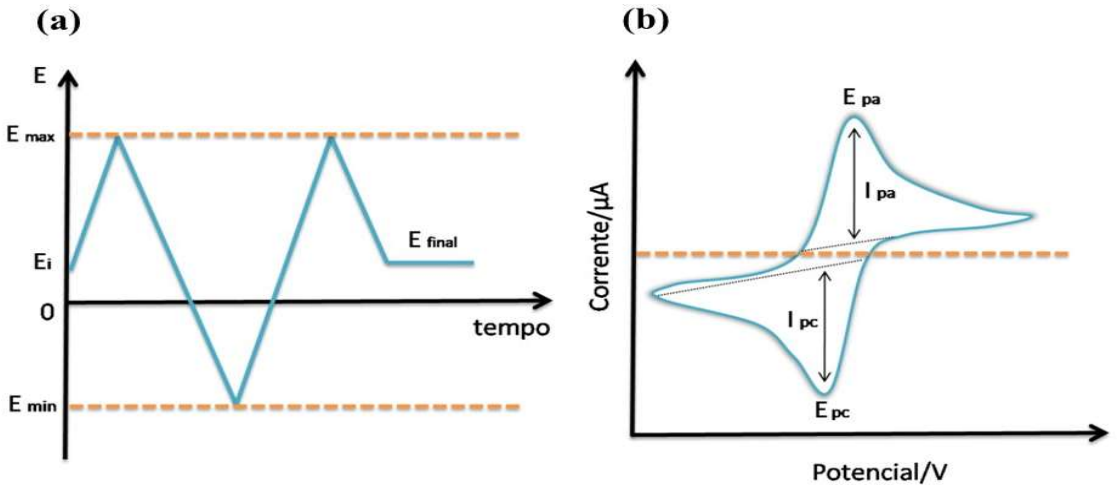

Source: Adapted from (151).
Note: (a) linear variation of potential vs. time (b) cyclic voltammogram indicating the main parameters to be analyzed.

A response to this disturbance is obtained by a pair of recorded cathodic and anode peaks in a voltammetric curve, denominated cyclic voltammogram, in which it is related to current variation (y-axis) Vs the potential variation (x-axis). In this way, a current graph is generated as a function of the potential variation known as cyclic voltammogram as can be seen in Figure 19. In the cyclic voltammogram, the main parameters analyzed are cathodic peak potentials (E_{pc}), anodic peak potentials (E_{pa}), cathodic (I_{pc}) and anodic (I_{pa}) peak currents. These data provide important information regarding the reversibility of electronic transfer. For a reversible reaction, a reaction that occurs with velocity high enough to establish a dynamic balance in the sensor interface, the I_{pa} and I_{pc} linearly vary with the square root of the sweep velocity of potential. In this system, the generated products can be oxidized or reduced on the electrode surface, resulting in cathodic and anodic peaks at symmetrical potentials respectively. Other criteria adopted for the determination of a reversible system are: the ratio between I_{pa} and I_{pc} and the non-variation of the peak potentials (E_{pa}/E_{pc}) relative to the speed.[153] Randles (1948) was the first who gave the theoretical analysis of a reversible system, according to which it is possible to obtain the peak current (Ip) as indicated in the following equation:

$$I_p = (2{,}26.10^5) n^{2/3} A D_0^{1/2} v^{1/2} C_0 \quad (3.8)$$

where n is the number of electrons involved in the process, A is the area of the electrode (cm^2), D_0 is the diffusion coefficient ($cm^2\ s^{-1}$), C_0 is the concentration of the species in solution ($mol\ cm^{-3}$) and v is the scanning speed (Vs^{-1}).

3.3.5 Square Wave Voltammetry (SWV)

The square wave voltammetry (SWV) is one of the faster and more sensitive voltammetry pulse techniques. The limits of detection may be compared to chromatographic and spectroscopic techniques. In addition, the characteristic parameters of this technique allow the kinetic and mechanistic evaluation of the electrode process under study. [154] The basic principle is the form of the resulting current peak coming from the overlap of potential pulses of height a (pulse amplitude), to a ladder of potentials of width ΔEs (incremental scan of potentials) and duration 2t

(period). Current measurements are made at the end of the direct and reverse pulses and the obtained signal after derivation is given as an intensity of the resulting current, presenting excellent sensitivity and high rejection to capacitive currents. The resulting voltammetric peak presents position, width and height characteristic of the redox type system. In practical terms, one of the advantages of SWV is the possibility of obtaining chains of well-defined peaks even in readings performed at high scanning speeds. Because it is a pulse technique, the Faradaic current can be collected in an appropriate time interval so that the contribution of the capacitive current has minimized. Another favorable point to use this technique is the reduction in background noise through repeated sweeps by observing the direct and inverse signals but if we obtain information analogous to those obtained through CV, with greater sensitivity due to the minimization of the contribution of the capacitive current. [154]

3.4 Structural and topographic characterization

The techniques of structural and topographic characterization have been of great importance in surface studies are being used by some authors in an attempt to find relationships between the surface morphology of the electrodes and their electrochemical performance. In this study, Fourier Transform Infrared Spectroscopy (FT-IR), Atomic Force Microscopy (AFM) and Scanning Electron Microscopy (SEM) were used for the characterization of developed sensor platforms.

3.4.1 Fourier Transform Infrared Spectroscopy (FT-IR)

FT-IR is an optical technique whose principle is based on the detection of absorbed radiation from the molecular bonds of different materials. By focusing Infrared light on a molecule causes the excitation of their chemical groups in vibrational modes. Similarly, when the radiant energy corresponds to the same vibrational energy level of the molecule in analysis, light is absorbed.[155][156] In the electromagnetic spectrum of light, Infrared radiation is located between visible and microwave region, comprising an extended spectrum between 14,000 and 10 cm^{-1}.

This region can be divided into three sub-regions: near infrared (14000 to 4000 cm^{-1}), medium infrared (4000 to 400 cm^{-1}) and far infrared (400 to 10 cm^{-1}). The portion of greater interest for the analysis of functional groups of organic structures fall between 4000 and 400 cm^{-1} i.e., medium infrared.[157]The infrared spectrum is obtained by plotting the intensity of radiation absorbed or transmitted by the molecule Vs. the wave number, which is proportional to the energy difference between the ground state and the excited states of vibration.[158] Each molecule has a unique absorption spectrum such as a fingerprint. From the knowledge of the location of the absorption vibrations of each functional group of the molecule investigated, it is possible to characterize the samples. For the preliminary examination, the region from 1300 to 4000 cm^{-1} (region of functional groups) is most important. In this region, the absorption occurs corresponding to important functional groups such as -OH, -NH and -C = O.[159][160] The main components of the Fourier transform infrared spectrometer are: infrared light source, an interferometer with a moving and a fixed mirror, a detector, an analog or digital converter and a computer as depicted in Figure 20.

Figure 20 - Geometrical representation of a FTIR spectrometer in the generation of a spectrum

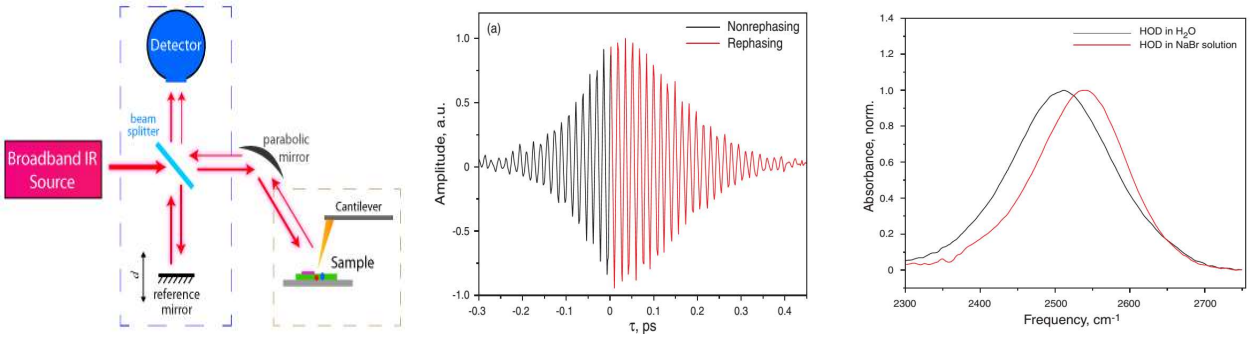

Source: Adapted from (161).

The interferometer allows you to split a beam of radiation from the external source into two waves and then recombine them so that the output beam intensity variations can be measured by a detector as a function of the path difference between the two beams. The technique uses two mirrors planes out of two, one is fixed perpendicular and other moved at constant speed. The radiation coming from the external source can be partially reflected in the fixed mirror and

partially transmitted to the moving mirror by a beam splitter which is present between two mirrors. The bundles of radiation then return to the beam splitter after pass through the sample and finally reach the detector. The signal produced is an interferogram which is a result of variation in the amplitude of light absorbed or transmitted as a function of the moving mirror scanning. The detected spectrum after reconstruction can be directly interpreted by applying the Fourier transform. The analyzed data represents the ratio of absorbance/transmittance of the chemical groups Vs. the frequency or wave number. [155]

3.4.2 Atomic Force Microscopy (AFM)

AFM analyses allow 2D- and 3D-images representative of the topography of the studied surface, with a spatial resolution that approximation of the atomic dimensions. The key components of an AFM are: ceramic cantilever attached to a tip at its end, a photodetector, a feedback system and a computer, which stores and processes the different probe deflections. [162] [163] The AFM system operates on the control of piezoelectric modulators that allow the vertical and horizontal movement of the tip as it approaches the surface of the sample, causing a deflection of the cantilever. This deflection is measured through the (angular) direction change of a collimated, emitted and reflected laser beam on the upper surface of the cantilever. Variations in position and intensity of light reflected laser beam are then captured by a photodetector. During tip displacement surface, the computer analyzes and reconstructing the topography of the sample at each position, the interaction force between the tip and the sample and plot a height diagram. Thus, the AFM technique dispenses with the sample preparation step with conductors, allowing the analysis of the same without loss of its properties. [164] The distance between the tip and the sample is of chief importance for the characterization of the material, for the resolution of the images and quality of the results. The forces interaction depending on the distance between the tip and the sample can be attractive or repulsive. As the tip approaches the sample, attractive force come to act (van der Waals force). As the level of approach to direct contact, repulsive force (electrostatic) prevail between the tip and the sample. According to the distance between the tip and the sample, three modes of operation are defined: 1) contact, 2) Non-contact, 3)

Intermittent contact. In first mode, repulsive interactions are predominant, allowing high resolution images to be obtained however it damages the sample. Non-contact, in 2nd mode of operation attractive interactions is predominant, having the advantage of not effecting the sample but the resolution usually limited to tens of nanometers due to the distance between tip and sample. The 3rd mode (intermittent contact) involve the tip oscillation on the surface of the sample, touching it periodically, bringing together the advantages of the two previous modes. (163)

3.4.3 Scanning Electron Microscopy (SEM)

SEM is one of the most versatile technique available for observation and analysis of the micro and Nano structural characteristics (Topography and morphology, Chemical composition, Crystallography orientation etc.) of solid materials. The principle of SEM is to use an accelerated electron beam focused to fine point which interact with the surface of the sample and sample is scanned line by line not necessary to penetrate the specimen. By a system of deflection coils, the electron from the beam can be guided by sweeping the surface of the sample so that the image signal results from the interaction of the incident beam with the surface of the sample. The interaction between the electron beam and the sample produces scattered electrons and photons that are registered by detector and converted into a video signal. The image formed from the signal picked up in the electronic scanning of a surface may present different characteristics, since the image results from the amplification of a signal obtained from a sample - electron interaction. The signals from the specimen surface are mainly due to secondary electrons (SE) and backscatter electrons (BSE) as well dependent on the surface curvature. The SE (low Energy Electrons) are generated by the electron-atom interactions of the sample, therefore, only those generated near the surface can be reissued and even these are very vulnerable to absorption by surface topography. The BSE (High Energy Electron) are come from a simple elastic collision, more superficial layers of the sample and contribute qualitatively to the sample composition. (165)

4 RESULTS AND DISCUSSION

Complex plasmonic nanostructures are proposed for sensing applications due to their high sensing ability without considering the broad nature of the LSPR peak that decrease the detection limit of the plasmonic sensor. In this section, we applied Full-wave field analysis/Mie theory to compute the optical characteristics and exploring the potential of dielectric shell with metallic core (Au/Ag@SiO_2) under probe model as a reliable sensor. On tuning the geometric parameters of the nano shells, we have calculated the optimized RIS×FoM. Furthermore, Campbell's model was exploited for molecular adsorption sensing on a size dependence approach.

4.1 Plasmonic Properties of Silica Coated Au/Ag nanoshells

Figure 21 (A & B) depicted the response of the λ_{LSPR} and extinction spectra of metallic core/dielectric shell nanoparticles to the refractive index of the neighboring medium respectively.

Figure 21 - The LSPR extinction for gold and silver nanoshells.

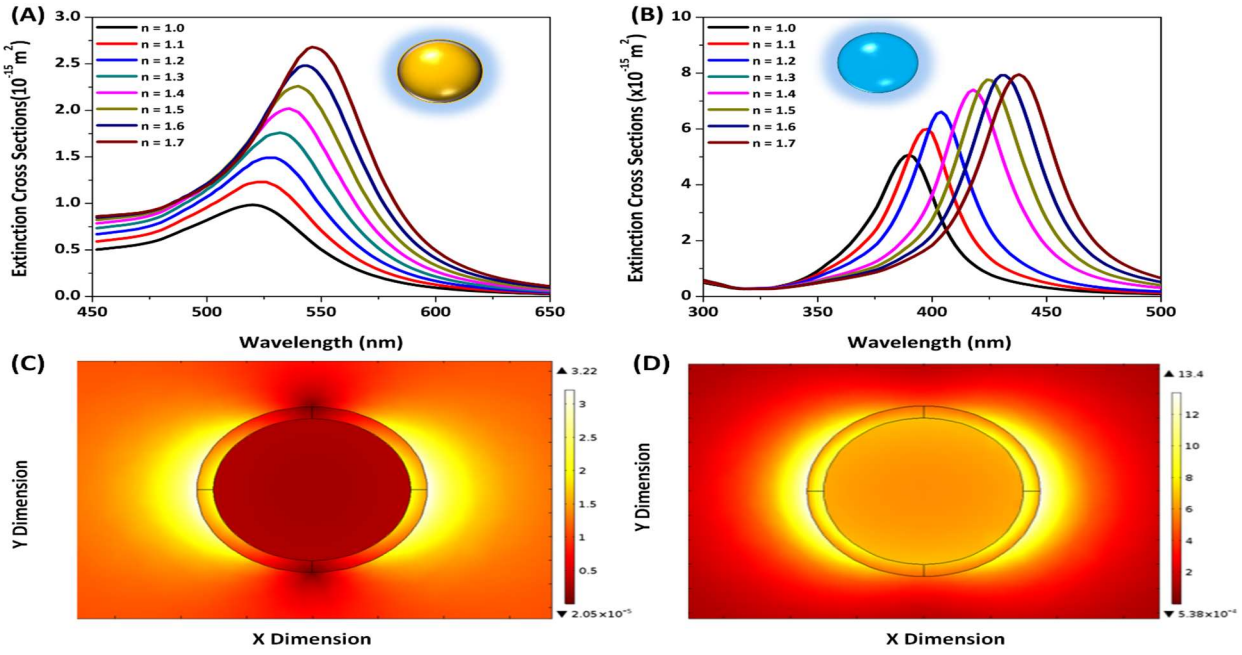

Source: The Author, 2019.

Note: (A) Gold (B) silver nanoshells. Electric field profile for gold (C) and silver nanoshells (D) in dielectric media water

In this probed model, our focus is on the optimization of the figure of merit by varying the refractive index of the surrounding medium. Despite their simplest core-shell based structure, these metallic nanostructures can still display refractive index tunability based on their LSPR effect. For both nanostructures, by varying the RI the extinction varied significantly in the visible regime and exhibits red shifts which obviously results increase in the intensity of the extinction peak. In case of Au@SiO_2 shell, the extinction spectra continued to red shift in the visible region and the peak wavelength approaches 540 nm. On contrary, the extinction peak of Ag@SiO_2 shell initially blue shifted near UV regime and eventually the peak wavelength was recognizable around 430 nm in the visible region. The E-field profile around the nanoshells for the dipole mode (gold and silver) can be observed in Figure 21C and Figure 21D, respectively.

Figure 22 - LSPR peak shift of gold and silver nanoshells on changing the refractive index of the surrounding.

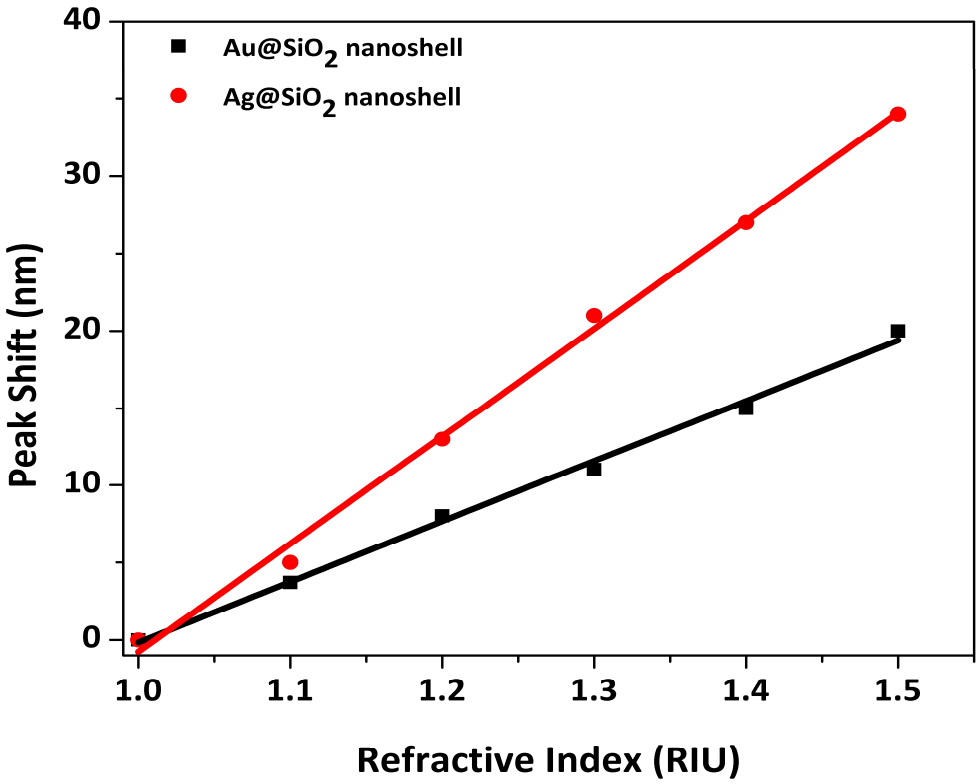

Source: The Author, 2019.

The changes in normalized electric field of nanoshells were compared at the LSPR wavelengths. For linear polarization, the electric field distribution is expressed by the two lobes which ensure

the influence of plasmon dipole resonance. LSPR peak position can be determined not only by the real part of nanostructure dielectric function, but also by the RI of the surrounding medium. In refractive index based LSPR sensors, bulk sensitivity reflects how LSPR peak position varies by changes in the RI of the local medium. Figure 22 depicts that surface plasmon wavelength as a function of RI which increases linearly along with refractive index range. In case of Ag@SiO_2 nanoparticles with radius of 30 nm, (t = 5 nm), there is red-shift effect from 390 to 424 nm ($\Delta\lambda \approx 27$nm), as observed in Figure 22 On the other hand, for the Au@SiO_2, the plasmonic shift influence is around $\Delta\lambda \approx 20$nm (Figure 22), indicating that Ag nanoshells show more sensitivity to surrounding environment. Moreover, one can see that the plasmon peak shift is linearly reliant on the RI of dielectric surrounding media. Figure 23 reflects the sensitivity response of the plasmonic sensor when R_c thickness of Ag and Au is fixed (30 nm) while SiO_2 shell radius is tuned from 2 to 18nm.

Figure 23 - The sensitivity of gold and silver nanoshells as a function of their respective silica shell thickness.

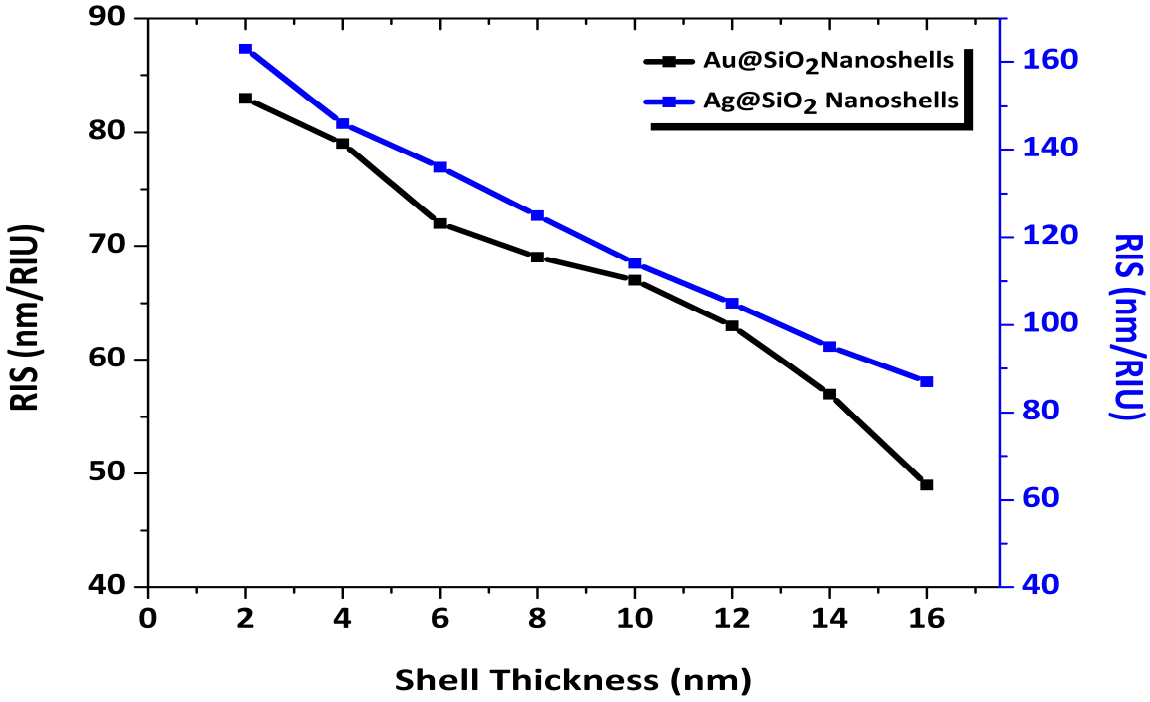

Source: The Author, 2019.

As expected, increasing the shell thickness results in decreasing the sensitivity for both metallic cores, specifically linearly for Ag nanoshell. Keeping in view this response based on this proposed structure, for high molecular sensing $Ag@SiO_2$ nanostructure could be more useful for molecular biosensing at small shell thickness (5 nm) as compared to $Au@SiO_2$ shell.

The effects of NP core radius on the bulk sensitivity and FoM determining nanoparticle sensing efficiency can be observed in Figure 24. Ag and Au nanoshells with radii 10 - 50 nm (t = 5nm) were analyzed. A theoretical analysis of the bulk sensitivity as function of core radius Figure 24 A indicates a linear behavior for the sensitivity values. As the core radius of the nanoparticles increases, a linear response in nanosensor bulk sensitivity from 20 -140 nm/RIU for gold, and 40 - 240 nm/RIU for silver nanoshells were respectively observed. As core shell radius increases, the sensing area as a function of radius of the core shell linearly increases, results in raising the sensitivity of the nanostructured platform.

Figure 24 - The bulk sensitivity of gold versus silver nanoshells as a function of core radius and their respective figure of merit.

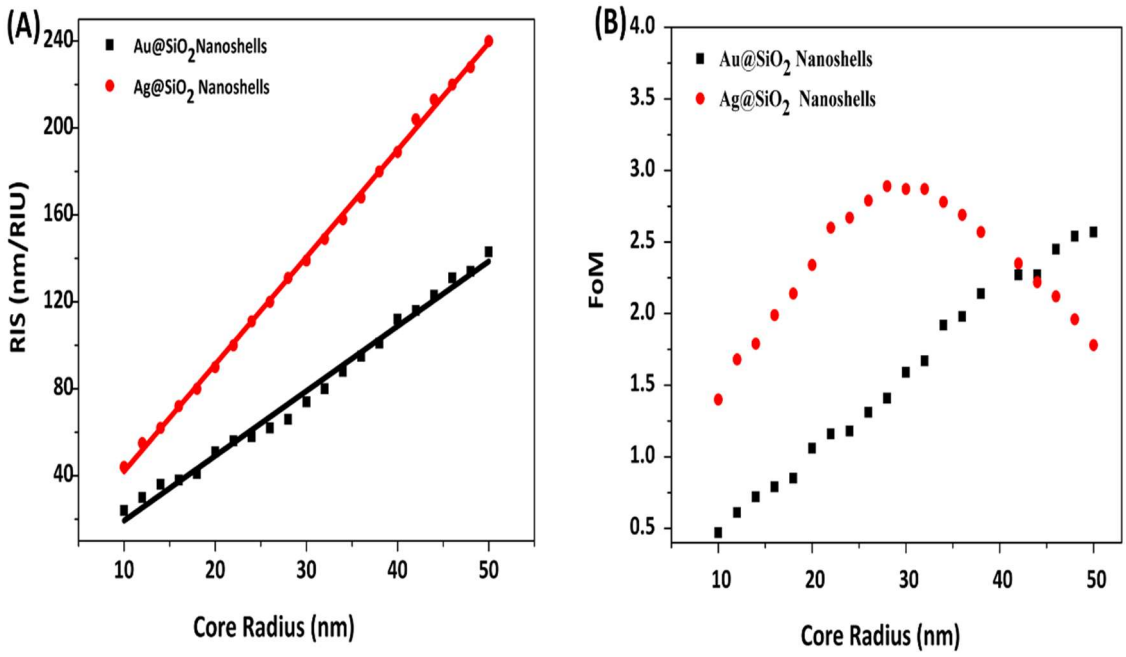

Source: The Author, 2019.

Note: (A) Bulk sensitivity of gold versus silver nanoshells (B) and their respective figure of merit.

Moreover, for small particle (r < 10 nm) the absorption process manly determines the light nanoparticle interaction. Scattering phenomenon enhance by increasing the particle size (r > 10 nm). In case of AuNP platform, with 20 nm < r < 40 nm bulk sensitivity is highly dependent on the nanostructure size. It can be seen (Figure 24) that bulk sensitivity of Ag nanoshells is highly influenced on size than Au nanoshells. As the Ag nanoshell radius increases, the FWHM increase due to radiation damping factor. [166] Therefore, FoM of Ag nanoshells decrease as the particle size grows, as shown in Figure 24 (B). Albeit, the ε_i value of Ag dielectric function is less than that of Au across visible region, therefore less damping occurs, resulting narrow FWHM in previous section (Figure 21) and high values of FoM for in previous section (Figure 21) and high values of FoM for silver particles. This is an advantage of Ag over Au nanoshells in biosensing applications. The calculated value of FoM (3.0) depicted in Figure 24 (B) for silver nanoshells (r = 30 nm) is higher than the reported values of more complex shapes, such as single Au nanorod (1.3) [55], Au nanostar (1.9) [167], Au pyramid (2.2) [50] Ag nanocube (1.6). [41]

Figure 25 - The product of RIS×FoM (unit: nm/RIU^2) for Au/Ag nanoshell with SiO_2 shell (5nm) and Au/Ag core (10-50nm).

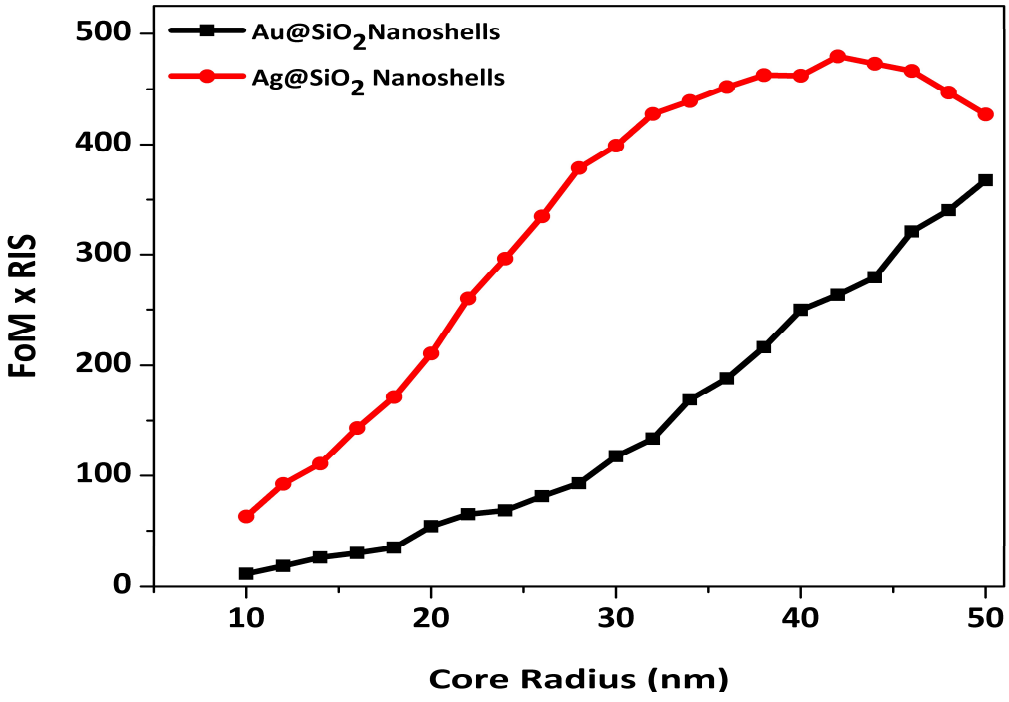

Source: The Author, 2019.

The FWHM of gold spectrum is not so affected by changing the surrounding medium, as compared to Ag nanoplatform. Therefore, the FoM response of AuNP is mainly determined by variations in bulk sensitivity. Furthermore, the relation RIS× FoM provides an over view of the sensing ability of LSPR sensor. Figure 25 depicts the RIS× FoM values for Au/Ag@SiO_2 nanoshell with different core radius, ranging from 10 to 50nm (shell thickness 5nm), indicating that Rc=30nm provides the best performance for the LSPR sensor at t = 5nm, where RIS×FoM is equal to 479 nm/RIU^2 for Ag as compare to Au nanoshells (364nm/RIU^2). For optical based biosensing, the EM field decay length (l_d) is considered an important parameter for molecular sensing. [84] Due to a molecular monolayer adsorption, the LSPR wavelength shift (Δλ) on a metallic NP surface can be ascribed by the Campbell's model as

$$\Delta\lambda = \eta_b(n_{ads} - n_m)(1 - e^{-\frac{2d}{l_d}}) \quad (4.1)$$

The Campbell's model (Eq.4. 1) indicates the Δλ decreases as the l_d value increases. Where l_d is the EM field decay length around the NP, adsorbate layer thickness d, η_b is the bulk sensitivity and n_{ads}, nm are respectively the RI of the adsorbate layer and the surrounding dielectric medium.[84]

Figure 26 - Plasmonic spectral shift as a function of the adsorbent layer thickness

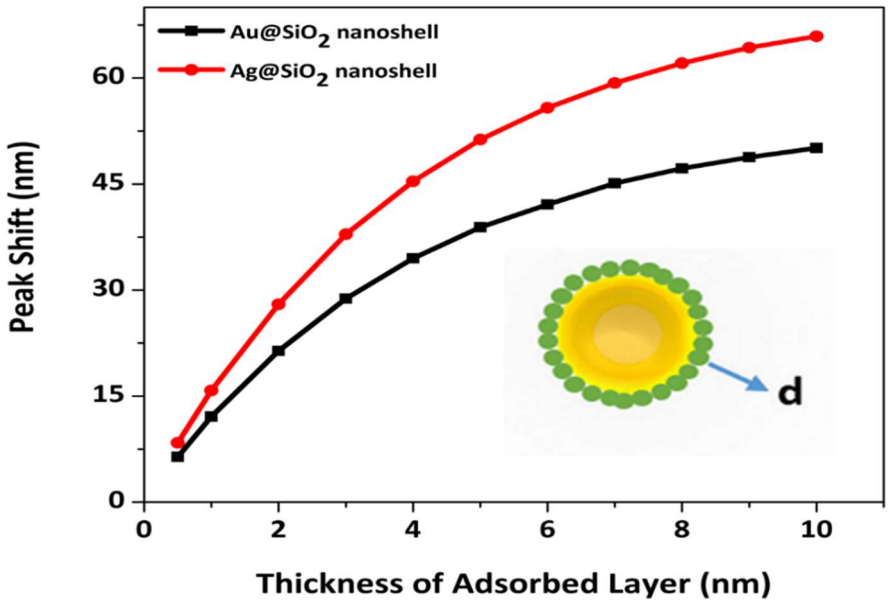

Source: The Author, 2019.

In Bio sensing, the adsorption of a molecular layer on a metallic NP surface enhances shifts in the LSPR spectrum according to the Campbell's model. Figure 26 depicts the trend of LSPR peak shift of the plasmonic nanoshells when the monolayer thickness (d) with RI (1.48) equal to protein on the NP surface is observed (d = 0.5 to 10 nm). For a 10 nm thick monolayer, a red-shift effect of $\Delta\lambda \approx 65.90$nm for $Ag@SiO_2$ and $\Delta\lambda \approx 50.10$nm in case of $Au@SiO_2$ respectively can be observed. However, Figure 26 demonstrates that $Ag@SiO_2$ are more sensitive to adsorbed layer as compared to $Au@SiO_2$ nanoshells (50 nm radius).

4.2 Gold nanorods dimer structure for sensing platform

The optical features of gold nanorod (AuNR) dimer linked end-to-end by thin silica cylinder had been investigated qualitatively. To study the influence of local environment changes by varying junction lengths and different aspect ratios of AuNR dimer, mathematical simulations in frequency domain were carried out. The light-dimer interactions were evaluated by the use of finite element method (FEM) with COMSOL Multiphysics. This computational approach focused on the assessment of the LSPR spectral peak position and spatial distribution of electromagnetic field enhancement near the surface of individual gold nanorod dimer, in order to understand the behavior of crucial parameters such as figure of merit and bulk sensitivity which predicts the LSPR sensor performance.

The LSPR peak shift of single AuNR and silica connected AuNR dimer in various surrounding mediums with different RI values is presented in Figure 27 LSPR peak position is linearly dependent on the variations of the surrounding medium RI, as shown in Figure 27 for individual Au rod as well as AuNR dimer. For gold dimer bridged by silica cylinder having length G = 2 nm and thickness d= 1 nm, LSPR peak position made a shift from 630 to 756 nm with RI increasing from 1.0 to 1.33, as depicted in Figure 27. Numerical values for the bulk sensitivity of AuNR dimer were identified as 381 nm/RIU, which is higher than single nanorod value (300 nm/RIU). The AuNR dimer also presents a higher figure of merit (11.7) after linked by silica cylinder with appropriate aspect ratio (AR = 3).

Figure 27 - LSPR peak shift of single AuNR and AuNR dimer connected with silica cylinder

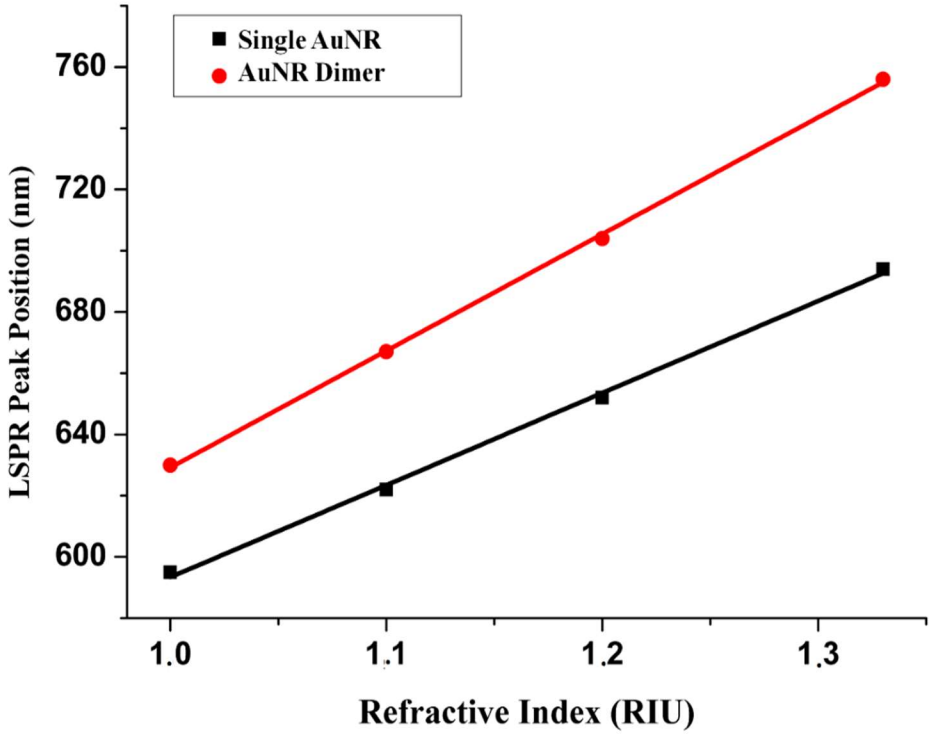

Source: The Author, 2019

As can be seen from Figure 28 (a), the aspect ratio of silica linked AuNR dimer increases, the bulk sensitivity of gold nanostructure enhances accordingly. The higher value of bulk sensitivity obtained at aspect ratio 6 (L = 30 nm, D = 5 nm), and the lower value at aspect ratio 1. Therefore, FoM of AuNR dimer varies as a function of aspect ratio as shown in Figure 28 (b). The maximum value of FoM calculated in this work is 16.9 at the aspect ratio 6. The calculated value of FoM (16.9) of gold nanorod dimer (AR = 6) is higher than the reported values of more complex shapes, such as Au nanorod (1.3) [55], Au nanosphere (1.5) [168], Au nano-cresent (2.4)[169], Au nanoshells (0.9) [170], Au bipiramide (4.5) [171] and Ag Nanoplate (2.5)[38] also illustrated in table 5.

Table 5 - Brief survey of Bulk sensitivity and Figure of Merit of plasmonic nanostructures

Nanostructures	Types	Bulk Sensitivity (nm/RIU)	FoM
Au NR-dimer	Ensemble	717	16.9
Au Nanoshells	Ensemble	314	0.9
Au Nanospheres	Ensemble	90	1.5
Au Nanorods	Ensemble	170	1.3
Au Nano-Cresent	Ensemble	596	2.4
Au bipyramid	Ensemble	352	4.5
Ag Nanoplate	Ensemble	406	2.5

Source: The Author, 2019.

The FWHM, dimer of gold nanorod spectrum is not so affected by increasing the aspect ratios, as compared to other ensemble shapes like spheres, shells etc. However, varying the aspect ratios of gold nanorod dimer can also affect the FoM due to change in radiation damping. Therefore, the FoM response of AuNR dimer is mainly dependent on the variations in bulk sensitivity and FWHM.

Figure 28 - Bulk sensitivity and FoM of AuNR dimer with various aspect ratios

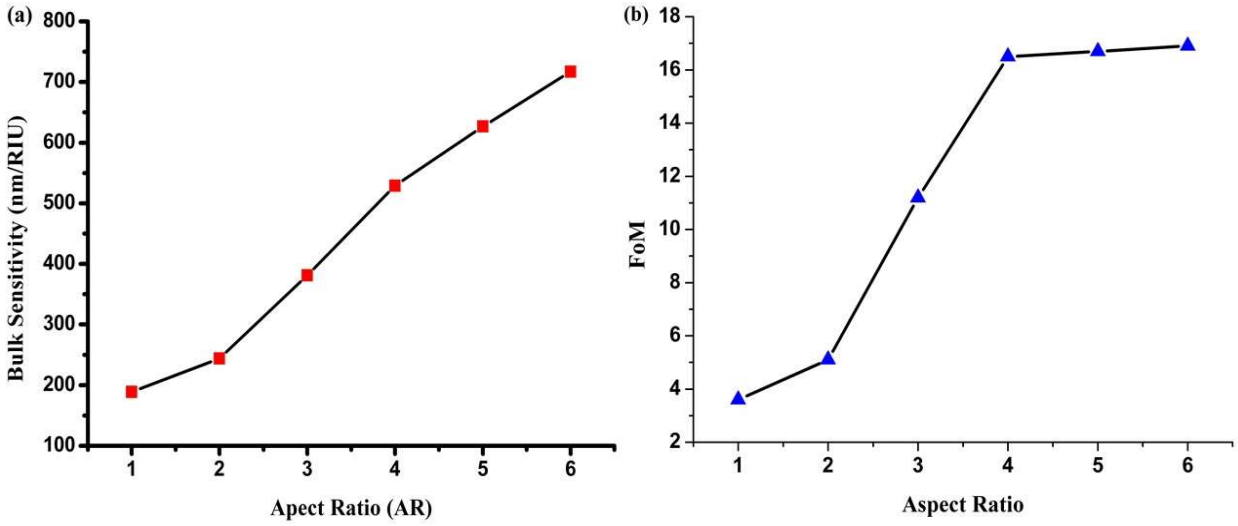

Source: The Author, 2019.
Note: Bulk sensitivity (a) and FoM (b) of AuNR dimer.

The impact of silica nano-cylinder junction, connecting head to head gold nanorods, with several lengths on the bulk sensitivity and FoM determining dimer-based sensing platform, can be observed in Figure 29. AuNR dimer with various silica junction lengths from 1 nm to 5 nm were analyzed. A computational analysis of the bulk sensitivity as a function of the junction length G (Figure 29) indicates an intensity map for the η_B values.

Figure 29 - Bulk sensitivity and FoM as a function of silica nano-cylinder with different lengths

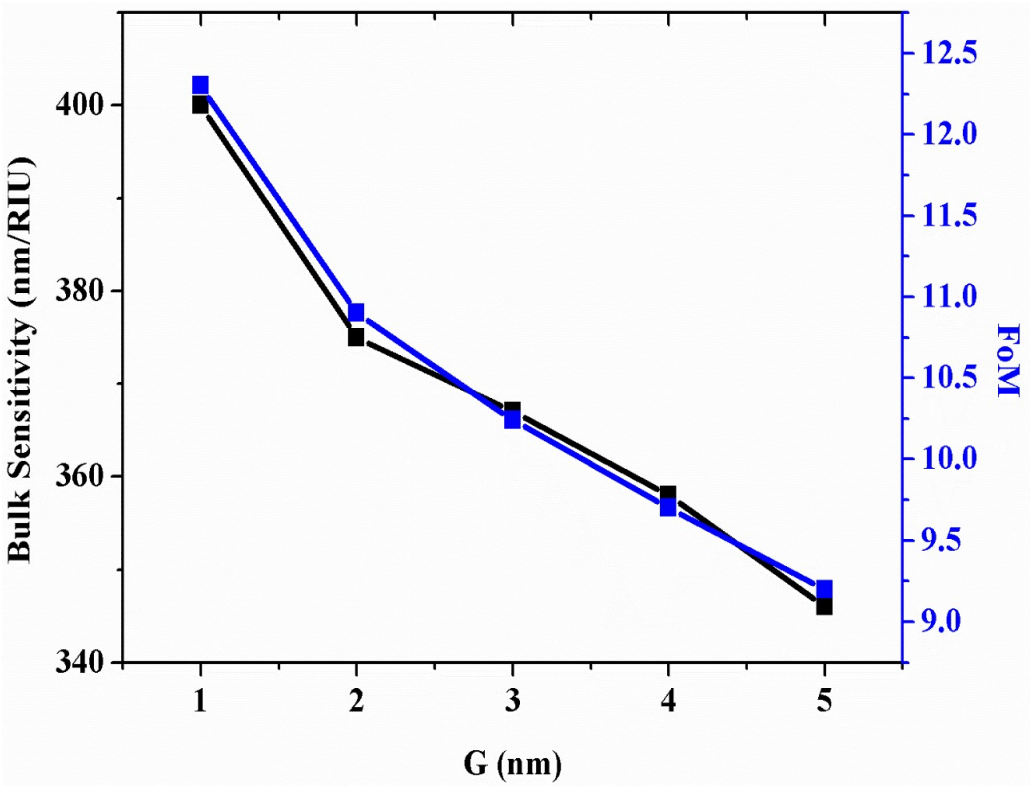

Source: The Author, 2019.

As silica linked cylinder length increases which in turn decreases the sensitivity of the nanostructured platform and FoM as well. Furthermore, scale bar of Figure 29 presents the FoM and bulk sensitivity response at different junction lengths. The higher FoM and sensitivity value obtained at 1 nm junction length was 12.25 and 397 nm/RIU respectively (shown in Figure 29). Simulations paved the way to choose the suggested nanostructure sensor for the effective LSPR sensing platform. In addition, the choice of the nano aggregate with best performances is

therefore dependent on the orientation and effective aspect ratio of the gold nanorod dimer, which might be measured by the use of colloidal medium or deposition on the substrate by classical SPR spectroscopy. The proposed approached can be extended to engineer an efficient and precise nanoscale sensor in molecular biosensing.

4.3 Construction of PEDOT-EDA film on the GCE for the detection of chikungunya.

The PEDOT:PSS based polymers configuration is combination of highly conductive, hydrophobic PEDOT and insulating, hydrophilic PSS chains, which leads to synergizes the good electrical conductivity and dispersibility of water. On the other hand, the excess ratio of PSS as compared to PEDOT inside PEDOT:PSS, can contribute towards low electrical conductivity as a result of reduced chain alignment.[172] To overcome this limitation in a facile way, different post treatment process such as solvent treatment, vapor treatment and electrochemical treatment has been widely utilized to enhance the charge carrier of PEDOT:PSS based materials. Primarily, this results from the reorientation of PEDOT chains and PSS chains. [172]

Figure 30 - Effect of different concentrations of EDA on PEDOT: PSS (a) Bare (b) 0.5% (c) 0.7% (d) 0.9%

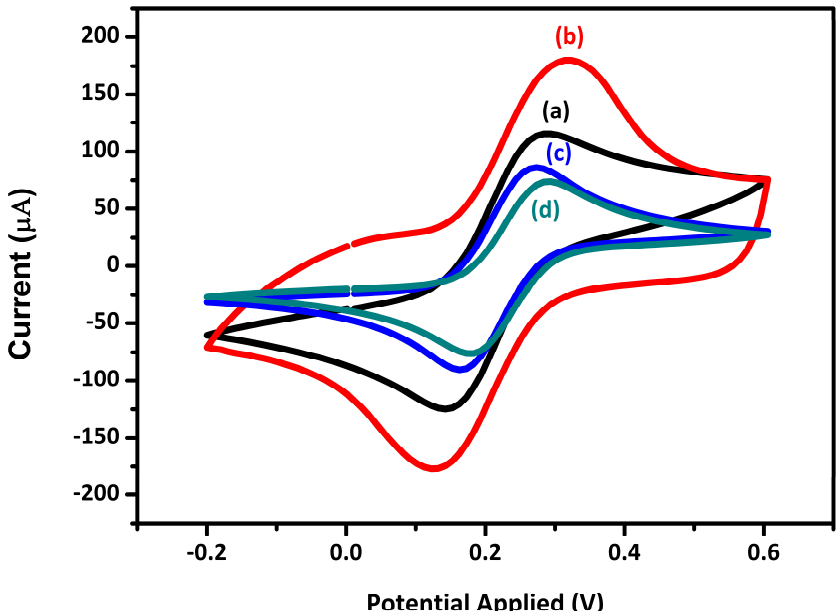

Source: The Author, 2019.

The cyclic voltammetry (CV) was used to investigate the redox characteristics of PEDOT: PSS and influence of different EDA concentrations (0.5%, 0.7%, 0.9%) inclusion. On average, the reduced response of CV has shown that water-soluble amines EDA incorporation contributed to the decreased oxidation and reduction peak currents indicating the domination of EDA as depicted in Figure 30. On contrary, it may be attributed that the low concentration of EDA comparatively provides higher binding sites between the amino groups of EDA and glassy carbon electrode (GCE) electrode, which may allow efficient electron transfer at the interfaces. One of the most important requirements in developing regular and homogeneous PEDOT-EDA electrode surfaces, includes a uniform and reproducible dispersion. Taking in account that the stability of the dispersion is also very important for preparing the modified electrodes with high reproducibility, EDA dispersion resulted in a black and homogenous solution.

Figure 31 - Schematic representation of nanostructured platform development and Cyclic voltammograms of the electrode modified

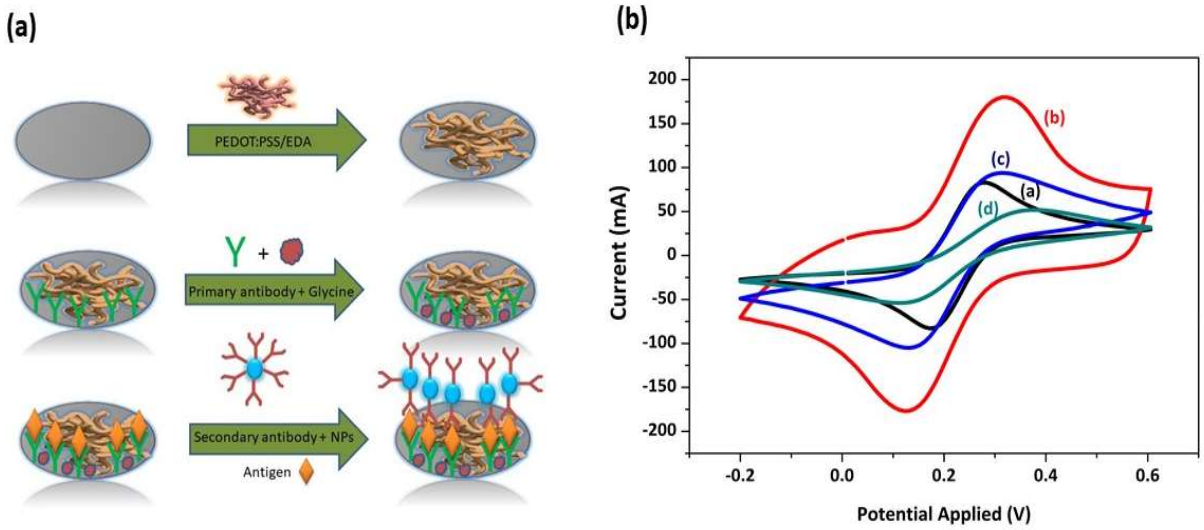

Source: The Author, 2019.

Note (a) Schematic representation of nanostructured platform development, (b) Cyclic voltammograms of the electrode modified as follows: (a) bare GCE (b) PEDOT-EDA, (c) PEDOT-EDA+ Glycine (d) PEDOT-EDA+ Glycine + PEDOT NPs at a scan rate of 100 mVs^{-1}

Different methods to form a polymeric film have been employed; among them drop coating is one of the more facile and simplest method was chosen in this study. A schematic diagram of all steps involved on the synthesis of anti-CHIK/ PEDOT@EDA-NPs/activated CHIK/activated anti-CHIK/PEDOT@EDA/GCE is depicted in Figure 31 (a).

In order to electrochemically characterize the model under probe as illustrated in Figure 31 (b), Modification of the electrode surface was accomplished by CVs using $K_3Fe(CN)_6/K_4Fe(CN)_6$ prepared in 100 mM KCl as redox probe. The electrochemical proprieties of the PEDOT-EDA resulted in an increase of the catalytic activity, confirmed by increase of the anodic and cathodic peaks compared with the bare GCE and PEDOT-EDA/GCE. After PEDOT NPs immobilization, a decrease in redox peak currents was observed due to the insulating nature of the PEDOT nanoparticles. [173] This same behaviour also occurred after blocking the non-specific bindings with incubation of the electrode in 50 mmol L^{-1} glycine solution. Scan rate studies were performed on the PEDOT-EDA/GCE varying from 10 mVs^{-1} to 120 mVs^{-1} (Fig.32).

Figure 32 - CVs obtained from the PEDOT-EDA/GCE and Plot of anodic and cathodic peak current

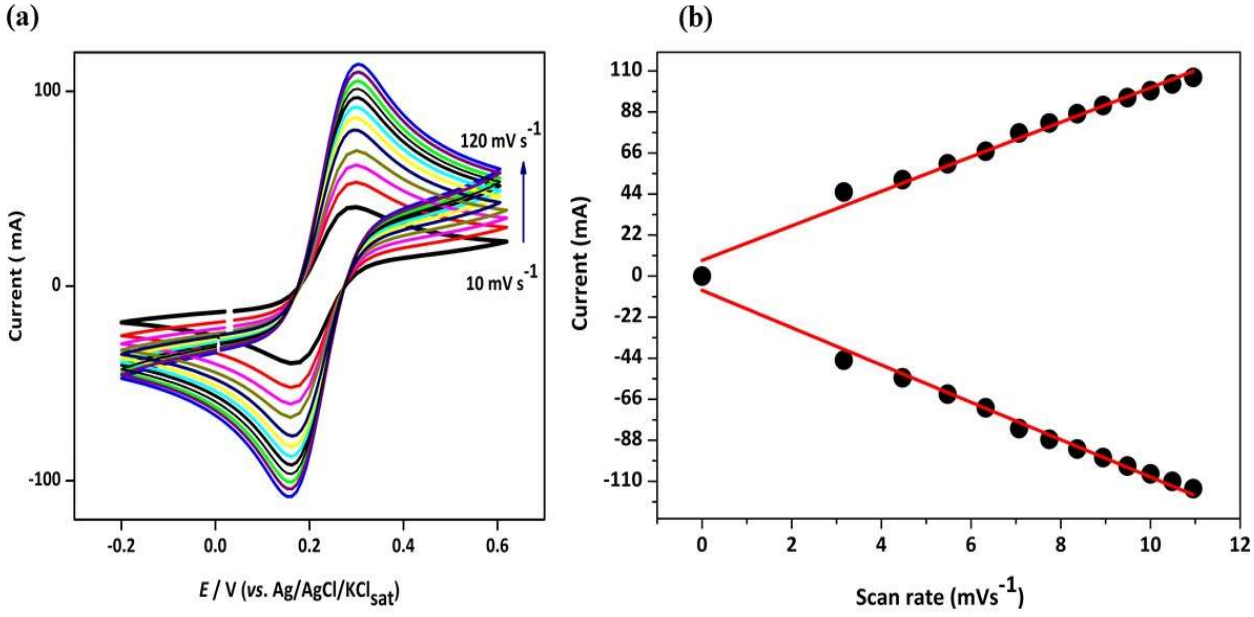

Source: The Author, 2019.

Note: (a) CVs obtained from the PEDOT-EDA/GCE in presence of redox probe of 5 mM $K_3Fe(CN)_6/K_4Fe(CN)_6$ prepared in 100 mM KCl at scan rates (inner to outer) 10, 20, 30, 40, 50, 60, 70, 80, 90, 100, 110, 120 mV/s. (b): Plot of anodic and cathodic peak current from CVs vs. scan rate.

The voltammograms presented highly symmetric redox peaks such as a voltammetry behavior close to the reversible process.[152] The currents of cathodic and anodic peaks increased linearly, indicating a diffusion controlled electron transfer [152] (Figure 32b). The stability of the PEDOT-EDA film on the GCE was checked by performing 15 consecutive voltammetric cycles in the potential range from –0.2 V to 0.7 V in 5 mmol L^{-1} $K_3Fe(CN)_6/K_4Fe(CN)_6$ solution. A discrete shift on redox peak potentials was detected which can be attributed a possible interaction between sulfur reactive species of PEDOT and iron species present in the ferrocyanide redox probe. The coefficients of variation were 0.04% and 0.09% for anodic and cathodic peaks, respectively, indicating good stability of PEDOT-EDA film. The results show a strong synergism of electrical conductivity between PEDOT: PSS and EDA.

The immunosensor performance is highly dependent on the amount of immobilized antibodies and antigen binding capacity (C. Wu et al.) In this study, PEDOT:PSS based polymer was used to promote a covalent immobilization of the anti-IgG antibodies via amide bonds. For covalent immobilization and as well as to activate the carboxyl groups of anti-IgG, EDC/NHS (1:1) was combined with antibody. For the sake of immunoassay sensitivity enhancement response, 5 μg/mL and 10 μg/mL anti- IgG concentrations were immobilized on the GCE modified by PEDOT-EDA. Different concentrations of for mentioned anti-IgG (0.5 to 10 μg mL^{-1}) previously dispersed in PBS (pH = 6.5) were immobilized on the sensor surface. The immunosensor response is presented in Figure 33 and optimization can be seen at 5 μg/mL of anti- IgG. Hence, this optimized concentration was chosen for onward experiments.

Figure 33 - Immunosensor response for Anti-IgG 5 µg/mL and Anti-IgG 10 µg/mL.

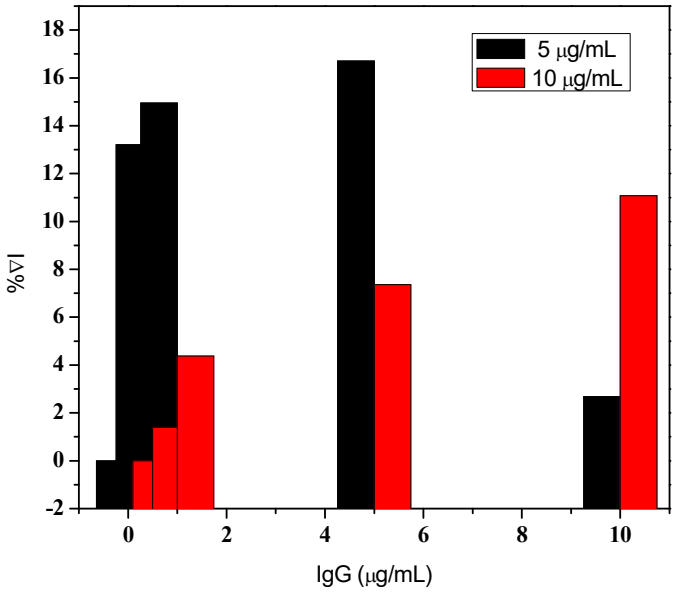

Source: The Author, 2019.

Adsorption of protein on the NPs surface can be influenced by various factors e.g. (1) Amount of proteins (2) Affinity towards the surface of NP (3) Capability to capture the surface [174] etc. NPs concentration which can be defines as the number of proteins per NP or surface area ratio [175] can be denoted as A_{ratio}, also influences the affinity. Although the optimal ratio will depend on the nanoparticle density and the proteins affinity to the NPs surface. There is an obvious effect of NPs and protein on the immunosensor performance. In this work, we have studied the effect of both NPs and protein separately upon sensor response with varying concentrations. On average, the peak current %ΔI relatively increases as the IgG ratio varies from (1:1 to 1:4) as Figure 34 represents. NPs ratio is kept constant while the protein molecules ratio was linearly increased. Morteza et al [175] claimed that, by decreasing A_{ratio}, proteins/NP is significantly decreased; therefore, more energy is transferred from the NPs to each protein molecule, resulting in a stronger binding and more conformational changes of the proteins on the NPs. On the other hand, for the lower ratios, the stronger binding between protein and NPs.

Figure 34 - Effect of Different Concentrations of IgG and Different Concentrations of NPs

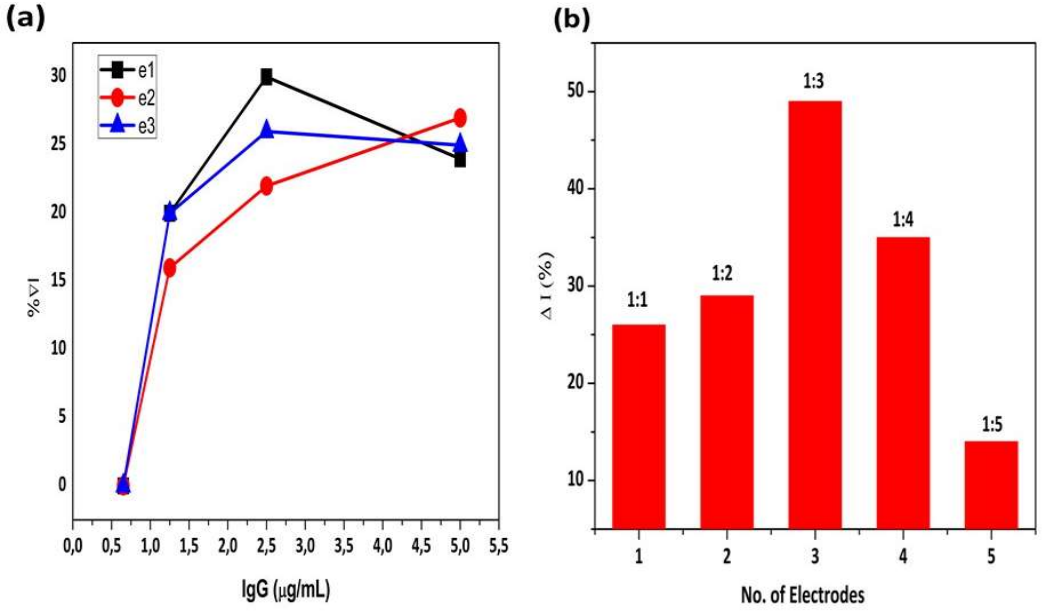

Source: The Author, 2019.

Note - (a) Different Concentrations of IgG (b) Different Concentrations of NPs

The matrix effect and selectivity were also tested with this immunosensor by using serum samples, since these complex samples contain a great number of interferers. As exclusion criteria in samples selections, hemolyzed or hypercholesteremic samples were not included. The assays were carried out by successive incubations with the positive serum (with 5 µg/mL Chikungunya in PBS) and negative serum (diluted in PBS 10 mM, pH 6.5) samples at the same electrode in each experiment (Figure.35). Plots represent cathodic peak currents of SWVs subtracted from the blank; SWV measurements performed.

Figure 35 - Matrix effect and selectivity studied on successive incubations in positive and negative serum.

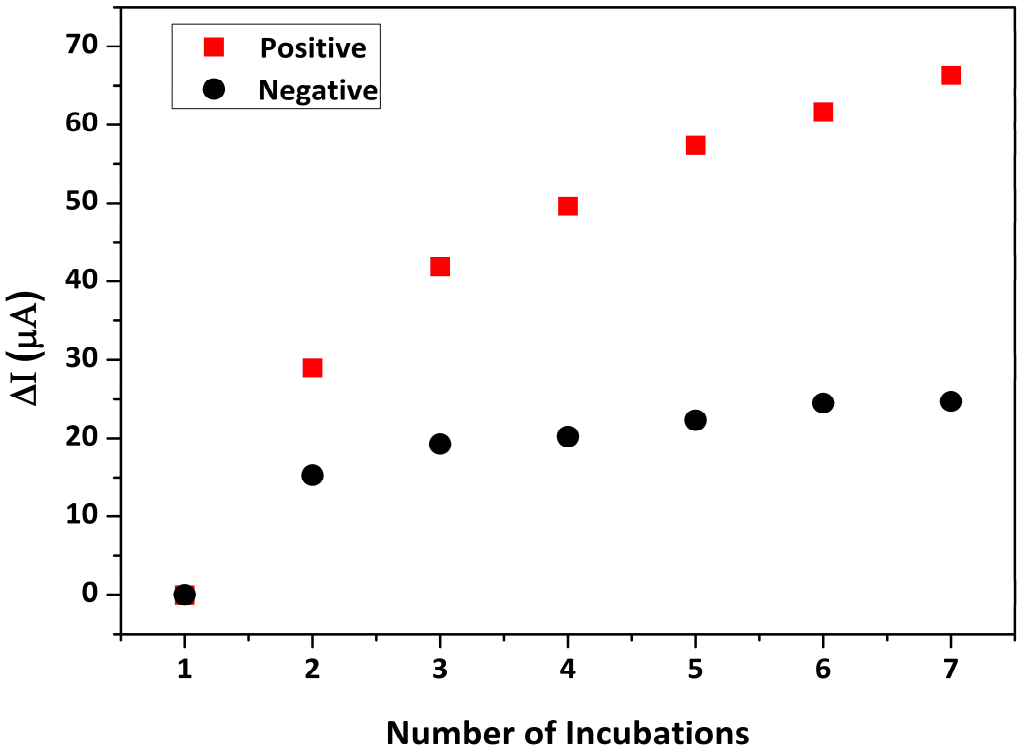

Source: The Author, 2019.

Analytical responses indicated a gradual decrease in the SWV peaks proportional to the increase of the Chikungunya concentrations of positive samples, contrary to the negative serum response. The selectivity of the immunosensor was tested by incubating positive and negative chikungunya serum samples for anti- chikungunya antibodies diluted at 1:1 in PBS. An increased frequency response was found when the immunosensor was incubated with positive chikungunya serum for anti- chikungunya antibodies and a practically constant response was found when incubated with negative serum, demonstrating that the immunosensor is selective regarding the identification of anti- chikungunya antibodies in chikungunya serum samples.

5 CONCLUSION

Noble metallic NPs possess remarkable optical and physical properties due to strong absorption as well as scattering characteristics. The shift in LSPR wavelength due to change in dielectric constant of local medium enables the plasmonic metallic NPs to apply them in facile, cost-effective and label free plasmonic sensing. Parameters that govern LSPR sensor performance such as bulk sensitivity, figure of merit and molecular sensing of various size and shapes of Au and Ag nanoparticles was investigated. FEM and Mie theory are related in good agreement to show scattering, absorption and extinction cross sections for metallic NPs. Sensing performance of the dielectric-metal core-shell (Au/Ag@SiO_2) had been investigated theoretically as a function of refractive index of the surroundings in connection with varying core radius and shell thickness. Furthermore, our results possess high figure of merit for Ag nano shell (3.0) as compared to Au nano shell (2.50) having the same silica shell thickness 5 nm but different metallic core radius (46 nm & 34 nm) for Au/Ag nano shells, respectively. Then we had investigated the optical behaviour of gold nanorod (AuNR) dimmer bridged by thin silica cylinder of varying length. Our results reveal that an increase in aspect ratio causes a red shift in dimer, leading to significantly higher sensitivity 717 nm/RIU and higher figure of merit 16.9 as compared to single AuNR having 300 nm/RIU sensitivity with similar dimensions. Due to high surface to volume ratio, Au nanorods prove good candidate for LSPR-based optical sensors as compared to Au/Ag nanoshells.In the second part of this study, a promising electrochemical immunosensor approach based on PEDOT-EDA as sensing plate form was demonstrated for chikungunya detection. Polymeric NPs and EDA nanocomposite had been successfully prepaid and applied to sandwich-type immunosensor. As polymers have advantages over metal or inorganic materials, for instance easy to synthesize and processing, structural and chemical diversity, light weight as well as better electrical and optical properties. The one-step synthesis by adding organic compound is an efficient, rapid and simple method for producing functionalized polymeric nanoparticles. Due to the extraordinary performance, the immunosensor presented in this work can be suitable for the rapid and on-site detection of the chikungunya protein, opening new ways for an early diagnosis of the acute chikungunya infection.

REFERENCES

[1] STRAUSS, J. H.; STRAUSS, E. G. The Alphaviruses: Gene Expression, Replication, and Evolution. **Microbiological Reviews**, v. 58, p. 491–562, 1994.

[2] MUKHOPADHYAY, S.; *et al*. Mapping the Structure and Function of the E1 and E2 Glycoproteins in Alphaviruses. **Structure**, v. 14, p. 63–73, 2006.

[3] MAYER, S. V.; *et al*. The Emergence of Arthropod-Borne Viral Diseases: A Global Prospective on Dengue, Chikungunya and Zika Fevers. **Acta Tropica**, v. 166, p. 155–63, 2017.

[4] SINGHAL, C.; *et al*. A Genosensor for Detection of Consensus DNA Sequence of Dengue Virus Using ZnO/Pt-Pd Nanocomposites. **Biosensors and Bioelectronics**, v. 97, p. 75–82, 2017.

[5] World Health Organization. **Chikungunya**. 2017. Disponível em: https://www.who.int/news-room/fact-sheets/detail/chikungunya. Acesso em: 08 set. 2019.

[6] MARC, F.; ERIN, S. Chikungunya Virus Spreads in the Americas - Caribbean and South America, **IstMMWR Morb Mortal Wkly Repv**, v.63(22), 2014.

[7] BRASIL. Ministério da Saúde. **Chikungunya**: Manejo Clínico. Brasília, 2017. Disponível em: http://portalarquivos.saude.gov.br/images/pdf/2016/dezembro/25/chikungunya-novo-protocolo.pdf.2017. Acesso em: 08 set. 2019.

[8] NUNES, Marcio, R. T.; *et al*. Emergence and Potential for Spread of Chikungunya Virus in Brazil. **BMC Medicine**, v. 13, 2015.

[9] SIMÃO, Estefani, P.; *et al*. Nanostructured Impedimetric Lectin-Based Biosensor for Arboviruses Detection. **Talanta**, vol. 208, p. 120338, 2020.

[10] PABBARAJU, Kanti, *et al*. Simultaneous Detection of Zika, Chikungunya and Dengue Viruses by a Multiplex Real-Time RT-PCR Assay. **Journal of Clinical Virology**, v. 83, p. 66–71, 2016.

[11] JOHNSON, Barbara. W.; *et al*. Laboratory Diagnosis of Chikungunya Virus Infections and Commercial Sources for Diagnostic Assays. **Journal of Infectious Diseases**, v. 214, p. S471–74, 2016.

[12] WANG, J. Electrochemical Nucleic Acid Biosensors. **Analytica Chimica Acta**, v. 469, p. 63–71, 2002.

[13] WILSON, M. S.; WEIYAN, N. Multiplex Measurement of Seven Tumor Markers Using an Electrochemical Protein Chip. **Analytical Chemistry**, v. 78, pp. 6476–83, 2006.

[14] ATES, M.; KARAZEHIRA, T.; SARAC, A. Conducting Polymers and their Applications.

Current Physical Chemistry, v. 2, p. 224-240, 2012.

[15] ADELOJU, S. B.; WALLACE, G. G. Conducting Polymers and the Bioanalytical Sciences: New Tools for Biomolecular Communications. A Review. **The Analyst**, v.121, p. 699, 1996.

[16] SUNG, W. Jun.; YOU, H. B. A Glucose Oxidase Electrode Based on Electropolymerized Conducting Polymer with Polyanion−Enzyme Conjugated Dopant. **Analytical Chemistry**, v. 72, p. 2177–2181, 2000.

[17] YOON, Hyeonseok, *et al*. Versatile Strategies for Fabricating Polymer Nanomaterials with Controlled Size and Morphology. **Macromolecular Research**, v. 16, p. 85–102, 2008.

[18] JANG, and JYONGSIK. Conducting Polymer Nanomaterials and Their Applications. **Advances in Polymer Science**, v. 199, p. 189–259, 2006.

[19] THAKUR, and HIMKUSHA, *et al*. Electrochemical Determination of M. Tuberculosis Antigen Based on Poly(3,4-Ethylenedioxythiophene) and Functionalized Carbon Nanotubes Hybrid Platform. **Talanta**, v. 171, p. 115–23, 2017.

[20] HONGLAN, Qi.; XIAOXIA, L. PEI, C. CHENGXIAO, Z. Electrochemical Detection of DNA Hybridization Based on Polypyrrole/Ss-DNA/Multi-Wall Carbon Nanotubes Paste Electrode. **Talanta**, v. 72, p. 1030–35, 2007.

[21] YONGWON, J.; JIN,Y. Jeonga.; BONG, H. C. Recent Advances in Immobilization Methods of Antibodies on Solid Supports. **The Analyst**, v. 133, p. 697, 2008.

[22] JUNHOE C.; JUNG, I. H.; YOUNG, C.; DAE, S. Y.; KWANG W. O.; GEUNBAE, L. DNA Hybridization Electrochemical Sensor Using Conducting Polymer. **Biosensors and Bioelectronics**, v. 18, p. 1241–47, 2003.

[23] THOMAS, C. A.; ZONG, K.; SCHOTTLAND, P.; Reynolds, J. R. Poly(3,4-Alkylenedioxypyrrole)s as Highly Stable Aqueous-Compatible Conducting Polymers with Biomedical Implications. **Advanced Materials**, v. 12, p. 222–25, 2000.

[24] ZAJDEL, J. T.; MOSHE, B.; GÁBOR, M. *et al*. PEDOT:PSS-Based Multilayer Bacterial-Composite Films for Bioelectronics. **Scientific Reports**, v. 8, 2018.

[25] ALVESA, R. da F.; SILVAA, G. da, A.; FERREIRAB L. F. *et al*. Synthesis and Characterization of a Material Derived from 4-Mercaptobenzoic Acid: A Novel Platform for Oligonucleotide Immobilization. **Talanta**, vol. 165 , p. 69–75, 2017.

[26] FENGA, j.; LIA, Y.; LIA, M.; LIA, F. *et al*. A Novel Sandwich-Type Electrochemical Immunosensor for PSA Detection Based on PtCu Bimetallic Hybrid (2D/2D) RGO/g-C3N4. **Biosensors and Bioelectronics**, v. 91, p. 441–48, 2017.

[27] ZHANG, C.; ZHANG S.;, JIA, Y.; LI, Y. *et al*. Sandwich-Type Electrochemical Immunosensor for Sensitive Detection of CEA Based on the Enhanced Effects of Ag NPs@CS Spaced Hemin/RGO. **Biosensors and Bioelectronics**, v. 126, p. 785–91, 2019.

[28] SWATI, S. Glassy Carbon: A Promising Material for Micro- and Nanomanufacturing. **Materials**, v. 11, p. 1857, 2018.

[29] BOHREN, C. F.; HUFFMAN, D. R. **Absorption and Scattering of Light by Small Particles**. Weinheim: Wiley-VCH Verlag GmbH & Co. KGaA. 2007.

[30] JANA, j.; GANGUNLY, M.; PAL. T. Enlightening Surface Plasmon Resonance Effect of Metal Nanoparticles for Practical Spectroscopic. **RSC Advances**, v. 6. P. 86174-86211, 2016.

[31] TAYLOR, A. D. Plasmonic Nanoparticles As Versatile Nanorulers For Sensing Applications: Developing The Nanoparticle-On-Mirror Architecture. **Wake Forest University.** Ph. D Thesis, 2016.

[32] ZEEV, Z.; IBRAHIM, A. Integrated Nanophotonic Devices. Elsevier, 2010.

[33] MÜLLER, H. Optical Properties of Metal Clusters. **Zeitschrift Für Physikalische Chemie**, v. 194, p. 278–79, 1996.

[34] SHERRY, L. J.; JIN, R. *et al*. Localized Surface Plasmon Resonance Spectroscopy of Single Silver Triangular Nanoprisms. **Nano Letters**, v. 6, p. 2060–65, 2006.

[35] AVERITT, R. D.; SARAH, L. *et al*. Linear Optical Properties of Gold Nanoshells. **Journal of the Optical Society of America B,** v. 16, p. 1824, 1999.

[36] MAIER, S. A. Plasmonics: Fundamentals and Applications. **Springer**, 2007.

[37] ARELLANO, A.; M. Ung, T.; BLANCO, Á.; MULVANEY, P.; LIZ, L. M. Silica-coated metals and semiconductors. Stabilization and nanostructuring. **Pure and Applied Chemistry**, v.72, p. 1–2, 257–267, 2000.

[38] FAROOQ, S.; NUNES, F. D. *et al*. Optical Properties of Silver Nanoplates and Perspectives for Biomedical Applications. **Elsevier** ,v. 31, p. 160–67, 2018.

[39] XUAN, Y.; YANG, M.; PANG, B. *et al*. Gold Nanomaterials at Work in Biomedicine. **Chemical Reviews**, v. 115, p. 10410–88, 2015.

[40] FREESTONE, I.; MEEKS, N.; *et al*. The Lycurgus Cup - A Roman Nanotechnology. **Gold Bulletin**, v. 40, p. 270–77, 2008.

[41] SHERRY, L. J.; CHANG, S. H. *et al*. Localized Surface Plasmon Resonance Spectroscopy of Single Silver Nanocubes. **Nano Letters**, v. 5, p. 2034–38, 2005.

[42] CHEN, T.; YANG, M.; WANG, X. *et al*. Controlled Assembly of Eccentrically Encapsulated Gold Nanoparticles. **J Am Chem Soc**, vol. 130, p. 11858-11859. 2008.

[43] MURRAY, W.; ANDREW, *et al*. Sensitivity of Localized Surface Plasmon Resonances to Bulk and Local Changes in the Optical Environment. **The Journal of Physical Chemistry C**, vol. 113, p. 5120–25, 2009.

[44] PETRYAYEVA, E.; ULRICH, J. K. Localized Surface Plasmon Resonance: Nanostructures,

Bioassays and Biosensing—A Review. **Analytica Chimica Acta**, vol. 706, p. 8–24, 2011.

[45] JENSEN, T. R. *et al*. Nanosphere Lithography: Effect of the External Dielectric Medium on the Surface Plasmon Resonance Spectrum of a Periodic Array of Silver Nanoparticles. **The Journal of Physical Chemistry B**, vol. 103, p. 9846–53, 1999.

[46] MAHMOOD, H. Z.; FAROOQ, S.; LINS, E. C. Optimizing the Plasmonic Sensing of Silica Coated Au/Ag Nanoshellse. **International Journal of Science and Engineering Investigations**, vol. 87, p. 140–45, 2019.

[47] FAROOQ, S,; WENDELL W. N. *et al*. Engineering a Plasmonic Sensing Platform for Candida Albicans Antigen Identification. **Journal of Nanophotonics**, v. 12, 2018.

[48] SCHULTZ, S. *et al*. Single-Target Molecule Detection with Nonbleaching Multicolor Optical Immunolabels. **Proceedings of the National Academy of Sciences of the United States of America**, v. 97, p. 996–1001, 2000.

[49] XIAOHUA, H. *et al*. Cancer Cell Imaging and Photothermal Therapy in the Near-Infrared Region by Using Gold Nanorods. **American Chemical Society** , 2006.

[50] LEE, K. S.; EL-SAYED M. A. Gold and Silver Nanoparticles in Sensing and Imaging: Sensitivity of Plasmon Response to Size, Shape, and Metal Composition. **The Journal of Physical Chemistry B**, v. 110, p. 19220–25, 2006.

[51] XU, Xia, *et al*. Gold Nanorods Based LSPR Biosensor for Label-Free Detection of Alpha-Fetoprotein. **Procedia Engineering**, v. 25, p. 67–70, 2011.

[52] CAPPI, G.; SPIGA, F. M. *et al*. Label-Free Detection of Tobramycin in Serum by Transmission-Localized Surface Plasmon Resonance. **American Chemical Society**, v. 87, p. 5278-5285, 2015.

[53] HODAK, J. H. *et al*. Size Dependent Properties of Au Particles: Coherent Excitation and Dephasing of Acoustic Vibrational Modes. **The Journal of Chemical Physics**, vol. 111, p. 8613, 1999.

[54] EUSTIS, S.; EL-SAYED, M. A. Why Gold Nanoparticles Are More Precious than Pretty Gold: Noble Metal Surface Plasmon Resonance and Its Enhancement of the Radiative and Nonradiative Properties of Nanocrystals of Different Shapes. **Chem. Soc. Rev.**, vol. 35, p. 209–17, 2006.

[55] MAYER, K. M. *et al*. A Label-Free Immunoassay Based Upon Localized Surface Plasmon Resonance of Gold Nanorods. **American Chemical Society**, v. 2, p. 687-692, 2008.

[56] MAYER, K. M. *et al*. Localized Surface Plasmon Resonance Sensors. **Chemical Reviews**, v. 111, p. 3828–57, 2011.

[57] WILLETS, K. A.,; VAN Duyne, R. P. Localized Surface Plasmon Resonance Spectroscopy and Sensing. **Annu. Rev. Phys. Chem**., vol. 58, p. 267–97, 2007.

[58] GANS, R. Über Die Form Ultramikroskopischer Goldteilchen. **Annalen Der Physik**, 1912.

[59] SONG, Yujun, *et al*. Correlation and Characterization of Three-Dimensional Morphologically Dependent Localized Surface Plasmon Resonance Spectra of Single Silver Nanoparticles Using Dark-Field Optical Microscopy and Spectroscopy and Atomic Force Microscopy. **The Journal of Physical Chemistry C**, vol. 114, p. 74–81, 2010.

[60] RINGE, E. *et al*. Plasmon Length: A Universal Parameter to Describe Size Effects in Gold Nanoparticles. **The Journal of Physical Chemistry Letters**, vol. 3, p. 1479–83, 2012.

[61] Countries and Territories Where Chikungunya Cases Have Been Reported as of May 29, 2018. **CDC**. Disponível em: https://www.cdc.gov/chikungunya/geo/index.html. Acesso em: 05 set. 2019.

[62] PATIL, P. O. *et al*. Antibody-Mediated Diagnosis of Biomolecules. **Nanobiosensors for Biomolecular Targeting,** p. 165–93, 2019.

[63] MOCK, J. J. *et al*. Shape Effects in Plasmon Resonance of Individual Colloidal Silver Nanoparticles. **The Journal of Chemical Physics**, vol. 116, p. 6755–59, 2002.

[64] CREIGHTON, J. A.; DESMOND, G. E. Ultraviolet–Visible Absorption Spectra of the Colloidal Metallic Elements. **J. Chem. Soc., Faraday Trans**., v. 87, p. 3881–91, 1991.

[65] LANGHAMMER, Christoph, *et al*. Plasmonic Properties of Supported Pt and Pd Nanostructures. **Nano Letters**, v. 6, p. 833–38, 2006.

[66] CHAN, G. H.; JING, Z.; Erin, M. H. *et al*. Plasmonic Properties of Copper Nanoparticles Fabricated by Nanosphere Lithography. **Nano Letters**, v. 7, p. 1947–52, 2007.

[67] CHAN, G. H.; JING Z.; GEORGE, C. S. *et al*. Localized Surface Plasmon Resonance Spectroscopy of Triangular Aluminum Nanoparticles. **The Journal of Physical Chemistry C**, vol. 112, p. 13958–63, 2008.

[68] CHEN, H. *et al*. Shape- and Size-Dependent Refractive Index Sensitivity of Gold Nanoparticles. **Langmuir**, vol. 24, p. 5233–37, 2008.

[69] MCMAHON, J. M. *et al*. Plasmonics in the Ultraviolet with the Poor Metals Al, Ga, In, Sn, Tl, Pb, and Bi. **Phys. Chem. Chem. Phys**., v. 15, p. 5415–23, 2013.

[70] HAES, A. J.; SHENGLI, Z. *et al*. Nanoscale Optical Biosensor: Short Range Distance Dependence of the Localized Surface Plasmon Resonance of Noble Metal Nanoparticles. **The Journal of Physical Chemistry B**, vol. 108, p. 6961–68, 2004.

[71] ROLF E. Hummel, P. WiÃŸmann. Handbook of Optical Properties, Optics of Small Particles, Interface, and Surface. **CRC Press,** v. II, 1997.

[72] HAES, A. J.; VAN DUYNE R. P. A Nanoscale Optical Biosensor: Sensitivity and Selectivity of an Approach Based on the Localized Surface Plasmon Resonance Spectroscopy of Triangular Silver Nanoparticles. **Journal of the American Chemical Society**, v. 124, p. 10596–

604, 2002.

[73] MARTINSSON, E. *et al*. Substrate Effect on the Refractive Index Sensitivity of Silver Nanoparticles. **The Journal of Physical Chemistry C**, v. 118, p. 24680–87, 2014.

[74] MILLER, M. M.; ANNE A. L. Sensitivity of Metal Nanoparticle Surface Plasmon Resonance to the Dielectric Environment. **The Journal of Physical Chemistry B**, v. 109, p. 21556–65, 2005.

[75] HAES, A. J.; LEI C. *et al*. Detection of a Biomarker for Alzheimer's Disease from Synthetic and Clinical Samples Using a Nanoscale Optical Biosensor. **Journal of the American Chemical Society**, v. 127, p. 2264–71, 2005.

[76] JUVÉ, V. *et al*. Size-Dependent Surface Plasmon Resonance Broadening in Nonspherical Nanoparticles: Single Gold Nanorods. **Nano Letters**, v. 13, p. 2234–40, 2013.

[77] MAHMOUD, M. A. *et al*. Effect of the Dielectric Constant of the Surrounding Medium and the Substrate on the Surface Plasmon Resonance Spectrum and Sensitivity Factors of Highly Symmetric Systems: Silver Nanocubes. **Journal of the American Chemical Society**, v. 134, p. 6434–6442, 2012.

[78] OTTE, M. A. *et al*. Identification of the Optimal Spectral Region for Plasmonic and Nanoplasmonic Sensing. **ACS Nano**, v. 4, p. 349–57, 2010.

[79] RASCHKE, G. *et al.* Biomolecular Recognition Based on Single Gold Nanoparticle Light Scattering. **Nano Letters**, v. 3, p. 935-938, 2003.

[80] JAIN, P. K.; WENYU H. *et al*. On the Universal Scaling Behavior of the Distance Decay of Plasmon Coupling in Metal Nanoparticle Pairs: A Plasmon Ruler Equation. **Nano Letters**, v. 7, p. 2080–88, 2007.

[81] HAMMOND, J. L. *et al*. Localized Surface Plasmon Resonance as a Biosensing Platform for Developing Countries. **Biosensors**, v. 4, p. 172–88, 2014.

[82] UNSER, S. *et al*. Localized Surface Plasmon Resonance Biosensing: Current Challenges and Approaches. **Sensors**, v. 15, p. 15684–716, 2015.

[83] BECKER, J. *et al.* The Optimal Aspect Ratio of Gold Nanorods for Plasmonic Bio-Sensing. **Plasmonics**, v. 5, p. 161–67, 2010.

[84] JUNG, L. S. *et al*. Quantitative Interpretation of the Response of Surface Plasmon Resonance Sensors to Adsorbed Films. **Langmuir**, v. 14, p. 5636–48, 1998.

[85] ZEMAN, E. J.; GEORGE, C. S. An Accurate Electromagnetic Theory Study of Surface Enhancement Factors for Silver, Gold, Copper, Lithium, Sodium, Aluminum, Gallium, Indium, Zinc, and Cadmium. **The Journal of Physical Chemistry**, v. 91, p. 634–43, 1987.

[86] VIDOTTI, M. *et al*. Biosensors Based on Gold Nanostructures. **Journal of the Brazilian Chemical Society**, v. 22, p. 3-20, 2011.

[87] PERUMAL, V.; HASHIM, U. Advances in Biosensors: Principle, Architecture and Applications. **Journal of Applied Biomedicine**, v. 12, p. 1-15, 2014,.

[88] VO-DINH, TUAN.; BRIAN Cullum. Biosensors and Biochips: Advances in Biological and Medical Diagnostics. **Journal of Analytical Chemistry**, v. 366. P. 540-551, 2000.

[89] LUZ, R. A. S. *et al*. Nanomaterials for Biosensors and Implantable Biodevices. **Nanobioelectrochemistry**, p. 27-48, 2013.

[90] RABA, J. *et al*. Analytical Biosensors for the Pathogenic Microorganisms Determination. **Formatex**, 2013.

[91] IBRAHIM, A. *et al*. Overview of Optical Biosensing Techniques. **Handbook of Biosensors and Biochips**, 2008,

[92] IBRAHIM A.; ZOUROB, M.; LAKHTAKIA A. Surface Plasmon Resonance for Biosensing: A Mini-Review. **Electromagnetics**, v. 28, p. 214-242, 2008.

[93] ASHA, C.; MALHOTRA, B. D. Mediated Biosensors. **Biosensors and Bioelectronics**, v. 17, p. 441-456, 2002.

[94] TOMÁŠ, B. *et al*. Electrochemical Lectin Based Biosensors as a Label-Free Tool in Glycomics. **Mikrochim Acta**, v. 180, p. 1-13, 2013.

[95] ELAINE, S. *et al*. High Sensitivity DNA Detection Using Gold Nanoparticle Functionalised Polyaniline Nanofibres. **Biosensors and Bioelectronics**, v. 26, p. 2613-2618, 2011.

[96] KAFI, A. K. M.; CROSSLEY, M. J. Synthesis of a Conductive Network of Crosslinked Carbon Nanotube/Hemoglobin on a Thiol-Modified Au Surface and Its Application to Biosensing. **Biosensors and Bioelectronics**, v. 42, p. 273-279, 2013.

[97] LU, Xianbo, *et al*. "Electrochemical Biosensing Platform Based on Amino Acid Ionic Liquid Functionalized Graphene for Ultrasensitive Biosensing Applications." **Biosensors and Bioelectronics**, v. 62, p. 134-139, 2014,

[98] SERGE, C.; KARYAKIN, A. Electropolymerization. **Wiley-VCH Verlag GmbH & Co. KGaA**, 2010.

[99] CUNNINGHAM, B. T. Label-Free Optical Biosensors: An Introduction. Label-Free Biosensors*:* Techniques and Applications, **Cambridge University Press**, 2009.

[100] ZHANG, X.; JU, H.; WANG, J. Electrochemical sensors, biosensors and their biomedical applications. New York: **Elsevier**, 2008.

[101] KRYSCIO, D. R.; PEPPAS, N. A. Critical Review and Perspective of Macromolecularly Imprinted Polymers. **Acta Biomaterialia**, v. 8, p. 461-473, 2012.

[102] GOPINATH, S. C. B. *et al*. Current Aspects in Immunosensors. **Biosensors and Bioelectronics**, v. 57, p. 292–302, 2014.

[103] ABBAS, A. K.; LICHTMAN, A. H.; PILLAI, S. Imunologia celular e molecular. 7th ed. Rio de Janeiro: **Elsevier**, p. 560, 2012.

[104] RAHMAN, Md. M. *et al*. A Comprehensive Review of Glucose Biosensors Based on Nanostructured Metal-Oxides. **Sensors**, v. 10, p. 4855–86, 2010.

[105] FARRÉ, M. *et al*. Advances in Immunochemical Technologies for Analysis of Organic Pollutants in the Environment. *TrAC* **Trends in Analytical Chemistry**, v. 26, p. 1100–1112, 2007.

[106] RAPP, B. E. *et al*. Biosensors with Label-Free Detection Designed for Diagnostic Applications. **Analytical and Bioanalytical Chemistry**, v. 398, p. 2403–2412, 2010.

[107] MATTOS, A. B. *et al*. A Dual Quartz Crystal Microbalance for Human Cardiac Troponin T in Real Time Detection. **Sensors and Actuators B**, v. 161, p. 439–446, 2012.

[108] TRILLING, A. K. *et al*. Antibody Orientation on Biosensor Surfaces: A Minireview. **The Analyst**, v. 138, p. 1619, 2013.

[109] BUČKO, M. *et al*. Immobilization in Biotechnology and Biorecognition: From Macro- to Nanoscale Systems. **Chemical Papers**, v. 66, p. 983-998, 2012.

[110] SASSOLAS, A. *et al*. Immobilization Strategies to Develop Enzymatic Biosensors. **Biotechnology Advances**, v. 30, p. 489–511, 2012.

[111] STEEN, R.; ERIK. *et al*. Protein Engineering For Directed Immobilization. **Bioconjugate Chemistry**, v. 24, p. 1761–1777, 2013.

[112] RICCI, F. *et al*. A Review of Experimental Aspects of Electrochemical Immunosensors. **Electrochimica Acta**, v. 84, p. 74–83, 2012.

[113] ERICSSON, E. Biosensor Surface Chemistry for Oriented Protein Immobilization and Biochip Patterning. **Linköping University, Sweden** ,2013.

[114] SEHGAL, D.; VIJAY, I. K. A Method for the High Efficiency of Water-Soluble Carbodiimide-Mediated Amidation. **Analytical Biochemistry**, vol. 218, p. 87–91, 1994.

[115] SCOTT, G. Degradation and Stabilization of Polymers. **European Polymer Journal**, vol. 5, p. 189–213, 1969.

[116] BĂNICĂ, F. G. Chemical Sensors and Biosensors. **John Wiley & Sons, Ltd**, 2012.

[117] INZELT, G. *et al*. Electron and Proton Conducting Polymers: Recent Developments and Prospects. **Electrochimica Acta**, v. 45, p. 2403–2421, 2000.

[118] LI, C. *et al*. Conducting Polymer Nanomaterials: Electrosynthesis and Applications. **Chemical Society Reviews**, v. 38, p. 2397, 2009.

[119] YANG, H. Enzyme-Based Ultrasensitive Electrochemical Biosensors. **Current Opinion in Chemical Biology**, v. 16, p. 422–428, 2012.

[120] RAVICHANDRAN, R. *et al*. Advances in Polymeric Systems for Tissue Engineering and Biomedical Applications. **Macromolecular Bioscience**, v. 12, p. 286–311, 2012.

[121] XIAO, X. *et al*. An Reagentless Glucose Biosensor Based on Direct Electrochemistry of Glucose Oxidase Immobilized on Poly(Methylene Blue) Doped Silica Nanocomposites. **Sensors and Actuators B**, v. 165, p. 126–132, 2012.

[122] GUAN, R. *et al*. Effect of Casting Solvent on the Morphology and Performance of Sulfonated Polyethersulfone Membranes. **Journal of Membrane Science**, v. 277, p. 148–156, 2006.

[123] PATRIC, J. Recent Developments in High-Temperature Proton Conducting Polymer Electrolyte Membranes. **Current Opinion in Colloid & Interface Science**, v. 8, p. 96–102, 2003.

[124] LITSTER, S.; MCLEAN, G. PEM Fuel Cell Electrodes. **Journal of Power Sources**, v. 130, p. 61–76, 2004.

[125] BAIG, N. *et al*. Recent Trends in Nanomaterial-Modified Electrodes for Electroanalytical Applications. **Trends in Analytical Chemistry**, v. 111, p. 47–61, 2019.

[126] CULEBRAS, M.; Igual-Muñoz, A.M. *et al*. Manufacturing Te/PEDOT Films for Thermoelectric Applications. **ACS Applied Materials & Interfaces**, v. 9, p. 20826–20832, 2017.

[127] BREIBY, D. W. *et al*. Smectic Structures in Electrochemically Prepared Poly(3,4-Ethylenedioxythiophene) Films. **Journal of Polymer Science**, **Part B: Polymer Physics**, v. 41, p. 945-952, 2003.

[128] CRISPIN, X. *et al*. The Origin of the High Conductivity of Poly(3,4-Ethylenedioxythiophene)-Poly(Styrenesulfonate) (PEDOT-PSS) Plastic Electrodes. **Chemistry of Materials**, v. 18, p. 4354-4360, 2006.

[129] PIGANI, L. *et al*. Pedot Modified Electrodes in Amperometric Sensing for Analysis of Red Wine Samples. **Food Chemistry**, v. 129, p. 226–33, 2011.

[130] GONÇALVES, A. R. *et al*. Preparation and Characterisation of Poly(3,4-Ethylenedioxythiophene) and Poly(3,4-Ethylenedioxythiophene)/Poly(Neutral Red) Modified Carbon Film Electrodes, and Application as Sensors for Hydrogen Peroxide. **Electrochimica Acta**, v. 56, p. 3685–9362, 2011.

[131] KAKHKI, S. *et al*. Development and Characterization of Poly(3,4-Ethylenedioxythiophene)-Coated Poly(Methylene Blue)-Modified Carbon Electrodes. **Synthetic Metals**, v. 161, p. 2718–26, 2012.

[132] SCHULLER, J. A. *et al*. Plasmonics for Extreme Light Concentration and Manipulation. **Nature Materials**, vol. 9, p. 193–204, 2010.

[133] FAROOQ, S.; ARAUJO, R.E. Engineering a Localized Surface Plasmon Resonance

Platform for Molecular Biosensing. **Open Journal of Applied Sciences**, vol. 08, p. 126–39, 2018.

[134] KELLY, K. L. *et al*. The Optical Properties of Metal Nanoparticles: The Influence of Size, Shape, and Dielectric Environment. **Journal of Physical Chemistry B**, v. 107, p. 668–677, 2003.

[135] DHAWAN, A. *et al*. Comparison of FDTD Numerical Computations and Analytical Multipole Expansion Method for Plasmonics-Active Nanosphere Dimers. **Optics Express**, v. 17, p. 9688, 2009.

[136] KHOURY, C. G. *et al*. Plasmonics of 3-D Nanoshell Dimers Using Multipole Expansion and Finite Element Method. **American Chemical Society**, v. 3, p. 2776-2788, 2009.

[137] OUBRE, C.; NORDLANDER, P. Finite-Difference Time-Domain Studies of the Optical Properties of Nanoshell Dimers. **The Journal of Physical Chemistry B**, v. 109, p. 10042-10051, 2005.

[138] TSAI, C. Y. *et al*. The Aspect Ratio Effect on Plasmonic Properties and Biosensing of Bonding Mode in Gold Elliptical Nanoring Arrays. **Optics Express,** v. 21, p. 14090-14096, 2013.

[139] WU, H. j. *et al*. Membrane-Protein Binding Measured with Solution-Phase Plasmonic Nanocube Sensors. **Nature Methods**, v. 9, p. 1189–1191, 2012.

[140] JOHNSON, P. B.; CHRISTY, R.W. Optical Constants of the Noble Metals. **Physical Review B**, v. 6, p. 4370–79,1972.

[141] KLANTSATAYA, E. *et al*. Surface Plasmon Scattering in Exposed Core Optical Fiber for Enhanced Resolution Refractive Index Sensing. **Sensors**, v. 15, p. 25090–25102, 2015.

[142] RIBEIRO, M. S. *et al*. Photodynamic Inactivation Assisted by Localized Surface Plasmon Resonance of Silver Nanoparticles: In Vitro Evaluation on Escherichia Coli and Streptococcus Mutans. **Photodiagnosis and Photodynamic Therapy**, v. 22, p. 191–96, 2018.

[143] MOCK, J. J. *et al*. Local Refractive Index Dependence of Plasmon Resonance Spectra from Individual Nanoparticles. **Nano Letters**, v. 3, p. 485–491, 2003.

[144] JAIN, P. K.; SUSIE, E. *et al*. Plasmon Coupling in Nanorod Assemblies: Optical Absorption, Discrete Dipole Approximation Simulation, and Exciton-Coupling Model. **Journal of Physical Chemistry B**, v. 110, p. 18243–18253, 2006.

[145] LEE, J. *et al*. Tuning the Thickness and Orientation of Single Au Pyramids for Improved Refractive Index Sensitivities. **Journal of Physical Chemistry C**, v. 113, p. 2205–2207, 2009.

[146] PRAMOD, P.; THOMAS. K. G. Plasmon Coupling in Dimers of Au Nanorods. **Advanced Materials**, v. 20, p. 4300–4305, 2008.

[147] ISHIMARU, A. Wave Propagation and Scattering in Random Media. **Elsevier**, 1978.

[148] SOUZA, D.; MACHADO, S.A.S.; AVACA, L. A. Square wave voltammetry. **Theoretical Aspects. New Chemistry**, v. 1, p. 81–89, 2003.

[149] ELGRISHI, N. *et al*. A Practical Beginner's Guide to Cyclic Voltammetry. **Journal of Chemical Education**, v. 95, p. 197–206, 2018.

[150] GRIESHABER, D. *et al*. Electrochemical Biosensors - Sensor Principles and Architectures. **Sensors**, v. 8, p. 1400–58, 2008.

[151] BRETT, C. M. A.; BRETT, A. M. O. Electrochemistry: Principles, Methods, and Applications. 1st ed. New York, **Oxford University Press**, p. 464 ,1993.

[152] BARD, J.; FAULKNER, L. R. Electrochemical Methods: Fundamentals and Applications. **2nd ed. New York: Wiley**, p. 864 ,2001.

[153] YUAN, X.; WANG, H.; SONG, C.; ZHANG, J. Electrochemical Impedance Spectroscopy in PEM Fuel Cells. Fundamentals and Applications. **Springer London**, 2010.

[154] DE Souza, D. *et al*. Voltametria De Onda Quadrada. Primeira Parte: Aspectos Teóricos. **Quim. Nova**, v. 26, 2003.

[155] GRIFFITHS, P. R.; JAMES A. D. Fourier Transform Infrared Spectrometry, Second Edition, **Wiley**, 2007.

[156] ALBERT, S. *et al*. High-Resolution Fourier Transform Infrared Spectroscopy. Handbook of High-Resolution Spectroscopy, **John Wiley & Sons, Ltd**, 2011.

[157] SILVERSTEIN, R.M.; BASSLER, G. C.; MORRILL, T. C. Spectrometric Identificationof Organic Compounds. 6th Ed., **Guanabara**, 2000.

[158] LARKIN, P. J. Infrared and Raman Spectroscopy; Principles and Spectral Interpretation. **Elsevier**, 2011.

[159] SMITH, B. C. Infrared Spectral Interpretation : A Systematic Approach. **CRC Press**, 1999.

[160] STUART, B. H. Infrared Spectroscopy : Fundamentals and Applications. **J. Wiley**, 2004.

[161] PARK, S. *et al*. Ultrafast 2D-IR Vibrational Echo Spectroscopy: A Probe of Molecular Dynamics. **Laser Physics Letters**, v. 4, p. 704–18, 2007.

[162] FERREIRA, PUPIM, A. A.; YAMANAKA. H. Atomic Force Microscopy Applied to Immunoassays. **Quimica Nova**, 2006.

[163] PAQUIM, A. M.; BRETT, A. M. Microscopia de Força Atômica de Moléculas de DNA Adsorvidas Na Superfície Do HOPG. **Boletim Da Sociedade Portuguesa de Química**, p. 57–68, 2009.

[164] MORITA, S.; WIESENDANGER, R.; MEYER, E. Noncontact Atomic Force Microscopy. **Springer Berlin Heidelberg**, 2002.

[165] ZHOU, W. *et al*. Fundamentals of Scanning Electron Microscopy (SEM). **Scanning Microscopy for Nanotechnology: Techniques and Applications**, 2007.

[166] HU, M. *et al*. Dark-Field Microscopy Studies of Single Metal Nanoparticles: Understanding the Factors That Influence the Linewidth of the Localized Surface Plasmon Resonance. **Journal of Materials Chemistry**, v. 18, p. 1949–60, 2008.

[167] NEHL, C. L. *et al*. Optical Properties of Star-Shaped Gold Nanoparticles. **Nano Letters**, v. 6, p. 683–88, 2006.

[168] UNDERWOOD, S.; MULVANEY, P. Effect of the Solution Refractive Index on the Color of Gold Colloids. **Langmuir**, v. 10, p. 3427–3430, 1994.

[169] BUKASOV, R.; JENNIFER S. S. P. Highly Tunable Infrared Extinction Properties of Gold Nanocrescents. **Nano Letters**, v. 7, p. 1113–1118, 2007.

[170] TAM, F. *et al*. Geometrical Parameters Controlling Sensitivity of Nanoshell Plasmon Resonances to Changes in Dielectric Environment. **Journal of Physical Chemistry B**, v. 108, p. 17290–17294, 2004.

[171] BURGIN, J. *et al*. Dielectric Sensing with Deposited Gold Bipyramids. **Journal of Physical Chemistry C**, v. 112, p. 19278–19282, 2008.

[172] ZHENG, Y. *et al*. Recent Advances in Conducting Poly(3,4-Ethylenedioxythiophene):Polystyrene Sulfonate Hybrids for Thermoelectric Applications. **Journal of Materials Chemistry C**, v. 6, p. 8858–8873, 2018.

[173] CULEBRAS, M.; JOSÉ, F. S. C. *et al*. Conducting PEDOT Nanoparticles: Controlling Colloidal Stability and Electrical Properties. **The Journal of Physical Chemistry C**, v. 122, p. 19197–19203, 2018.

[174] SAPTARSHI, S. R. *et al*. Interaction of Nanoparticles with Proteins: Relation to Bio-Reactivity of the Nanoparticle. **Journal of Nanobiotechnology**, v. 11, 2013.

[175] MAHMOUDI, M. *et al*. Protein-Nanoparticle Interactions: Opportunities and Challenges. **Chemical Reviews**, v. 111, p. 5610–5637, 2011.

APÊNDIX A - Articles and Conference Contributions

- Optimizing the Plasmonic Sensing of Silica Coated Au/Ag Nanoshells, **Article,** April 2019, International Journal of Engineering Science and Investigation.
- Sandwiched type Immunosensor PEDOT nanoparticles-based supported on GCE for the detection of chikungunya virus. , **Article** (TO be Submitted).
- Optimizing gold nanorods dimer structure for sensing platform, **Conference Paper**, September ,2018 SBFoton International Optics and Photonics Conference (SBFoton IOPC), Sao Paulo- Brazil
- The Optical Response of Bare Versus Coated Gold Nanorods For Sensing Applications", **Poster Paper**, 10th International Conference on Nanophotonics, July 02-05,2017, Recife-PE- Brazil (ICNP2017).
- Exploiting the Sensing Efficiency of Bare versus silica coated Au Nanorods, **Poster Paper**, XVII Brazilian MRS Meeting, September 16-20, 2018, Natal-RN- Brazil.
- A comparative study based on Optimizing the Figure of merit of Au versus Ag nanoshells, **Poster Paper**, XVII Brazilian MRS Meeting, September 16-20, 2018, Natal-RN- Brazil.
- Surface modification and spectroelectrochemical responseof PEDOT nanoparticles on glassy carbon electrode by template free solution method, **Poster Paper**, December 3-5,2018, Recife-PE- Brazil
- Plasmonic Response of Gold- silica and Silver- silica metal core nanoshells by optimizing the figure of merit. **Presentation**, February 18-20, 2019, 3rd International Conference On Materials Science & Nanotechnology- Pakistan.
- Effects of Different Aspect Ratios and Junction Lengths on the Coupled Plasmon Gold Nanorod Dimers, **Presentation**, July17-19. University of Aveiro, Aveiro, Portugal (ANM2019).